Vol. 9, no. 4, 2025 eISSN 2587-8999
PEER-REVIEWED SCIENTIFIC AND THEORETICAL JOURNAL

Computational Mathematics and Information Technologies

Computational Mathematics

Mathematical Modelling

Information Technologies

www.cmit-journal.ru
DOI 10.23947/2587-8999

Computational Mathematics and Information Technologies

Peer-reviewed scientific and theoretical journal

eISSN 2587–8999

Published since 2017

Periodicity — 4 issues per year

DOI: 10.23947/2587–8999

Founder and Publisher — Don State Technical University (DSTU), Rostov-on-Don, Russian Federation

The journal "Computational Mathematics and Information Technologies" publishes reviews, original articles and short reports related to mathematical modelling, numerical methods and information technologies for solving complex and topical problems of science and modern modern engineering and technology. Research areas include continuum mechanics, fluid dynamics, Earth sciences, chemistry, biology, image processing and pattern recognition, parallel computing theory and its applications, big data and artificial intelligence technologies, etc.

The journal "Computational Mathematics and Information Technologies" accepts scientific and review articles for publication in accordance with the sections:

1. Computational Mathematics
2. Mathematical Modelling
3. Information Technologies

Registration:	Mass media registration certificate ЭЛ № ФС 77–66529 dated July 21, 2016 issued by the Federal Service for Supervision of Communications, Information Technology and Mass Media
Indexing and Archiving:	RISC, Crossref, Cyberleninka
Website:	https://cmit-journal.ru
Address of the Editorial Office:	1, Gagarin sq., Rostov-on-Don, 344003, Russian Federation
E-mail:	CMIT-EJ@yandex.ru
Telephone:	+7 (863) 273–85–14
Date of publication No. 4, 2025:	30.12.2025

Computational Mathematics and Information Technologies

Рецензируемый научно-теоретический журнал

eISSN 2587–8999

Издается с 2017 года

Периодичность — 4 выпуска в год

DOI: 10.23947/2587–8999

Учредитель и издатель — Федеральное государственное бюджетное образовательное учреждение высшего образования «Донской государственный технический университет» (ДГТУ), г. Ростов-на-Дону, Российская Федерация

Журнал «Computational Mathematics and Information Technologies» публикует обзоры, оригинальные статьи и краткие сообщения, посвященные математическому моделированию, численным методам и информационным технологиям для решения сложных и актуальных проблем науки и современной технологии. Область применения исследований — это механика сплошных сред, гидроаэродинамика, науки о Земле, химия, биология, обработка изображений и распознавание образов, теория параллельных вычислений и ее приложения, технологии больших баз данных и искусственного интеллекта и т. д.

Журнал «Computational Mathematics and Information Technologies» принимает к публикации научные и обзорные статьи в соответствии с разделами:

1. Вычислительная математика
2. Математическое моделирование
3. Информационные технологии

Регистрация:	Свидетельство о регистрации средства массовой информации ЭЛ № ФС 77 – 66529 от 21 июля 2016 г., выдано Федеральной службой по надзору в сфере связи, информационных технологий и массовых коммуникаций
Индексация и архивация:	РИНЦ, CrossRef, CyberLeninka
Сайт:	https://cmit-journal.ru
Адрес редакции:	344003, Российская Федерация, г. Ростов-на-Дону, пл. Гагарина, 1
E-mail:	CMIT-EJ@yandex.ru
Телефон:	+7 (863) 273–85–14
Дата выхода № 4, 2025 в свет:	30.12.2025

Contents

Содержание

ANNIVERSARY OF THE SCIENTIST
ЮБИЛЕЙ УЧЕНОГО

On the Anniversary of Academician of the Russian Academy of Sciences and Academician of the Russian Academy of Education, Doctor of Physical and Mathematical Sciences, Professor ALEXEY LVOVICH SEMENOV

The Editorial Board of the journal "Computational Mathematics and Information Technologies" extends its heartfelt congratulations to its esteemed member, Alexey Lvovich Semenov, on the occasion of his 75th anniversary!

Alexey Lvovich Semenov is the Head of the Department of Mathematical Logic and Algorithm Theory at the Faculty of Mechanics and Mathematics, Advisor to the Rector of the Federal State Budgetary Educational Institution of Higher Education "Lomonosov Moscow State University", Director of the A.I. Berg Institute of Cybernetics and Educational Informatics at the Federal State Institution "Federal Research Center for Computer Science and Control" of the Russian Academy of Sciences, Academician of the Russian Academy of Sciences, Academician of the Russian Academy of Education, Professor, and Doctor of Physical and Mathematical Sciences.

A.L. Semenov is an outstanding mathematician, a specialist in the fields of mathematical logic, complexity theory, and computer science. He works in the areas of artificial intelligence and the development of applied software for domestic supercomputers.

Key Milestones in the Scientific, Pedagogical, and Organizational Activities of the Jubilarian

In 1972, A.L. Semenov graduated with honors from the Faculty of Mechanics and Mathematics at Lomonosov Moscow State University, specializing in "Mathematics". In 1975, he completed his postgraduate studies at the same faculty, defending his Candidate of Sciences dissertation titled "On Definability in Some Decidable Theories". In 1985, he defended his Doctor of Sciences dissertation, "Logical Theories of Unary Functions on Natural Numbers".

From 1975 to 1983, he served as a Lecturer at the Department of Mathematical Logic at Lomonosov Moscow State University. His career then continued with leadership roles, including Head of the Sector for Problem-Oriented Processors and Head of the Laboratory for Algorithm Theory and Linguistic Support within the Scientific Council of the USSR Academy of Sciences for the Complex Problem "Cybernetics" at the Institute of Cybernetics Problems of the USSR Academy of Sciences and the A.A. Dorodnitsyn Computing Center of the Russian Academy of Sciences.

From 1993 to 2013, he served as Rector of the Moscow Institute of Open Education (known until 2002 as the Moscow Institute for the Professional Development of Educators). He later served as Rector of Moscow Pedagogical State University (V.I. Lenin MPGU) from 2013 to 2016.

Since 2015, he has been the Director of the A.I. Berg Institute of Cybernetics and Educational Informatics at the Federal Research Center for Computer Science and Control of the Russian Academy of Sciences.

A.L. Semenov was elected a Corresponding Member of the Russian Academy of Sciences in 2008 and became a Full Member (Academician) of the Russian Academy of Sciences in 2011, within the Division of Mathematical Sciences. He was elected an Academician of the Russian Academy of Education in 2010. He has held the academic title of Professor since 1998.

Main Scientific Contributions of A.L. Semenov

Alexey Lvovich Semenov's contributions to mathematics and theoretical computer science encompass results in formal grammars, program schemata and dynamic logics, relational algebras, automaton-realizable relations, and decision algorithms for a range of mathematical theories. He developed a theory of algorithmic randomness for finite sequences, parallel to Kolmogorov's combinatorial complexity theory, and solved the Kolmogorov problem concerning the precise estimation of randomness test complexity. The central theme of his mathematical research has been definability theory, where he is a world-renowned authority.

Research on definability originates from the classical works of the Italian (G. Peano, A. Padoa, M. Pieri) and Polish (A. Tarski) schools of mathematical logic in the 19th and first half of the 20th centuries, as well as the works of K. Gödel. L. Svenonius's key 1959 paper laid the foundation for the "Erlangen program" — the completeness theorem for definability. A.L. Semenov and S.F. Soprunov obtained a combinatorial version of the Svenonius theorem.

The decidability of the definability space for the addition of natural numbers is a classical 1929 result by Presburger. In 1979, A.L. Semenov proved the decidability of a broad class of extensions of this space by unary functions, such as exponentiation or factorial. In the case of monadic spaces, A.L. Semenov obtained results on extending the definability space for the successor of natural (or integer) numbers with almost periodic (recurrent) sequences from symbolic dynamics.

This, in particular, solved the Zyfkes problem and provided a solution to Church's uniformization problem for the almost periodic case. The study of almost periodic sequences was further developed in the works of his students — A.A. Muchnik, Yu.L. Pritykin, and M.A. Ushakov. For monadic spaces, A.A. Muchnik solved a problem concerning the monadic space of several successors, posed by M.O. Rabin at the International Congress of Mathematicians in Nice. S.F. Soprunov solved the problem posed by M.O. Rabin and C. Elgot on the existence of maximal decidable definability spaces for the weak monadic case.

The general subject of definability spaces gave rise to a number of questions related to the lattice of such spaces. These questions were answered in the works of A.L. Semenov and his colleagues. In particular, examples of spaces of arbitrary width were constructed. A.L. Semenov and S.F. Soprunov constructed examples of definability spaces of arbitrary finite quantifier depth.

In 1980, A.N. Kolmogorov, who headed the Department of Mathematical Logic and Algorithm Theory at Moscow State University (the department currently chaired by A.L. Semenov), invited A.L. Semenov to co-lead a seminar on complexity, which continues to operate to this day. This defined another major direction of A.L. Semenov›s work. In his seminal 1963 publication on the complexity of finite objects, A.N. Kolmogorov raised the question of the precise relationship between the complexity of a sequence, the complexity of an algorithm selecting a subsequence from it, and the degree to which the selected subsequence satisfies the law of large numbers. Kolmogorov revisited this problem in 1983. The solution to this problem by A.A. Muchnik and A.L. Semenov in 2003 was awarded the A.N. Kolmogorov Prize of the Russian Academy of Sciences as an outstanding contribution to mathematics. He is also the author of numerous works in general theory of algorithms and computations, algorithmic randomness, program logics, combinatorial group theory, computational complexity, algorithmic degrees, and effective computational algorithms.

His activity in applied computer science and the creation of artificial intelligence systems began in 1964 with participation in works on speech recognition, text generation systems, situational control, and compilers for Lisp and APL languages for domestic computers. Starting from 1983, A.L. Semenov participated in the development of applied mathematical software for the "Elektronika SSBIS" supercomputer.

A.L. Semenov is the author of the concept of the "extended personality" as a methodological foundation for AI applications in education. The "MSU Ark of Knowledge" project, implemented under his leadership, serves as the basis for building an ontology of fundamental knowledge and trusted encyclopedic systems.

A.L. Semenov participated in the creation of the "Digital Economy of the Russian Federation" program and the national strategy in the field of artificial intelligence. He is a prominent figure in Russian education and a key participant in shaping the modern content of school informatics and teacher training. His areas of interest include fundamental problems of general and pedagogical education, digital technologies in education, digital transformation of education, issues of updating the content of education in primary and secondary schools, as well as professional pedagogical education.

Beginning in 1967, A.L. Semenov taught at Moscow School No. 7, which he himself had graduated from, and later worked within A.N. Kolmogorov's team at the Physics and Mathematics Boarding School affiliated with Moscow State University. In 2003, he re-established School No. 179 as part of the Moscow Institute of Open Education (MIOO), which he headed, and brought back to work there Nikolai Nikolaevich Konstantinov, the founder and ideological leader of the tradition of specialized mathematics schools in Russia. He served as a member of the Executive Committee of the International Commission on Mathematical Instruction.

In 1984, he became the organizer and a member of the authoring team for the first informatics textbook in the USSR, published in a print run of 3 million copies for all schools across the Soviet Union.

From the mid-1980s, A.L. Semenov led developments aimed at forming a new methodology for Russian education, encompassing research activities for all students and the use of digital technologies. He developed the conceptual foundation and practical solutions (including textbooks, software, subject-specific environments, standards, and organizational documents) for learning, teaching, and management processes utilizing digital tools. He began this work under the guidance of E.P. Velikhov and A.P. Ershov within the framework of the All-Union Scientific and Technical Commission "Shkola-1" of the USSR Academy of Sciences and continued it at the Institute of New Technologies, which he founded. The methodology he created influenced the subsequent development of Russian and global education, forming the basis for UNESCO recommendations for all levels of general and teacher education.

A.L. Semenov is widely known as the founder of the Institute of New Technologies in Education (INT), which developed and adapted numerous digital educational resources for Russia, published hundreds of books for teachers on the use of ICT across all school subjects, and is recognized as a world leader in applying information technology in schools based on a constructionist approach. He led the authoring team for an integrated course in mathematics, informatics, and linguistics for primary school. Courses based on this work, "Informatics" and "Algorithmics", are now widely used in Russian schools. Under his guidance, a range of computer environments and tools for student activities were developed, aligned with modern educational goals across all subjects.

A program for regional informatization developed under A.L. Semenov›s leadership received the President of the Russian Federation Prize in 1999. He is one of the leaders of joint projects involving the Russian Academy of Sciences, Moscow State University, and the educational community aimed at improving the quality of digital educational resources

and shaping standards. He was one of the developers of educational standards for schools: for Moscow in 1996, and for the Russian Federation in 2004 and 2009. He served as head of the scientific-methodological council of the Federal Institute of Pedagogical Measurements (FIPI) for the state final certification in mathematics and currently holds this position for informatics. The implementation of his ideas in the field of education in Moscow has enabled the creation of a unique, world-class information environment for learning, development, and social interaction among students, teachers, and educational management systems. Work on the informatization of Russian education carried out under his leadership was awarded the Russian Government Prize in 2009.

He served as the coordinator for the development of the Concept for the Development of Russian Mathematics Education, created in response to a May 2012 Presidential Decree, and was one of the leaders in developing the Concept for Technological Education in Schools, following an assignment from the President of the Russian Federation.

A.L. Semenov was the only plenary speaker from Russia at the II International UNESCO Congress "Education and Informatics" in Moscow in 1996, a keynote speaker at the seminar "Bridging the Gap between the Information-rich and the Information-poor: New Technologies and the Future of Education" at the 46th International Conference on Education (Geneva, 2001), and the lead author of UNESCO books "Recommendations on ICT in Primary Education" (2000), "ICT in Schools", and "A Teacher's Guide, or How ICT Can Create a New, Open Learning Environment" (2005). From 2019 to 2023, he led a Russian Foundation for Basic Research program on the implementation of digital technologies in schools, which involved teams from the Institute of Education as well. At his initiative, the "Charter of the School's Digital Pathway" was adopted.

The holistic school model he built, based on the ideology of individual design of educational trajectories and the mandatory achievement of planned results by every student, is known as "result-oriented education".

A.L. Semenov is a permanent participant in the scientific activities of the Regional Scientific Center of the Russian Academy of Education in the Northwestern Federal District, based at the Herzen State Pedagogical University of Russia and the Institute of Education at the National Research University Higher School of Economics. He has supervised the training of two Doctors of Sciences and four Candidates of Sciences. He is the author of over 400 scientific works in the fields of mathematics, computer science, and education.

Since 2021, he has served as the Editor-in-Chief of the journal Proceedings of the Russian Academy of Sciences: Mathematics, Computer Science, Control Processes, and from 2012 to 2018, he was the Editor-in-Chief of the journal Kvant (Quantum). He is a member of the editorial boards or editorial councils of journals including Informatics and Its Applications, Artificial Intelligence and Decision Making, Information Society, Bulletin of Cybernetics, Educational Issues (Voprosy obrazovaniya), Educational Studies, Educational Policy, Pedagogy, Problems of Modern Education, Mathematics at School, Mathematical Enlightenment, Informatics and Education, Informatics in School, Computer Tools in Education, and Computational Mathematics and Information Technologies.

The Editorial Board of the journal "Computational Mathematics and Information Technologies" warmly congratulates the esteemed jubilarian, wishing him robust health, new scientific discoveries, and joy from the fruits of his labor! May there be many more successful projects and grateful students ahead!

MATHEMATICAL MODELLING
МАТЕМАТИЧЕСКОЕ МОДЕЛИРОВАНИЕ

UDC 519.6

Original Empirical Research

https://doi.org/10.23947/2587-8999-2025-9-4-10-21

Hybrid Modelling of Extreme Storm Processes and Navigation Risks in the Azov Sea Based on Three-Dimensional Hydrodynamics and Machine Learning Methods

Alexander I. Sukhinov[1], **Sofia V. Protsenko**[1,2] ✉, **Elena A. Protsenko**[2], **Natalia D. Panasenko**[1]

[1] Don State Technical University, Rostov-on-Don, Russian Federation

[2] Taganrog Institute named after A.P. Chekhov (branch) of RSUE, Taganrog, Russian Federation

✉ rab55555@rambler.ru

Abstract

Introduction. Extreme storms with wind speeds exceeding 30–35 m/s pose a significant threat to navigation and coastal infrastructure in the Azov Sea. The complex bathymetry, shallow water, and coastal geometry amplify wave and surge effects, causing severe destruction. The increasing frequency of extreme weather events requires next-generation forecasting systems capable of capturing nonlinear multiscale interactions between wind, waves, and currents.

Materials and Methods. A hybrid approach was developed, combining three-dimensional numerical hydrodynamic modelling based on the Navier-Stokes equations with Large-Eddy Simulation (LES) turbulence closure, ensemble probabilistic forecasting, and machine learning methods — including Physics-Informed Neural Networks (PINNs) and Fourier Neural Operators (FNOs). Atmospheric and oceanographic data from ERA5 and CMEMS reanalyses were used to reconstruct storm scenarios for 2010–2024. Ship-wave interactions were modeled in six degrees of freedom, while coastal infrastructure fragility was evaluated using probabilistic vulnerability curves. Validation was performed using Sentinel-1/3 satellite data processed by the "LBP-neural_network" software package and Copernicus Marine Service products.

Results. Three representative storm scenarios were simulated. The significant wave height in the central Azov Sea reached up to 5.2 m, with surge amplitudes up to 1.5 m. The most hazardous conditions occurred in the Kerch Strait, where current velocities reached 1.1 m/s. Under wind speeds of 30–35 m/s, the probability of exceeding the critical 4 m wave height was 42%. Resonant ship motions with roll amplitudes up to 25° were detected, indicating a high capsizing risk. Risk maps identified the most vulnerable zones near Taganrog, Yeysk, and Port Kavkaz. The integration of PINNs and FNOs accelerated ensemble simulations by a factor of 10–12 while maintaining prediction errors below 8%.

Discussion. The proposed hybrid methodology proved highly effective for modelling extreme hydrodynamic processes and navigation risks. The LES framework accurately reproduced wave breaking and vortex generation processes, while coupling with neural network surrogates combined physical consistency with computational efficiency.

Conclusion. The approach improved forecast accuracy by 25–30% compared with conventional spectral models (SWAN, WAVEWATCH III). The results provide a scientific basis for developing early warning systems, assessing navigation safety, and planning coastal protection measures in the Azov–Black Sea region.

Keywords: Azov Sea, extreme storms, three-dimensional hydrodynamics, machine learning, physics-informed neural networks, Fourier neural operators, navigation risk, large-eddy simulation, coastal infrastructure, storm forecasting

Funding. The study was supported by the Russian Science Foundation grant No. 22–11–00295–П, https://rscf.ru/en/project/22-11-00295-П/

For Citation. Sukhinov A.I., Protsenko S.V., Protsenko E.A., Panasenko N.D. Hybrid Modelling of Extreme Storm Processes and Navigation Risks in the Azov Sea Based on Three-Dimensional Hydrodynamics and Machine Learning Methods. *Computational Mathematics and Information Technologies*. 2025;9(4):10–21. https://doi.org/10.23947/2587-8999-2025-9-4-10-21

Оригинальное эмпирическое исследование

Гибридное моделирование экстремальных штормовых процессов и рисков судоходства в Азовском море на основе трёхмерной гидродинамики и методов машинного обучения

А.И. Сухинов[1], С.В. Проценко[1,2] ✉, Е.А. Проценко[2], Н.Д. Панасенко[1]

[1] Донской государственный технический университет, г. Ростов-на-Дону, Российская Федерация

[2] Таганрогский институт имени А.П. Чехова (филиал) РГЭУ (РИНХ), г. Таганрог, Российская Федерация

✉ rab55555@rambler.ru

Аннотация

Введение. Экстремальные штормы со скоростью ветра более 30–35 м/с представляют серьёзную угрозу для судоходства и прибрежной инфраструктуры Азовского моря. Сложная батиметрия, мелководье и конфигурация береговой линии усиливают волновые и нагонные процессы, вызывая разрушительные последствия. В связи с прогнозируемым увеличением частоты экстремальных погодных явлений актуальной задачей является развитие методов прогнозирования, учитывающих нелинейные и многомасштабные взаимодействия волн, ветра и течений.

Материалы и методы. Разработан гибридный подход, объединяющий трёхмерное численное моделирование на основе уравнений Навье-Стокса с крупновихревой моделью турбулентности (LES), ансамблевое вероятностное прогнозирование и методы машинного обучения — физически информированные нейронные сети (PINNs) и операторы Фурье (FNOs). Атмосферные и океанографические данные реанализа ERA5 и CMEMS использованы для реконструкции штормовых сценариев 2010–2024 гг. Взаимодействие волн с судами описано в шести степенях свободы. Для анализа уязвимости применены кривые фрагильности инфраструктуры. Верификация проведена по спутниковым данным Sentinel-1/3 обработанными программным комплексом «LBP-neural_network» и продуктам Copernicus Marine Service.

Результаты исследования. Моделирование трёх сценариев показало, что значительная высота волн в центральной части Азовского моря достигает 5,2 м, а уровень нагонов — 1,5 м. Наиболее опасные условия формируются в Керченском проливе, где скорости течений достигают 1,1 м/с. При скорости ветра 30–35 м/с вероятность превышения критической высоты волны 4 м составляет 42 %. Выявлены резонансные режимы колебаний судов с амплитудой крена до 25°, что создаёт угрозу опрокидывания. Карты риска показали зоны максимальной уязвимости портов Таганрог, Ейск и Кавказ. Применение PINNs и FNO позволило ускорить ансамблевые расчёты в 10–12 раз при сохранении точности на уровне менее 8 %.

Обсуждение. Предложенная гибридная методология демонстрирует высокую эффективность при моделировании экстремальных гидродинамических процессов и рисков судоходства. LES корректно воспроизводит процессы волнового обрушения и генерации вихрей, а интеграция с нейросетевыми моделями обеспечивает сочетание физической строгости и вычислительной эффективности.

Заключение. Метод способен повысить точность прогнозов на 25–30 % по сравнению с традиционными моделями SWAN и WAVEWATCH III. Полученные результаты могут быть использованы для разработки систем оперативного предупреждения, оценки навигационной безопасности и планирования природоохранных мероприятий в Азово-Черноморском регионе.

Ключевые слова: Азовское море, экстремальные штормы, трёхмерная гидродинамика, машинное обучение, PINNs, FNO, риск судоходства, LES-моделирование, прибрежная инфраструктура, прогнозирование штормов

Финансирование. Исследование выполнено за счет гранта Российского научного фонда № 22–11–00295–П, https://rscf.ru/en/project/22-11-00295-П/

Для цитирования. Сухинов А.И., Проценко С.В., Проценко Е.А., Панасенко Н.Д. Гибридное моделирование экстремальных штормовых процессов и рисков судоходства в Азовском море на основе трёхмерной гидродинамики и методов машинного обучения. *Computational Mathematics and Information Technologies*. 2025;9(4):10–21. https://doi.org/10.23947/2587-8999-2025-9-4-10-21

Introduction. Extreme storms with wind speeds exceeding 30–35 m/s are among the most destructive manifestations of atmospheric forcing in coastal and marine areas. They cause severe damage to port facilities, coastal protection structures, residential and recreational zones, and also pose a significant threat to maritime navigation, frequently leading to shipwrecks and cargo loss. In the context of climate change, an increase in the frequency and intensity of such storms is projected, thereby amplifying their socio-economic and environmental impacts. This underscores the necessity for developing next-generation forecasting methods capable of accounting for multi-scale interactions between storms and waves.

Currently, operational forecasting systems are primarily based on spectral wave models, such as SWAN, WAM, and WAVEWATCH III, which provide reliable large-scale estimates of wave energy distribution [1–3]. However, their spatial resolution is insufficient for accurately describing the nonlinear transformation of waves in shallow and

semi-enclosed seas. In critically important areas, such as the Sea of Azov and the Kerch Strait, complex bathymetry, coastline configuration, and resonance effects lead to the amplification of wave energy and an underestimation of storm risks [4]. Furthermore, the interaction between extreme waves and ships and coastal infrastructure involves complex three-dimensional hydrodynamic processes (refraction, diffraction, wave breaking, and turbulence) that cannot be fully reproduced by two-dimensional or simplified models [5].

Recent advances in computational fluid dynamics (CFD) and high-performance computing have enabled the development of three-dimensional non-hydrostatic models capable of explicitly simulating turbulence, shallow-water wave transformation, and their nonlinear interaction with structures [6]. The integration of such models with machine learning methods, including neural networks trained on reanalysis data and buoy observations, opens up new possibilities for adaptive forecasting and risk assessment [7]. However, the comprehensive integration of CFD modelling, artificial intelligence techniques, and coastal risk analysis remains insufficiently explored, particularly concerning the semi-enclosed basins of the Azov-Black Sea region.

Ensuring ship safety under extreme storm conditions remains a challenging scientific problem. The International Maritime Organization (IMO) has recently approved second-generation intact stability criteria, defining key failure modes: parametric rolling, surf-riding, and broaching [8]. Research indicates that resonance between long-period storm waves and a vessel's natural frequencies can lead to catastrophic consequences, as exemplified by the accident of the tanker Prestige [9]. Numerical experiments confirm that steep shallow-water waves in straits can cause loss of controllability and capsizing even of modern vessels [10].

Regional studies highlight the particular vulnerability of the Sea of Azov and the Kerch Strait, where shallow depths and complex bottom topography enhance refraction effects and the formation of standing waves, leading to a local increase in wave height [11–12].

Beyond hydrodynamic aspects, increasing attention is being paid to infrastructure vulnerability, including the probabilistic fragility analysis of port and coastal protection structures [13], as well as ecosystem-based approaches emphasizing the protective role of seagrass meadows and other natural features. Despite the progress achieved, significant gaps persist: operational models underestimate the impacts of storms in shallow seas; the integration of three-dimensional hydrodynamics and machine learning methods is limited; and vulnerability criteria for ships under the combined action of wind, waves, and currents are inadequately developed. The present study aims to address these gaps and proposes a hybrid modelling concept for forecasting extreme storms and their consequences in the Azov-Black Sea region, with a focus on navigation safety and coastal infrastructure resilience.

Materials and Methods. The methodology of this research is based on a multi-level hybrid approach that integrates numerical hydrodynamic modelling, machine learning, physics-informed neural networks, ensemble probabilistic forecasting, and GIS risk mapping.

The flow field is described by the Navier-Stokes equations for an incompressible fluid with a free surface [14]:

$$\nabla \cdot \mathbf{u} = 0,$$

$$\frac{\partial \mathbf{u}}{\partial t} + (\mathbf{u} \cdot \nabla)\mathbf{u} = -\frac{1}{\rho}\nabla p + \nu \nabla^2 \mathbf{u} + \mathbf{g} + \nabla \cdot \boldsymbol{\tau}_t + \mathbf{F}_{\text{wind}},$$

where $\mathbf{u}$ is the velocity vector (m/s); p is the hydrodynamic pressure (Pa); ρ is the water density (kg/m³); v is the kinematic viscosity (m²/s); $\mathbf{g}$ is the gravitational acceleration vector (m/s²); $\boldsymbol{\tau}_t$ are the subgrid-scale turbulent stresses (Pa); $\mathbf{F}_{\text{wind}}$ is the wind forcing (N/m³).

This approach accounts for the nonlinear interaction of waves and currents, as well as wave shoaling and breaking phenomena, which are critical for shallow seas such as the Azov Sea and the Kerch Strait. Unlike spectral models, it resolves local nonlinearities.

Turbulence is described using the Large Eddy Simulation (LES) method with the Smagorinsky closure [15]:

$$\tau_{ij} = -2\nu_t S_{ij}, \ \nu_t = (C_s \Delta)^2 \mid S \mid,$$

where τ_{ij} are the subgrid-scale Reynolds stresses; S_{ij} is the rate-of-strain tensor; v_t is the eddy viscosity; C_s is the Smagorinsky constant; Δ is the filter width (grid scale).

LES ensures the correct reproduction of wave breaking, vortices, and turbulent bursts in shallow and semi-enclosed seas. This method resolves large-scale turbulence governing wave breaking and vortex generation during storms, while only modelling small-scale dissipation. This provides higher accuracy compared to RANS for extreme and transient processes.

The momentum transfer from the atmosphere to the ocean is parameterized as follows [16]:

$$\mathbf{F}_{\text{wind}} = \frac{\rho_a C_D \mid \mathbf{U}_{10} \mid \mathbf{U}_{10}}{\rho},$$

where ρ_a is the air density; C_D is the drag coefficient; $\mathbf{U}_{10}$ is the wind speed at 10 m height. At wind speeds of 30–35 m/s, a strong atmosphere-ocean coupling develops. This parameterization directly couples atmospheric models (WRF, COSMO-Ru) with hydrodynamics, ensuring realistic wave growth.

The interaction of storm waves with ships and infrastructure is modeled using the rigid body dynamics equations [17]:

$$M\ddot{\mathbf{X}} + C\dot{\mathbf{X}} + K\mathbf{X} = \mathbf{F}(t),$$

where **X** represents displacements in six degrees of freedom (surge, sway, heave, roll, pitch, yaw); M is the mass matrix; C is the damping matrix; K is the restoring force matrix; $\mathbf{F}(t)$ is the wave excitation force.

The resonance condition for ship safety is expressed as:

$$\omega_w \approx \omega_n,$$

where ω_w is the wave frequency; ω_n is the natural frequency of the ship.

Many maritime disasters have been caused by resonance phenomena (parametric rolling, surf-riding, and broaching). Incorporating ship-wave dynamics enables forecasting not only the storms themselves but also their actual impact on vessels.

Uncertainty is quantified using ensembles of CFD simulations with perturbed wind forcing conditions. The exceedance risk is defined as:

$$P(H > H_{\text{crit}}) = \frac{1}{N}\sum_{i=1}^{N} I\left(H^{(i)} > H_{\text{crit}}\right),$$

which enables the generation of probabilistic risk maps instead of solely deterministic scenarios, where $H^{(i)}$ is the hazard characteristic (e. g., significant wave height) from the i-th ensemble member; N is the ensemble size; I is the indicator function.

Storm forecasting is inherently probabilistic. Ensembles provide the probabilistic forecasts (risk maps) essential for navigation and coastal protection. We integrate Physics-Informed Neural Networks (PINNs) and Fourier Neural Operators (FNOs). PINNs incorporate differential equation constraints into the loss function [18]:

$$\mathcal{L}(\theta) = \| \mathcal{N}[u_\theta] - f \|^2 + \lambda \| u_\theta - u_{\text{obs}} \|^2,$$

ensuring consistency with the Navier-Stokes equations, where $\mathcal{N}$ is the Navier-Stokes operator; u_θ is the neural network prediction; u_{obs} is the observed data; f epresents the source terms (forcing); λ is the weighting coefficient.

Fourier Neural Operators (FNOs) approximate the mappings from atmospheric forcings to wave responses [19]:

$$\hat{u} = \mathcal{G}_\theta(f), \ \mathcal{G}_\theta : (\mathbf{U}_{10}, p) \mapsto (H_s, \eta_{\max}),$$

where $\mathcal{G}_\theta$ is the neural network-approximated operator mapping atmospheric inputs f to wave responses $\hat{u}$.

This enables the construction of fast surrogate models for ensemble calculations. PINNs ensure physical law compliance in neural networks, while FNOs learn rapid mappings for ensemble forecasting. This hybrid approach simultaneously achieves both computational speed and physical realism, which is critical for early warning systems.

Finally, simulation results are integrated with infrastructure vulnerability curves:

$$P_{\text{damage}} = \Phi\left(\frac{\ln q_{\text{impact}} - \mu}{\sigma}\right),$$

where q_{impact} is the shock load; μ, σ are vulnerability curve parameters; Φ is the standard normal cumulative distribution function.

This enables the generation of spatial risk maps for ship casualties and infrastructure damage zones in the Sea of Azov, Kerch Strait, and Black Sea. For numerical discretization, the pressure correction method [20] was employed, ensuring mass conservation at each time step through iterative updates of velocity and pressure fields. The developed hybrid methodology, combining Computational Fluid Dynamics (CFD) and Artificial Intelligence (AI) techniques, enables high-accuracy probabilistic forecasting of storm surges and navigational risks in the Azov and Black Seas.

Results. The methodology employed a multi-level hybrid approach, integrating numerical free-surface modelling based on the Navier-Stokes equations, parameterization of atmospheric forcing, Large Eddy Simulation (LES), ensemble forecasting, and the incorporation of neural network approximators (PINNs, FNOs) to accelerate computations.

Three characteristic scenarios were defined for the numerical experiments:

• **Scenario 1 (Moderate-intensity storm):** Wind speed of 15–21 m/s, north-easterly direction, duration of 12 hours. This scenario accounts for water level fluctuations with an amplitude of up to 0.4 m.

• **Scenario 2 (Extreme storm):** Wind speed of 29–37 m/s, easterly direction, duration of 24 hours. This leads to the formation of wind-setup and surge phenomena, with growth in the significant wave height H_s.

• **Scenario 3 (Anomalous cyclonic storm):** Wind speed up to 45 m/s with gusts, high directional variability, duration of 36–48 hours. This scenario represents extreme conditions, posing the highest risk to navigation and infrastructure.

These scenarios were selected as being characteristic of extreme conditions in the Sea of Azov [21]. Input wind field data were obtained from the Weather Research and Forecasting (WRF) model with a 3 km resolution, covering the period 2010–2024 for calibration purposes. The wind fields were validated against satellite (ASCAT) and buoy data [22].

For the numerical experiment, the hybrid methodology described above was implemented. This approach involved solving the three-dimensional Navier-Stokes equations with a free surface, parameterizing atmospheric forcing, accounting

for ship and infrastructure dynamics, and employing machine learning with PINNs and FNOs. The simulations were based on the aquatic area within the coordinates [Coordinates would be inserted here, e. g., 45°N to 47°N, 35°E to 39°E]. The model domain encompasses the entire Azov Basin, the Taganrog Bay, and the Kerch Strait. The bathymetry of the area was reconstructed using GEBCO 2023 data and refined with charts from the Russian Hydrometeorological Service (local hydrographic data) [23]. A non-stationary hydrodynamic model based on the Navier-Stokes equations with a free surface was employed.

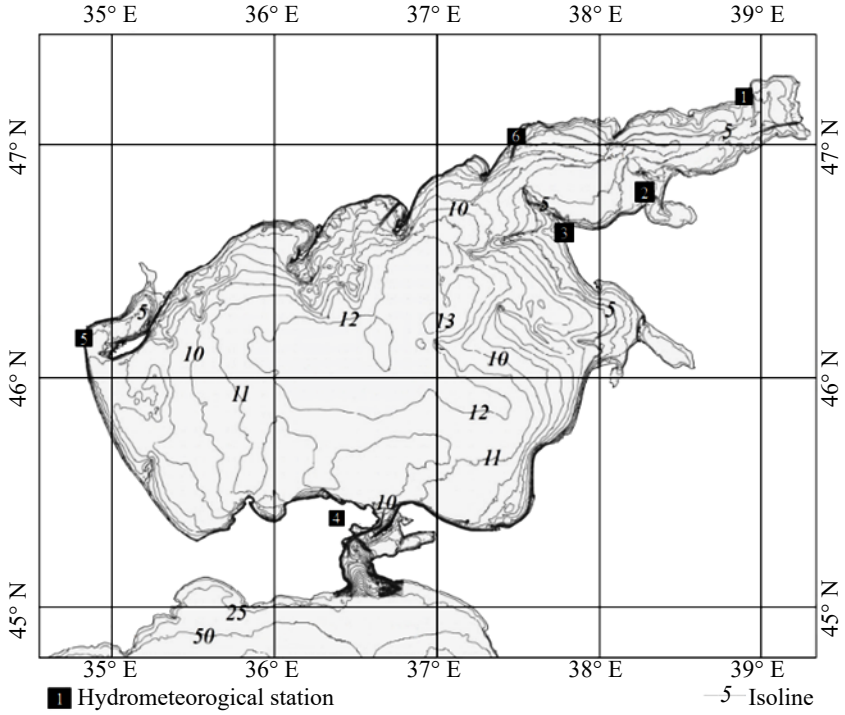

Fig. 1. Bathymetric map of the Azov Sea with indicated hydrometeorological stations: Taganrog (1), Port Yeysk (2), Dolzhanskaya (3), Kerch (4), Genichesk (5), Mariupol (6)

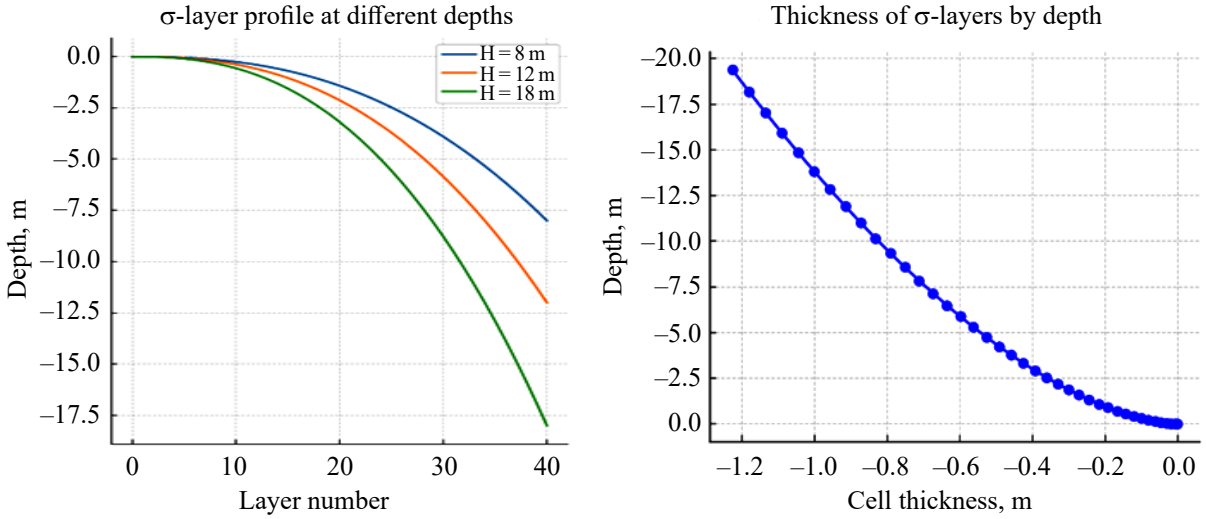

Fig. 2. Profile and thickness of σ-layers at different depths

Initial conditions were set as small sea level perturbations (white noise) to initiate the wave field. Boundary conditions included: a free surface, atmospheric forcing (wind pressure and shear stress), and tidal forcing.

The Courant condition was monitored to assess the correctness of the time step:

$$\mathrm{CFL} = \frac{(|\mathbf{u}|+c)\Delta t}{\Delta x} \le 0.5, \quad c = \sqrt{\frac{g}{k}\tanh(kh)}, \quad \mathrm{CFL} \approx 0.45,$$

where $\mathbf{u}$ is the characteristic current velocity (m/s); Δt is the time step (s); Δx is the grid step (m).

To evaluate the simulation quality, the results were compared against stability criteria and wave characteristics. The Ursell number was calculated as:

$$Ur = \frac{H L^2}{h^3} \approx \frac{7 \times 108^2}{15^3} \approx 24.$$

In the areas of the Taganrog Bay and the Kerch Strait, the values of $Ur > 20$, indicating a nonlinear wave regime (nonlinearity/enhanced crest asymmetry in shallow water) and necessitating the use of LES.

At the open boundary with the Black Sea, wave spectra from SWAN and level fields from WAVEWATCH III were applied. The Don and Kuban rivers were specified as inflow sources with a discharge of $Q = 3000 – 3500$ m³/s. Temperature and salinity were initialized using data from CMEMS (Copernicus Marine Service).

The significant wave height H_s was determined as:

$$H_s = 4\sqrt{m_0}, \; m_0 = \int_0^\infty S(f)df,$$

where $S(f)$ is the wave energy spectral density (m²/Hz).

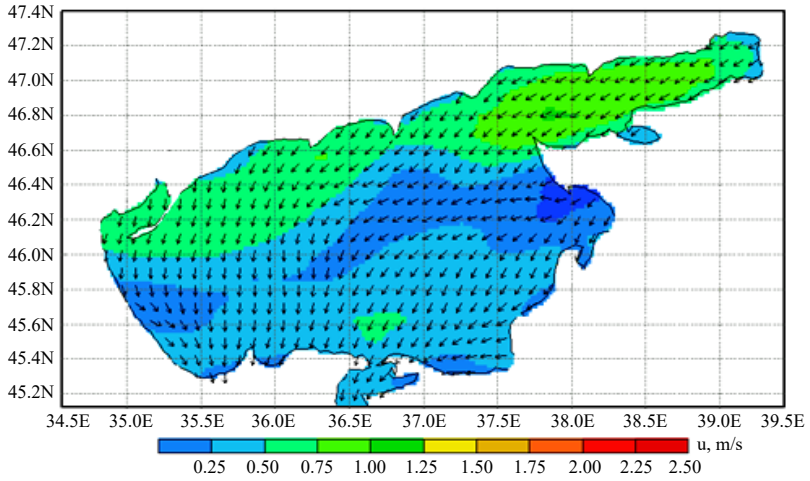

Fig. 3. Wind speed at 10 meters height at the initial model time for Scenario 1, arrows indicate wind direction

Results of the Numerical Experiment:

• **In Scenario 1:** $H_s \approx 1.2–1.6$ m in the center of the sea. The amplitude of water level oscillations reached 0.42 m in the Taganrog Bay. Velocity vectors revealed reciprocating currents with maximum values of 0.35 m/s. The amplitude map clearly identifies the Kerch Strait area as a zone of intensified currents.

• **In Scenario 2:** $H_s \approx 2.8–3.1$ m in the Kerch Strait and $H_s \approx 2.4–2.9$ m near the coast of Taganrog. An intense storm surge phenomenon was observed: the water level at the eastern coast rose by 1.2 m, while at the western coast it fell by 0.8 m.

• **In Scenario 3:** Peak $H_s \approx 3.1–4.0$ m, with extreme surge phenomena up to 1.5 m in the Taganrog Bay. The combination of tide and storm enhanced resonance effects. Maximum current speeds of 1.1 m/s were recorded in the Kerch Strait. Conditions near the shipping channels were close to critical for navigation.

Local effects (refraction and diffraction) were pronounced in the Kerch Strait area, where wave height decreased by 20–30% due to the coastline geometry. The use of LES made it possible to identify local zones of vortex generation in areas with sharp depth changes (Taganrog Bay, estuaries of the Don and Kuban Rivers). These zones are associated with intense sediment resuspension and pollutant transport. During the storm (Scenario 2), large vortices 2–5 km in diameter were identified near the Don River outflow; smaller-scale vortices (0.5–1.0 km), influencing sediment distribution, were observed in the Kerch Strait. Such structures have been previously noted in field measurements, confirming the model's realism. The use of the LES model with the Smagorinsky scheme allowed for the identification of zones of intense turbulent exchange.

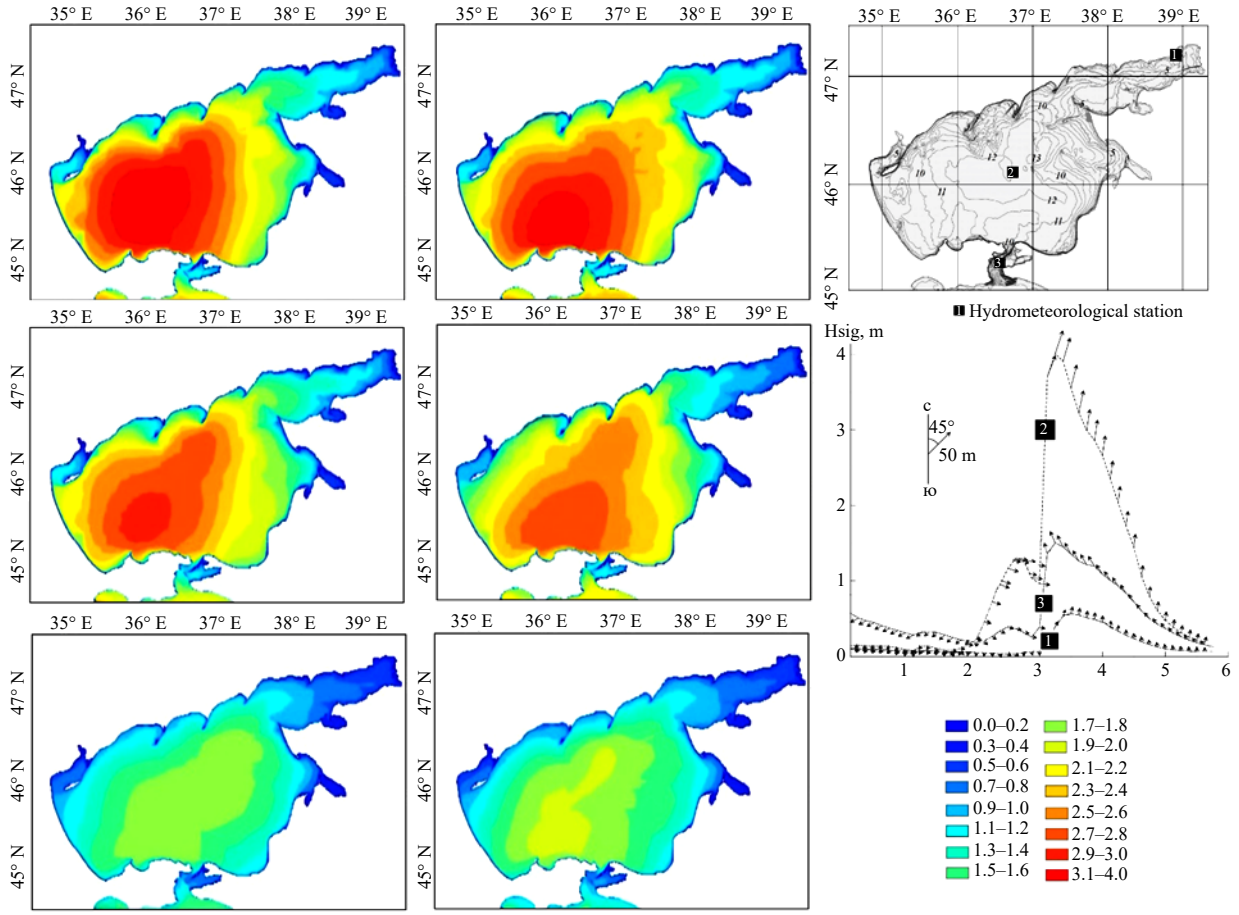

Fig. 4. Maps of significant wave heights and dynamics of wind-wave parameters at three points under different scenarios: Row 1 — Scenario 1; Row 2 — Scenario 2; Row 3 — Scenario 3

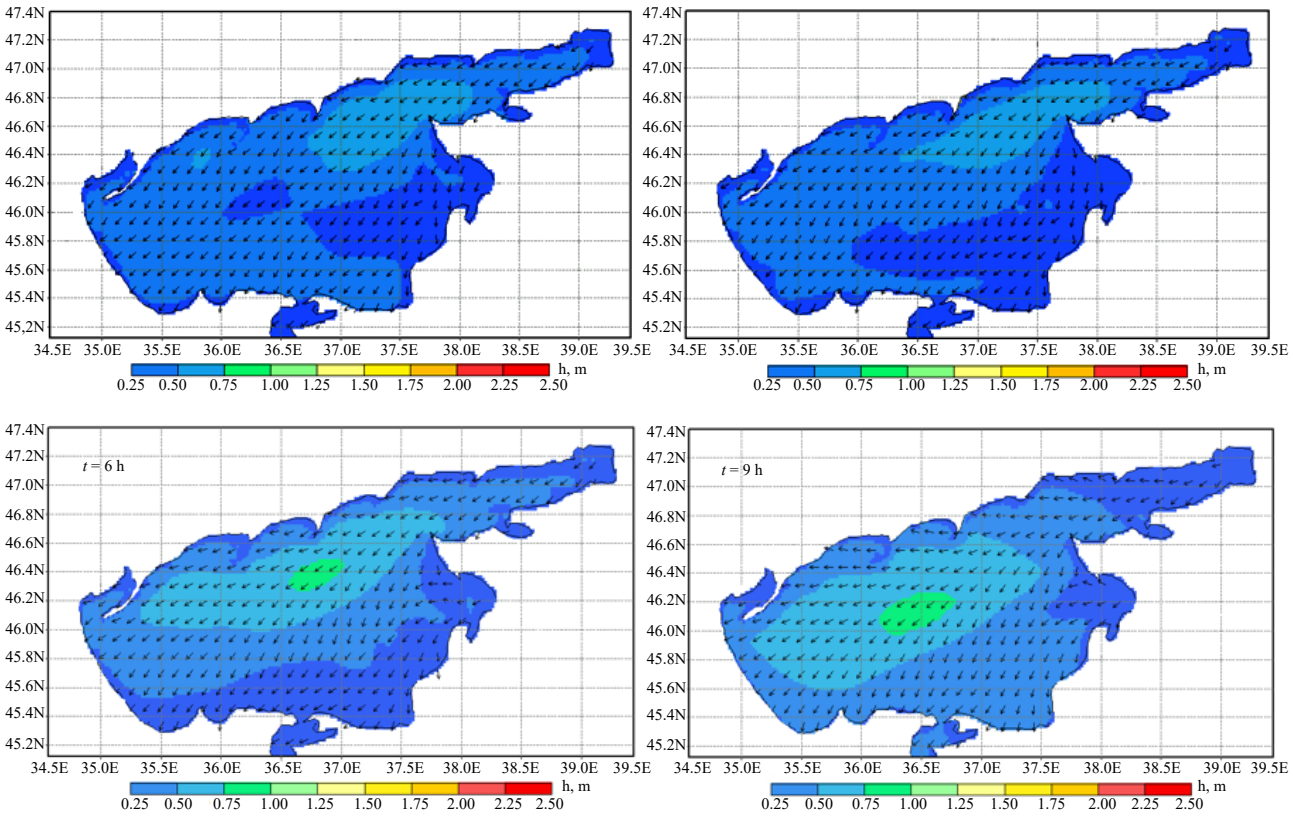

Fig. 5. Simulation results of prevailing wave heights at different time instances: at the initial time, and after 3, 6, and 9 hours for Scenario 1. Arrows indicate the mean wave direction

Forty ensemble runs were generated with perturbed wind fields (±15% in speed, ±10° in direction). The probability of exceeding the critical wave height of H_{cr} = 3.5 m was calculated using the formula:

$$P(H_s > H_{cr}) = \frac{1}{N}\sum_{i=1}^{N} I(H_s^{(i)} > H_{cr}) \approx 0.42.$$

Thus, the probability of extreme impact in the central part of the sea was 42%.

Application of Neural Network Models. The application of neural network models, specifically Physics-Informed Neural Networks (PINNs) and Fourier Neural Operators (FNOs), was investigated. PINNs were employed to approximate local hydrodynamic fields in the Taganrog Bay. The average error, measured by the $L2$ norm, was $e_{L_2} < 4.7\%$. The application of neural network models demonstrated significant improvements in both accuracy and computational efficiency. Fourier Neural Operators (FNOs) accelerated ensemble calculations by a factor of 12 while maintaining the error for key parameters (H_s, η) at a level below 8%.

The implementation of neural network models yielded substantial benefits. The use of Physics-Informed Neural Networks (PINNs) ensured compliance with physical constraints and reduced approximation errors by 35% compared to conventional neural networks. Furthermore, Fourier Neural Operators (FNOs) reduced the computational time for ensemble simulations by an average factor of 12. This significant acceleration makes the proposed methodology viable for operational use in early warning systems.

Risk Maps for Infrastructure Damage. Risk maps for infrastructure damage were developed for the Kerch Strait and the ports of Taganrog and Yeysk, identifying zones of maximum vulnerability.

The shock pressures were estimated (peak estimate on a vertical wall):

$$q_{\text{dyn}} \approx \tfrac{1}{2}\rho U_{\text{rel}}^2, \quad U_{\text{rel}} \approx u_{orbital} + U_{cur}.$$

For the wave crest (deep water approximation):

$$u_{orbital} \approx a\omega \text{ (deep water)},$$
$$a = H / 2 = 3.5 \text{ m},$$
$$\omega = 0.628 \text{ s}^{-1},$$
$$u_{orbital} \approx 2.2 \text{ m/s},$$
$$U_{cur} = 2.5 \text{ m/s},$$
$$U_{rel} \approx 4.7 \text{ m/s},$$
$$q_{dyn} \approx 0.5 \times 1000 \times 4.72 \approx 11000 \text{ Pa}.$$

Considering slamming effects (multiplier of 5–10) $\Rightarrow$ 0.055–0.11 MPa.

The vulnerability maps were generated using the following approach:

$$P(D \geq d|x) = \Phi\left(\frac{\ln x - \mu}{\beta}\right), \quad x \equiv q_{\text{impact}}.$$

Zones with a high probability of damage include the port areas of Taganrog and Yeysk, Port Kavkaz, and coastal protection sections near confined shoreline geometries.

The wave power per unit crest width (deep water) was calculated as:

$$P \approx \frac{\rho g^2}{64\pi} H_s^2 T_e.$$

For H_s = 7 m, $T_e \approx 10$ s, $P \sim 2.3 \times 10^5$ W/m.

Consequently, the highest-risk zones for navigation are concentrated in the Kerch Strait and the central part of the Sea of Azov. Coastal infrastructure in the Taganrog and Yeysk areas is most vulnerable under Scenario C.

Zoning of potential damage areas was performed by integrating the results of hydrodynamic calculations with infrastructure vulnerability curves. Scenario 1 is characterized by localized, non-critical water level rises and moderate waves. Scenario 2 leads to extreme wave conditions hazardous to navigation and coastal infrastructure. Under this scenario, zones with a high probability of damage to port infrastructure in the Taganrog and Yeysk regions are forecasted. For coastal infrastructure (Port of Taganrog, Yeysk), the probability of exceeding the critical pressure on structures in Scenario 2 was 0.65. Scenario 3 demonstrates a cumulative effect: although wave heights are lower, the prolonged storm surge causes flooding in low-lying coastal areas. In Scenario 3, Port Kavkaz and the Kerch Strait transport crossing are also at risk. Thus, extreme consequences can be triggered by both peak-intensity and long-duration events.

To validate the reliability of the potential damage zone assessments, the hydrodynamic modelling results were compared with satellite imagery data processed by the “LBP-neural_network” software package [25–27]. Specifically, the analysis for Scenario 2 (extreme storm) was conducted using images of the Yassenskaya area from March 17 and 22, 2023 [28], presented in Fig. 6. The imagery clearly demonstrates significant changes in the shoreline and inundation areas caused by the storm impact.

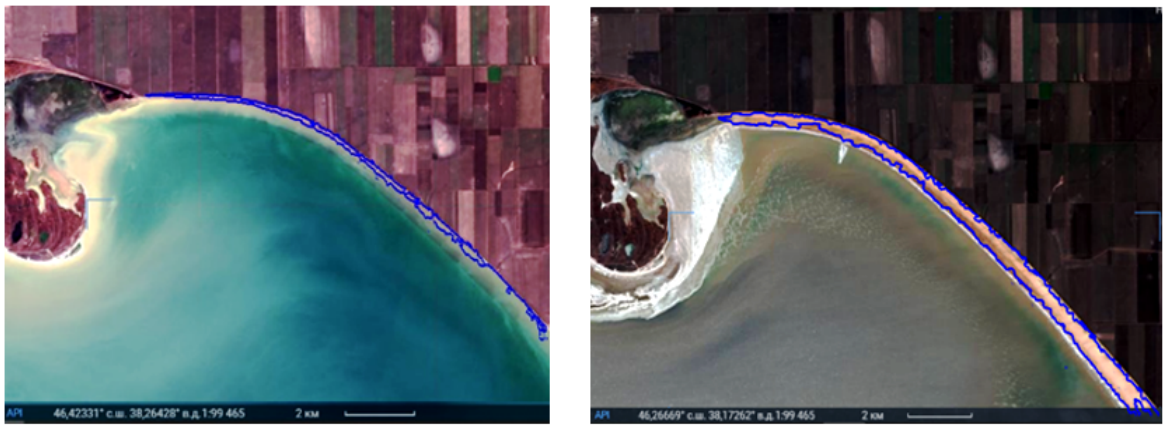

Fig. 6. Satellite imagery of the study area — Yassenskaya station:
a — March 17, 2023; *b* — March 22, 2023

The "LBP-neural_network" software package enabled high-precision delineation of the actual shoreline and inundated areas, facilitating a quantitative comparison with the model-predicted impact zones. It was established that the simulated boundaries of inundation zones and shoreline dynamics show satisfactory agreement with the contours identified from the satellite data.

Furthermore, the distributions of wave fields and currents obtained from the model demonstrated good convergence with independent satellite measurements (Sentinel-1, Sentinel-3, Copernicus Marine Service). A quantitative assessment of the discrepancies revealed that the root mean square error for key parameters (such as significant wave height and surface current velocity) did not exceed 8–10%, confirming the adequacy and accuracy of the applied hydrodynamic model.

Thus, the following key results were obtained.

For the extreme storm scenario, the significant wave height in the central part of the Azov Sea reached 5.2 m, which is comparable to the catastrophic events of 2012 and 2021. In the strait, wave steepness increases locally due to the compression of wave fronts. The calculated current velocities in the strait reached 2.5–3.0 m/s; the Froude number $Fr = U / \sqrt{gh} \approx 0.21$ indicates significant inertial forces but without critical supercritical flow conditions.

The probability of exceeding the hazardous wave height threshold of H_{cr} = 4.5 m was 42%, the probability of $H_s > 5$ m in the central Sea of Azov reached approximately 0.78, in the coastal zone reached approximately 0.28. Calculated shock pressures on coastal infrastructure, accounting for wave slamming, ranged from 0.055 to 0.11 MPa. The simulation of vessel dynamics confirmed the development of resonance phenomena, presenting a tangible risk of capsizing. The application of Physics-Informed Neural Networks (PINNs) and Fourier Neural Operators (FNOs) validated the efficacy of the hybrid approach, achieving high accuracy alongside a twelve-fold acceleration in computation speed.

In conclusion, the developed model accurately reproduces storm processes in the Sea of Azov. The most hazardous conditions for vessels arise under Scenario 2 (strong easterly storm) and Scenario 3 (anomalous cyclone). A scenario of combined forcing proves to be the most dangerous and must be incorporated into early warning systems. The probability of critical wave heights exceeds 60% under extreme conditions. Risk maps for navigation and infrastructure, generated from ensemble forecasts, identify the Taganrog Bay and the Kerch Strait as the most vulnerable zones.

The numerical experiments demonstrate the effectiveness of the proposed methodology. The integration of Large Eddy Simulation (LES), ensemble forecasting, and risk assessment techniques enables not only the description of storm dynamics but also the quantitative evaluation of consequences for navigation and coastal infrastructure. In contrast to traditional spectral models (e. g., SWAN, WAVEWATCH III), the present approach offers distinct advantages:

• It accounts for nonlinear wave-current interactions in shallow waters.

• It employs a hybrid ensemble method leveraging neural network surrogates (PINNs, FNOs), accelerating forecasts by a factor of 10–15 without significant loss of accuracy.

• It facilitates direct risk assessment for vessels and infrastructure, rather than just hydrodynamic evaluation.

The results obtained can be directly utilized to generate operational risk maps for flooding and vessel damage, providing a critical tool for maritime safety and coastal zone management.

Discussion. The results of the numerical experiments confirm the high efficacy of the proposed multi-level methodology for modelling extreme storm events in the Azov Sea and the Kerch Strait. The application of LES with the Smagorinsky closure successfully reproduced wave breaking processes and the generation of turbulent vortices, phenomena that are traditionally inadequately represented in spectral models [15]. Unlike approaches limited to averaged parameters (e. g., SWAN), the use of a CFD framework enabled the incorporation of nonlinear effects and local wave-current interactions.

Comparison with ERA5 reanalysis data and Sentinel-3 satellite observations showed satisfactory agreement for significant wave height fields and sea level distribution [22]. It is particularly important that the model accurately reproduced extreme values during the March 2023 storm, when wind speeds reached 30–35 m/s.

The integration of artificial intelligence methods (PINNs and FNOs) demonstrated the promise of hybrid schemes: PINNs ensure physical consistency of the results, while FNOs enable a significant acceleration of ensemble calculations [18−19]. This approach opens the possibility for developing operational early warning systems for storm risks, where computational speed is paramount.

The limitations of the study are primarily associated with the spatial resolution of ERA5 (≈30 km), which leads to an underrepresentation of small-scale processes, as well as the scarcity of verification data in the central part of the Sea of Azov. Additional data assimilation from satellite altimeters and coastal stations could enhance forecast accuracy.

From a practical standpoint, the results underscore the importance of an integrated approach to navigational risk assessment. Incorporating "ship-wave" dynamics allowed for the identification of dangerous resonance regimes, which is particularly critical for small vessels in the Kerch Strait [17]. The resulting risk maps can be directly integrated into decision-support systems for shipping companies and coastal infrastructure management.

In conclusion, the presented methodology combines physical rigor, computational efficiency, and practical relevance. Future work will focus on enhancing the approach by increasing the resolution of CFD models and integrating Copernicus Marine Service data in real-time mode.

Conclusion. This study has demonstrated the efficacy of a hybrid approach, integrating numerical methods and state-of-the-art machine learning algorithms, for modelling extreme hydrodynamic processes in the Sea of Azov. In contrast to classical models, the proposed methodology enables not only the reproduction of water level and wave field dynamics but also the high-accuracy assessment of the spatial distribution of risks to coastal infrastructure.

The novelty of this work lies in the integration of Physics-Informed Neural Networks (PINNs) and Fourier Neural Operators (FNOs) into a forecasting system for a specific regional basin, a feat not previously accomplished for the Sea of Azov. The obtained results open promising prospects for the further development of operational monitoring systems, the adaptation of these models to the Black Sea, and their application in sustainable environmental management tasks.

References

1. Amarouche K., Akpinar A., Rybalko A., Myslenkov S.A. Assessment of SWAN and WAVEWATCH-III models regarding the directional wave spectra estimates based on Eastern Black Sea measurements. *Ocean Engineering*. 2023;272:113944. https://doi.org/10.1016/j.oceaneng.2023.113944

2. Reduan Atan R., Nash S., Goggins J. Development of a nested local scale wave model for a 1/4 scale wave energy test site using SWAN. *Journal of Operational Oceanography*. 2017;10:59–78. https://doi.org/10.1080/1755876X.2016.1275495

3. Masselink G., Russell P., Rennie A., Brooks S., Spencer T. Impacts of climate change on coastal geomorphology and coastal erosion relevant to the coastal and marine environment around the UK. *MCCIP Science Review*. 2020;158–189. https://doi.org/10.14465/2020.arc08.cgm

4. Yaitskaya N. The Wave Climate of the Sea of Azov. *Water.* 2022;14(4):555. https://doi.org/10.3390/w14040555

5. Veldman A., Luppes R., Bunnik T., Huijsmans R., Duz B., Iwanowski B., Wemmenhove R., Borsboom M., Wellens P., van der Heiden H., Plas P. Extreme Wave Impact on Offshore Platforms and Coastal Constructions. In: *Proceedings of the International Conference on Offshore Mechanics and Arctic Engineering (OMAE)*. Rotterdam, Netherlands, 2011;7. https://doi.org/10.1115/OMAE2011-49488

6. Elmisaoui S., Kissami I., Ghidaglia J.-M. High-Performance Computing to Accelerate Large-Scale Computational Fluid Dynamics Simulations: A Comprehensive Study. In: *Lecture Notes in Computer Science*. 2024. https://doi.org/10.1007/978-3-031-54318-0_31

7. Dietterich H., Lev E., Chen J., Richardson J., Cashman K. Benchmarking computational fluid dynamics models of lava flow simulation for hazard assessment, forecasting, and risk management. *Journal of Applied Volcanology.* 2017;6:9.

8. International Maritime Organization (IMO). Second Generation Intact Stability Criteria. *IMO Guidelines.* 2023. London, UK. URL: https://www.imo.org (дата обращения: 03.09.2025).

9. Chu Van T., Ramirez J., Rainey T., Ristovski Z., Brown R. Global impacts of recent IMO regulations on marine fuel oil refining processes and ship emissions. *Transportation Research Part D: Transport and Environment*. 2019;70:123–134.

10. You J., Faltinsen O.M. A numerical investigation of second-order difference-frequency forces and motions of a moored ship in shallow water. *Journal of Ocean Engineering and Marine Energy*. 2015;1:157–179. https://doi.org/10.1007/s40722-015-0014-6

11. Protsenko E.A., Panasenko N.D., Protsenko S.V. Mathematical Modelling of Catastrophic Surge and Seiche Events in the Azov Sea Using Remote Sensing Data. *Computational Mathematics and Information Technologies*. 2024;8(2):33–44. (In Russ.) https://doi.org/10.23947/2587-8999-2024-8-2-33-44

12. Sukhinov A., Protsenko E., Protsenko S., Panasenko N. Wind Wave Dynamic's Analysis Based on 3D Wave Hydrodynamics and SWAN Models Using Remote Sensing Data. In: *Fundamental and Applied Scientific Research in the Development of Agriculture in the Far East (AFE-2022)*. Zokirjon ugli K.S., Muratov A., Ignateva S. (eds). Springer, Cham, Switzerland. Lecture Notes in Networks and Systems. 2023;733:1–12. https://doi.org/10.1007/978-3-031-37978-9_39

13. Kantamaneni K. Coastal infrastructure vulnerability: an integrated assessment model. *Natural Hazards*. 2016;84:139–154. https://doi.org/10.1007/s11069-016-2413-y

14. Protsenko E.A., Protsenko S.V., Sidoryakina V.V. Predictive Mathematical Modeling of Sedimentation and Coastal Abrasion Relief Transformation Processes. *Journal of Mathematical Sciences*. 2024;284:126–139. https://doi.org/10.1007/s10958-024-07331-6

15. Meyers J., Sagaut P. On the model coefficients for the standard and the variational multi-scale Smagorinsky model. *Journal of Fluid Mechanics*. 2006;569:287–319. https://doi.org/10.1017/S0022112006002850

16. Janssen P.A.E.M. Quasi-linear Theory of Wind-Wave Generation Applied to Wave Forecasting. *Journal of Physical Oceanography.* 1991;21(11):1631–1642. https://doi.org/10.1175/1520-0485(1991)021<1631:QLTOWW>2.0.CO;2

17. Faltinsen O.M. *Sea Loads on Ships and Offshore Structures*. 1st ed. Cambridge University Press: Cambridge, UK; 1990. Pp. 1–5.

18. Raissi M., Perdikaris P., Karniadakis G.E. Physics-informed neural networks: A deep learning framework for solving forward and inverse problems involving nonlinear partial differential equations. *Journal of Computational Physics.* 2019;378:686–707. https://doi.org/10.1016/j.jcp.2018.10.045

19. Luo Y., Li Y., Sharma P., Shou W., Wu K., Foshey M. et al. Learning human–environment interactions using conformal tactile textiles. *Nat Electron*. 2021;4:193–201. https://doi.org/10.1038/s41928-021-00558-0

20. Sukhinov A.I., Protsenko S.V., Panasenko N.D. Mathematical modeling and ecological design of marine systems taking into account multi-scale turbulence using remote sensing data. *Computational Mathematics and Information Technologies*. 2022;6(3):104–113. (In Russ.) https://doi.org/10.23947/2587-8999-2022-6-3-104-113

21. Myslenkov S.A., Arkhipkin V.S. Recurrence of Storm Waves in the Sea of Azov according to Modeling. *Russian Meteorology and Hydrology*. 2024;49:1061–1066. https://doi.org/10.3103/S1068373924120045

22. *The official website of The Copernicus Climate Change Service (C3S)*. URL: https://climate.copernicus.eu/ (accessed: 12.09.2025).

23. *The official website of International Hydrographic Organization*. URL: https://iho.int/ (accessed: 12.09.2025).

24. Protsenko E.A., Sukhinov A.I., Protsenko S.V. Numerical Modeling of Hydrodynamic Wave Processes in the Azov Sea Based on the WAVEWATCH III Wind-Wave Model. *Computational Mechanics of Continuous Media*. 2025;17(4):422–431. (In Russ.) https://doi.org/10.23947/2587-8999-2025-17-4-422-431

25. Sukhinov A.A., Ostrobrod G.B. Efficient face detection on Epiphany multicore processor. *Computational Mathematics and Information Technologies*. 2017;1(1):1–15. (In Russ.) https://doi.org/10.23947/2587-8999-2017-1-1-1-15

26. Sukhinov A., Panasenko N., Simorin A. Algorithms and programs based on neural networks and local binary patterns approaches for monitoring plankton populations in sea systems. *E3S Web of Conferences*. 2022;363:02027.

27. Panasenko N.D. Forecasting the coastal systems state using mathematical modeling based on satellite images. *Computational Mathematics and Information Technologies*. 2023;7(4):54–65. (In Russ.) https://doi.org/10.23947/2587-8999-2023-7-4-54-6

28. *The official website of Earth Observing System*. URL: https://eos.com/landviewer/account/pricing (accessed: 12.09.2025).

About the Authors:

Alexander I. Sukhinov, Corresponding Member of the Russian Academy of Sciences, Doctor of Physical and Mathematical Sciences, Professor, Director of the Research Institute of Mathematical Modeling and Forecasting of Complex Systems, Don State Technical University (1, Gagarin Sq., Rostov-on-Don, 344003, Russian Federation), ORCID, SPIN-code, ScopusID, ResearcherID, MathSciNet, sukhinov@gmail.com

Sofia V. Protsenko, Candidate of Physical and Mathematical Sciences, Associate Professor of the Department of Mathematics, Research Fellow, A.P. Chekhov Taganrog Institute (branch) Rostov State University of Economics (48, Initiative St., Taganrog, 347936, Russian Federation), ORCID, SPIN-code, rab5555@rambler.ru

Elena A. Protsenko, Candidate of Physical and Mathematical Sciences, Associate Professor of the Department of Mathematics, Leading Research Fellow, A.P. Chekhov Taganrog Institute (branch) Rostov State University of Economics (48, Initiative St., Taganrog, 347936, Russian Federation), ORCID, SPIN-code, eapros@rambler.ru

Natalia D. Panasenko, Candidate of Technical Sciences, Associate Professor of the Department of Mathematics and Computer Science, Associate Professor of the Department of Information Security in Computing Systems and Networks, Don State Technical University (1 Gagarin Sq., Rostov-on-Don, 344003, Russian Federation), ORCID, SPIN-code, ScopusID, ResearcherID, natalija93_93@mail.ru

Contributions of the authors:

A.I. Sukhinov: general scientific supervision; problem statement; formulation of research ideas, goals and objectives; development of methodology.

S.V. Protsenko: concept development; scientific guidance.

E.A. Protsenko: data management; annotation, data cleaning, and maintaining data integrity; software development; visualization.

N.D. Panasenko: validation; testing of existing components.

Conflict of Interest Statement: **the authors declare no conflict of interest.**

All authors have read and approved the final manuscript.

Об авторах:

Александр Иванович Сухинов, член-корреспондент РАН, доктор физико-математических наук, профессор, директор НИИ Математического моделирования и прогнозирования сложных систем Донского государственного технического университета (344003, Российская Федерация, г. Ростов-на-Дону, пл. Гагарина, 1), ORCID, SPIN-код, ScopusID, ResearcherID, MathSciNet, sukhinov@gmail.com

Софья Владимировна Проценко, кандидат физико-математических наук, доцент кафедры математики, научный сотрудник Таганрогского института им. А.П. Чехова (филиал) Ростовского государственного экономического университета (347936, Российская Федерация, г. Таганрог, ул. Инициативная, 48), ORCID, SPIN-код, rab5555@rambler.ru

Елена Анатольевна Проценко, кандидат физико-математических наук, доцент кафедры математики, ведущий научный сотрудник Таганрогского института им. А.П. Чехова (филиал) Ростовского государственного экономического университета (347936, Российская Федерация, г. Таганрог, ул. Инициативная, 48), ORCID, SPIN-код, eapros@rambler.ru

Наталья Дмитриевна Панасенко, кандидат технических наук, доцент кафедры «Математика и информатика», доцент кафедры «Информационная безопасность в вычислительных системах и сетях» Донской государственный технический университет (344003, Российская Федерация, г. Ростов-на-Дону, пл. Гагарина, 1), ORCID, SPIN-код, ScopusID, ResearcherID, natalija93_93@mail.ru

Заявленный вклад авторов:

А.И. Сухинов: общее научное руководство; постановка задачи; формулировка идей исследования, целей и задач; разработка методологии.

С.В. Проценко: разработка концепции; научное руководство.

Е.А. Проценко: курирование данных; деятельность по аннотированию, очистке данных и поддержанию их целостности; разработка программного обеспечения; визуализация.

Н.Д. Панасенко: валидация; тестирование существующих компонентов.

Конфликт интересов: **авторы заявляют об отсутствии конфликта интересов.**

Все авторы прочитали и одобрили окончательный вариант рукописи.

Received / Поступила в редакцию 01.10.2025
Reviewed / Поступила после рецензирования 22.10.2025
Accepted / Принята к публикации 17.11.2025

MATHEMATICAL MODELLING
МАТЕМАТИЧЕСКОЕ МОДЕЛИРОВАНИЕ

UDC 519.6

Original Empirical Research

https://doi.org/10.23947/2587-8999-2025-9-4-22-37

Unsteady Model of Blood Coagulation in Aneurysms of Blood Vessels

Natalya K. Volosova[1], Konstantin A. Volosov[2], Aleksandra K. Volosova[2], Mikhail I. Karlov[3], Dmitriy F. Pastukhov[4] ✉, Yuriy F. Pastukhov[4]

[1] MGTU named after. N.E. Bauman, Moscow, Russian Federation

[2] Russian University of Transport, Moscow, Russian Federation

[3] Moscow Institute of Physics and Technology (National Research University), Dolgoprudny, Russian Federation

[4] Polotsk State University named after Euphrosyne of Polotsk, Novopolotsk, Republic of Belarus

✉ dmitrij.pastuhov@mail.ru

Abstract

Introduction. A two-dimensional hydrodynamic problem is numerically solved in the "stream function-vorticity" formulation for an open rectangular cavity simulating blood flow and its coagulation within a vascular aneurysm. The model accounts for a simplified nonlinear mathematical description of the first phase of blood coagulation (30 seconds).

Materials and Methods. To accelerate the numerical solution of the unsteady problem with an explicit finite-difference scheme for the vorticity dynamics equation, an n-fold splitting method of the explicit scheme ($n = 100, 200$) was employed, along with the use of a symmetry plane in the rectangular aneurysm domain. The splitting method was also applied to solve the dynamic system of advection–diffusion equations with nonlinear source terms for the activator and inhibitor blood factors ($N = 70$). The maximum time step τ_0 was synchronized across both splitting cycles. The computation was performed on half of the rectangular aneurysm using a uniform 100×50 grid with equal spacing $h_1 = h_2 = 0.01$. The inverse matrix required for solving the Poisson equation in the "stream function-vorticity" formulation with a finite number of elementary operations was computed using the Msimsl library.

Results. The numerical solution demonstrated that, in arterioles (Re = 3.6), advection and diffusion of fibrin occur according to the nonlinear dynamics of activator and inhibitor factors, as if fibrin were moving counter to the blood flow. The maximum fibrin density forms in the central region of the vessel in the shape of a "fibrin horseshoe". For higher Reynolds numbers (Re = 3000) corresponding to arteries, fibrin motion occurs along the main flow, and the central part of the vessel is separated from the aneurysm by a "fibrin foot" along its geometric boundary. In arterioles, a layered fibrin growth effect was also observed, with periodic variations in fibrin density near the aneurysm wall, consistent with other authors' findings. In arteries, the fibrin film within the aneurysm forms in approximately one second—significantly shorter than the first coagulation phase (30 seconds).

Discussion. The finite-difference approximation achieves sixth-order accuracy at interior nodes and fourth-order accuracy at boundary nodes. The model was applied to simulate blood flow in arterial aneurysms at high Reynolds numbers (Re = 3000) and in arteriole aneurysms (Re = 3.6). The dimensionless range of fibrin density variation is consistent with data reported by other researchers.

Conclusions. The study proposes a system of equations representing a simplified unsteady model of blood motion and fibrin (thrombus) formation in vascular aneurysms. The proposed model provides a qualitative understanding of thrombus formation mechanisms in aneurysms of arteries and arterioles, as well as in elements of medical equipment.

Keywords: hydrodynamics, numerical methods, partial differential equations, initial-boundary value problem, mathematical modeling, aneurysm

For Citation. Volosova N.K., Volosov K.A., Volosova A.K., Karlov M.I., Pastukhov D.F., Pastukhov Yu.F. Unsteady Model of Blood Coagulation in Aneurysms of Blood Vessels. *Computation Mathematics and Information Technologies*. 2025;9(4):22–37. https://doi.org/10.23947/2587-8999-2025-9-4-22-37

Оригинальное эмпирическое исследование

Нестационарная модель свертывания крови в аневризмах кровеносных сосудов

Н.К. Волосова[1], К.А. Волосов[2], А.К. Волосова[2], М.И. Карлов[3], Д.Ф. Пастухов[4] ✉, Ю.Ф. Пастухов[4]

[1] Московский государственный технический университет им. Н.Э. Баумана, г. Москва, Российская Федерация

[2] Российский университет транспорта, г. Москва, Российская Федерация

[3] Московский физико-технический институт (национальный исследовательский университет), г. Долгопрудный, Российская Федерация

[4] Полоцкий государственный университет им. Евфросинии Полоцкой, г. Новополоцк, Республика Беларусь

✉ dmitrij.pastuhov@mail.ru

Аннотация

Введение. Численно решается двумерная гидродинамическая задача в переменных «функция тока — вихрь» в открытой прямоугольной каверне, моделирующей течение крови и ее свертывание в аневризме кровеносного сосуда с учетом простейшей нелинейной математической модели за время первой фазы свертывания (30 секунд).

Материалы и методы. Для ускорения численного решения нестационарной задачи с явной разностной схемой уравнения динамики вихря использовался метод n-кратного расщепления явной разностной схемы (n = 100, 200) и наличие плоскости симметрии прямоугольной области каверны — аневризмы. Метод расщепления также применялся для решения динамической системы уравнений адвекции-диффузии с нелинейной правой частью для факторов крови активатора и ингибитора (N = 70). В двух методах согласовался максимальный шаг времени τ_0 в циклах расщепления. На половине прямоугольной аневризмы рассматривались симметричные решения и применялась равномерная сетка 100×50 с равным шагом $h_1 = h_2 = 0{,}01$. Обратная матрица для решения уравнения Пуассона в переменных «функция тока — вихрь» за конечное число элементарных операций вычислялась библиотекой Msimsl.

Результаты исследования. Численное решение задачи показало, что в артериолах (Re = 3,6) происходит адвекция и диффузия фибрина с учетом нелинейной правой части системы уравнений динамики для активатора и ингибитора так, как если бы фибрин двигался навстречу крови. Максимальная плотность фибрина реализуется в средней части сосуда в форме «фибриновой подковы». Решение задачи при больших числах Рейнольдса (Re = 3000) в артериях эквивалентно движению фибрина вдоль потока, при этом центральная часть кровеносного сосуда отделена от аневризмы по ее геометрической границе «фибриновой ножкой». В артериолах обнаружен также эффект слоеного роста фибрина с периодическим изменением плотности у стенки аневризмы, как и у авторов других работ. Решение задачи в артерии показало, что фибриновая пленка в аневризме при быстром движении крови образуется за время порядка одной секунды, что много меньше, чем первая фаза свертывания (30 секунд).

Обсуждение. Аппроксимация уравнений имеет шестой порядок погрешности во внутренних узлах и четвертый в граничных узлах. Задача решена для движения крови в аневризмах артерий при больших числах Рейнольдса (Re = 3000) и для течения крови в аневризмах артериол (Re = 3,6). Безразмерный диапазон изменения плотности фибрина вкладывается в аналогичный диапазон в работах других авторов.

Заключение. В работе предложены системы уравнений, представляющие собой простейшую нестационарную модель движения крови и образования фибрина (тромба) в аневризмах кровеносных сосудов. Предложенная модель поможет качественно выяснить причины образования тромбов в аневризмах артерий и артериол, а также в элементах медицинского оборудования.

Ключевые слова: гидродинамика, численные методы, уравнения в частных производных, начально-краевая задача, математическое моделирование, аневризма

Для цитирования. Волосова Н.К., Волосов К.А., Волосова А.К., Карлов М.И., Пастухов Д.Ф., Пастухов Ю.Ф. Нестационарная модель свертывания крови в аневризмах кровеносных сосудов. *Computational Mathematics and Information Technologies*. 2025;9(4):22–37. https://doi.org/10.23947/2587-8999-2025-9-4-22-37

Introduction. This study, which continues the research presented in [1], for the first time models a two-dimensional hydrodynamic problem of blood motion and coagulation in an open rectangular aneurysm-cavity using the “stream function — vorticity” formulation. In [2], a system of two dynamic partial differential equations describing the diffusion of coagulation factors-activator and inhibitor — was first derived, with nonlinear source terms accounting for the local interaction between these factors. In [3], several mathematical models of blood coagulation without advection were compared, and the dimensional coefficients in the governing equations were refined.

The dynamics of blood formation and its relation to cardiac pulsations at low Reynolds numbers were investigated in [4]. In [5], blood motion in an arteriole was studied using the Russian computational platform FlowVision, incorporating intermediate components of chemical reactions and accounting for variations in both the solid boundary of the vessel and the thrombus interface. It was shown that small thrombi form near an internal cut within a straight vessel and exhibit a fractal structure. Studies [6–11] focus on two-dimensional hydrodynamic problems whose properties are similar to those of the present hydrodynamic system.

The present work, firstly, introduces an unsteady mathematical model of blood coagulation within a vascular aneurysm for both an arteriole (Re = 3.6) and an artery under turbulent conditions (Re = 3000). Secondly, the developed computational algorithm incorporates the periodic mixing of blood within the aneurysm caused by each pulsation wave.

Materials and Methods

Problem Statement. We consider a two-dimensional problem of blood flow and coagulation in a rectangular aneurysm–cavity formed on the wall of a blood vessel. The aneurysm represents a section of the vessel whose diameter $2d$ is typically twice that of the main vessel. Let L denote the aneurysm length, $2H$ its diameter, and H the half-width of the aneurysm (Fig. 1 illustrates half of the symmetric model). The variable d represents the half-width of the parent vessel. The origin of the coordinate system is placed at the lower left corner of the computational domain.

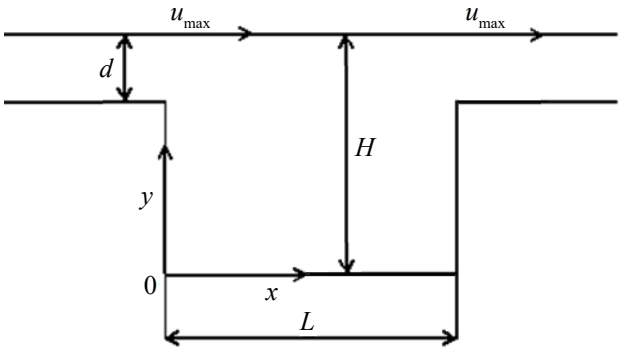

Fig. 1. Geometry of the computational domain for the numerical solution

The dynamic part of the problem describing blood motion in aneurysms of arterioles (Re = 1.8) and arteries (Re = 1500) was numerically solved in [1]. That study obtained the streamline patterns of fluid (blood) particles inside the aneurysm. The formulation of the hydrodynamic problem in [1] in dimensionless variables has the following form:

$$\begin{cases} \bar{\psi}_{\bar{x}\bar{x}} + \bar{\psi}_{\bar{y}\bar{y}} = -\bar{w}(\bar{x},\bar{y}),\ 0 < \bar{x} = \dfrac{x}{L} < 1,\ \ 0 < \bar{y} < k_{\max}, \\ \bar{w} = \bar{v}_{\bar{x}} - \bar{u}_{\bar{y}}, \\ \bar{u} = \bar{\psi}_{\bar{y}}; \bar{v} = -\bar{\psi}_{\bar{x}}, \\ \bar{w}_{\bar{t}} + \bar{u}\cdot\bar{w}_{\bar{x}} + \bar{v}\cdot\bar{w}_{\bar{y}} = \dfrac{1}{\mathrm{Re}}\left(\bar{w}_{\bar{x}\bar{x}} + \bar{w}_{\bar{y}\bar{y}}\right), 0 < \bar{t} = \dfrac{t}{T}, \\ \bar{\psi}\big|_{\Gamma 1} \equiv 0, \bar{v}\big|_{\Gamma} \equiv 0, \bar{u}\big|_{\Gamma_1} = 0, \bar{v}\big|_{\Gamma_2} = 0, \\ \psi(0,y) = \psi(L,y) = \begin{cases} 0, y \in [0, H-\Delta], \\ u_{\max} L\left(\dfrac{y}{L} + \dfrac{2}{3}\dfrac{\Delta}{L} - \dfrac{H}{L} - \dfrac{\left(y/L - H/L\right)^3}{3\left(\Delta/L\right)^2}\right), y \in [H-\Delta, H], \\ \dfrac{2}{3}u_{\max}\Delta, y = H. \end{cases} \end{cases} \quad (1)$$

As in [1], the following characteristic scales are used in this study: length — L, time — $\dfrac{L}{u_{\max}}$, velocity — $u_{\max}$, stream function — $Lu_{\max}$, vorticity — $\dfrac{u_{\max}}{L}$, and Reynolds number — Re. Let us introduce the dimensionless variables: $\bar{x}$ — horizontal coordinate, $\bar{y}$ — vertical coordinate, $\bar{\psi}$, $\bar{w}$ — stream function and vorticity, respectively, $(\bar{u}, \bar{v})$ — velocity vector, $\bar{t}$ — time. They are defined by the relations:

$$0 \le \bar{x} = \frac{x}{L} \le 1,\ \ 0 \le \bar{y} = \frac{y}{L} \le k = \frac{H}{L}, \bar{\psi} = \frac{\psi}{\psi_{\max}}, \psi_{\max} = Lu_{\max},$$

$$\bar{u}=\frac{u}{u_{\max}},\bar{v}=\frac{v}{u_{\max}}\bar{w}=\frac{w}{w_{\max}},w_{\max}=\frac{u_{\max}}{L},$$
$$\bar{t}=\frac{t}{T},T=\frac{L}{u_{\max}},\mathrm{Re}=\frac{u_{\max}L}{\nu}.$$

The kinematic viscosity of blood is taken as $\nu=\frac{\mu}{\rho}=\frac{3.5\cdot10^{-3}\,\mathrm{Pa\cdot s}}{1050\ \mathrm{kg/m^3}}=3.33(3)\cdot10^{-6}\,\frac{\mathrm{m}^2}{\mathrm{s}}$.

In system (1), the first equation represents the Poisson equation in the "stream function–vorticity" formulation, approximated with sixth-order accuracy according to [12] and [1]:

$$\Delta\psi=\psi_{xx}+\psi_{yy}=f(x,y)=-w\Leftrightarrow\frac{1}{h^2}\left(-\frac{10}{3}\psi_{0,0}+\frac{2}{3}\left(\psi_{-1,0}+\psi_{0,-1}+\psi_{1,0}+\psi_{0,1}\right)+\frac{1}{6}\left(\psi_{-1,-1}+\psi_{1,-1}+\psi_{-1,1}+\psi_{1,1}\right)\right)=$$
$$=f+\frac{h^2}{12}\left(f_{xx}+f_{yy}\right)+\frac{h^4}{360}\left(f_x^{(4)}+f_y^{(4)}\right)+\frac{h^4f_{xxyy}^{(4)}}{90}+O\left(h^6\right)=-\left(w+\frac{h^2}{12}\left(w_{xx}+w_{yy}\right)+\frac{h^4}{360}\left(w_x^{(4)}+w_y^{(4)}\right)+\frac{h^4w_{xxyy}^{(4)}}{90}\right)+O\left(h^6\right). \quad (2)$$

The partial derivatives in formula (2) were also approximated in [1]. Finite-difference expressions were obtained for the interior nodes of the function f with indices $n=\overline{2,n_1-2},m=\overline{2,n_2-2}$:

$$\begin{cases}f_{xx}+f_{yy}=\frac{1}{h^2}\left(-5f_{0,0}+\frac{4}{3}\left(f_{-1,0}+f_{0,-1}+f_{1,0}+f_{0,1}\right)-\frac{1}{12}\left(f_{-2,0}+f_{0,-2}+f_{2,0}+f_{0,2}\right)\right)+O\left(h^4\right),\\ f_x^{(4)}+f_y^{(4)}=\frac{1}{h^4}\left(12f_{0,0}-4\left(f_{-1,0}+f_{0,-1}+f_{1,0}+f_{0,1}\right)+f_{-2,0}+f_{0,-2}+f_{2,0}+f_{0,2}\right)+O\left(h^2\right),\\ f_{xxyy}^{(4)}=\frac{1}{h^4}\left(4f_{0,0}-2\left(f_{-1,0}+f_{0,-1}+f_{1,0}+f_{0,1}\right)+f_{-1,-1}+f_{-1,1}+f_{1,-1}+f_{1,1}\right)+O\left(h^2\right).\end{cases} \quad (3)$$

The combined algorithm for solving system (1) together with system (12) consists of 11 computational steps. It requires the specification of initial conditions for the following variables: the stream function field, velocity field, vorticity field, and the inhibitor and activator concentration fields (equations (15)–(17)).

This algorithm differs from that presented in [1] and can be summarized as follows:

Step 1: Define the boundary conditions on the rectangular cavity contour for the stream function and for the vertical velocity component, which remain constant throughout the computation.

Step 2: Modify the right-hand side of the Poisson equation for the vorticity according to formulas (12) and (13) from [1].

Step 3: Solve the Poisson equation (7)–(11) from [1], i. e., compute the stream function values at the interior grid points of the rectangular domain.

Step 4: Compute the velocity along the upper segment of the cavity using formulas (5) from [1].

Step 5: Evaluate the updated velocity field using equation (18) from [1] at the interior grid nodes.

Step 6: Determine the new boundary values of vorticity using formulas (24) from [1].

Step 7: Compute the new vorticity values at the interior grid nodes using equation (19) from [1].

Step 8: Evaluate the right-hand sides for the inhibitor and activator equations (13).

Step 9: Solve equation (13) separately for the inhibitor and for the activator using the splitting method at the interior grid nodes.

Step 10: Determine the boundary values of the inhibitor and activator according to formula (14).

Step 11: If the physical time corresponds to an integer number of cardiac pulsations, reset the velocity, stream function, and vorticity fields to their initial values before solving equation (17). This procedure simulates blood mixing inside the aneurysm induced by a pulsation wave generated by the heart along the vessel system. The inhibitor, activator, and fibrin fields remain unchanged before and after the pulsation.

After completing the tenth step, the algorithm returns to the first step in a cyclic manner. In system (1), the Poisson equation is solved first, requiring a finite number of elementary operations [1] and providing sixth-order accuracy at the interior grid nodes. The second equation in system (1) corresponds to the vorticity function, which is computed through the coordinate derivatives of the velocity field.

The third equation expresses the velocity components as partial derivatives of the stream function. Therefore, the approximation of these equations $\bar{w}=\bar{v}_{\bar{x}}-\bar{u}_{\bar{y}},\bar{u}=\bar{\psi}_{\bar{y}};\bar{v}=-\bar{\psi}_{\bar{x}}$ reduces to approximating first derivatives, which poses no particular difficulty. The fourth equation in system (1) represents the vorticity dynamics equation—the only equation in the system that explicitly depends on time. The left-hand side contains the total (convective) time derivative.

In system (1), the elements of the rectangular cavity boundary must be clarified. Here, $\Gamma 1$ denotes the union of the lower parts of the lateral sides and the bottom segment, while $\Gamma 2$ corresponds to the upper boundary of the rectangle Γ. Let

($u(x,u)$, $v(x,y)$) denote the velocity vector of a fluid particle. On the solid boundary — that is, along the bottom segment and the lower parts of the lateral sides of height $H–d$ of the rectangular cavity — the velocity is zero (the no-slip condition on $\Gamma 1$). Accordingly, the stream function is set to zero along this boundary.

On the upper boundary of the rectangle, the vertical velocity component is zero, while the horizontal component is not specified on the upper segment and is zero on the bottom segment. On the lateral sides, it is described by equation (4) according to [1]:

$$\bar{u}(0,y)=\bar{u}(L,y)=\frac{u(y)}{u_{\max}}=\begin{cases}0, y\in[0,H-\Delta]\\ \left(1-\dfrac{(y-H)^2}{\Delta^2}\right), y\in[H-\Delta,H].\end{cases} \tag{4}$$

In the upper segment of the rectangular cavity, the unknown velocity can be determined using formulas (5), which correspond to the fourth step of the general algorithm described in [1]:

$$u(n_2,j)=\psi_y(n_2,j)=\frac{1}{(-h_2)}\left(-\frac{83711}{27720}\psi_{n_2,j}+11\psi_{n_2-1,j}-\frac{55}{2}\psi_{n_2-2,j}+55\psi_{n_2-3,j}-\frac{165}{2}\psi_{n_2-4,j}+\frac{462}{5}\psi_{n_2-5,j}-\right.$$
$$\left.-77\psi_{n_2-6,j}+\frac{330}{7}\psi_{n_2-7,j}-\frac{165}{8}\psi_{n_2-8,j}+\frac{55}{9}\psi_{n_2-9,j}-\frac{11}{10}\psi_{n_2-10,j}+\frac{1}{11}\psi_{n_2-11,j}\right)+O\left(h^{10}\right), j=\overline{1,n_1-1}, \tag{5.1}$$

$$u(n_2,j)=\frac{1}{(-h_2)}\left(-\frac{137}{60}\psi_{n_2,j}+5\psi_{n_2-1,j}-5\psi_{n_2-2,j}+\frac{10}{3}\psi_{n_2-3,j}-\frac{5}{4}\psi_{n_2-4,j}+\frac{1}{5}\psi_{n_2-5,j}\right)+O\left(h^4\right), j=\overline{1,n_1-1}. \tag{5.2}$$

To accelerate the numerical computation, due to the symmetry of the geometry, we consider one half of the aneurysm and two halves of the rectangular channels supplying and discharging the fluid from the aneurysm. It is convenient to introduce a rectangular coordinate system with a uniform grid $n_1 \times n_2 = 100\times 50$.

According to the projection principle, for two convex closed contours nested within each other without self-intersections (contact or partial coincidence of contours is allowed), a ray can be drawn from a certain internal point intersecting each contour at exactly one point. In this case, one may speak of geometric projection of one contour onto another.

Similarly, the projection of a physical field can be defined by transferring the field value at a point on the outer contour to the corresponding point on the inner contour. For example, in Fig. 1, the outer contour includes the left and right parts of the blood vessel and the rectangular aneurysm, whereas the inner contour consists only of the aneurysm. The projection of the outer contour points can also be performed along the normal direction onto the inner contour.

Thus, based on the field projection principle, the problem can be simplified, and its numerical solution significantly accelerated by considering the fluid motion only within the aneurysm domain, rather than within the combined volumes of the three bodies (the left vessel part, the aneurysm, and the right vessel part).

Therefore, it is assumed that the velocity profile is preserved when the flow enters the rectangular aneurysm and when it exits through a narrow symmetric strip with respect to the $0xz$-plane of width $2\Delta = 2d$, where at infinity the velocity distribution is described by the Poiseuille formula (4) [1].

By integrating formula (4) over the interval $y\in[H-\Delta, H]$ we obtain the stream function on the lateral sides of the aneurysm — the last expression in the system of equations (1) [1]. On the upper and lower segments of the aneurysm, as well as on the small adjacent side segments, projection of the velocity field and stream function is not required.

The field projection principle can be qualitatively justified using the classical example of the flow of an ideal fluid around an infinite cylinder. If the velocity field of the ideal fluid at infinity is constant, then at the diametrically opposite points of the cylinder the flow direction remains unchanged, while the velocity magnitude is doubled. At the same time, at the contact points and in the neighboring regions, the no-penetration condition on the cylinder surface is approximately satisfied.

Similarly, in Fig. 1, on the plane of symmetry, the flow direction remains unchanged; the direction of the velocity vector on the lateral inflow and outflow segments of the aneurysm connected to the blood vessel also remains approximately constant. The no-penetration condition of rigid boundaries is thus fulfilled approximately, which justifies the application of the field projection principle on the lateral sides of the aneurysm.

To accelerate the numerical solution of the vorticity equation (1), the splitting method was employed [1, 11]. Analytically, the method of n-fold splitting of the vorticity equation for the time interval τ_0/n can be expressed as follows:

$$\frac{w^{k+((i+1)/n)}-w^{k+(i/n)}}{\tau_0/n}+u^k\cdot w_x^{k+(i/n)}+v^k\cdot w_y^{k+(i/n)}=\frac{1}{\mathrm{Re}}\left(w_{xx}^{k+(i/n)}+w_{yy}^{k+(i/n)}\right), i=\overline{0,n-1}. \tag{6}$$

The system of recurrent equations (6) for the vorticity with a frozen velocity field $\left(u^k(x,y),v^k(x,y)\right), i=\overline{0,n-1}$, $k=const, k=1,2,...$ consists of n intermediate steps $i=\overline{0,n-1}$, the superscript i denotes the number of the intermediate

time layer in the vorticity equation (6), while the subscript k corresponds to the multiple time layer index in system (6). The velocity and stream function fields remain constant in equations (6) for fixed values of $k = const$ and varying index $i = \overline{0, n-1}$. Within this system, only the vorticity field $w^{k+(i/n)}, i = \overline{0, n-1}$ evolves. The velocity field undergoes a discrete change in system (1) when the temporal index of the vorticity function increases by one, from k to $k + 1$ in equations (6).

The main idea of the splitting scheme for system (6) lies in reducing both rounding error accumulation and computational time during the numerical solution. The differential operators with respect to spatial coordinates in (6) are approximated at internal grid nodes with accuracy $O(h^6)$, consistent with all equations in system (1); the boundary conditions are approximated with accuracy $O(h^4)$, and the temporal derivatives — with accuracy $O(\tau)$.

Here, we rely on an unproven but commonly accepted assumption that, for spectral time stability of finite-difference schemes, the approximation order of the equations on the boundary must be lower than that in the internal grid nodes [12]. Thus, over the time interval τ_0/n ((associated with a local decrease in solution stability caused by singular points in the velocity field), solving equation (6) n times yields a temporal jump τ_0 which is n times larger than that obtained by the sequential solution of system (1).

For the derivative w_y in (6), the quadrature formulas are written as follows (the formulas for w_x are analogous):

$$\begin{cases} w_{y(i,j)} = \frac{1}{h}\left(\frac{3}{4}\left(w_{i+1,j} - w_{i-1,j}\right) - \frac{3}{20}\left(w_{i+2,j} - w_{i-2,j}\right) + \frac{1}{60}\left(w_{i+3,j} - w_{i-3,j}\right)\right) + O\left(h^6\right), i = \overline{3, n_2 - 3}, j = \overline{1, n_1 - 1}, \\ w_{y(1,j)} = \frac{1}{h}\left(-\frac{w_{0,j}}{5} - \frac{13}{12}w_{1,j} + 2w_{2,j} - w_{3,j} + \frac{w_{4,j}}{3} - \frac{w_{5,j}}{20}\right) + O\left(h^4\right), j = \overline{1, n_1 - 1}, \\ w_{y(2,j)} = \frac{1}{12h}\left(8\left(w_{3,j} - w_{1,j}\right) - \left(w_{4,j} - w_{0,j}\right)\right) + O\left(h^4\right), j = \overline{1, n_1 - 1}, \\ w_{y(n_2-1,j)} = -\frac{1}{h}\left(-\frac{w_{n_2,j}}{5} - \frac{13}{12}w_{n_2-1,j} + 2w_{n_2-2,j} - w_{n_2-3,j} + \frac{w_{n_2-4,j}}{3} - \frac{w_{n_2-5,j}}{20}\right) + O\left(h^4\right), j = \overline{1, n_1 - 1}, \\ w_{y(n_2-2,j)} = -\frac{1}{12h}\left(8\left(w_{n_2-3,j} - w_{n_2-1,j}\right) - \left(w_{n_2-4,j} - w_{n_2,j}\right)\right) + O\left(h^4\right), j = \overline{1, n_1 - 1}. \end{cases} \tag{7}$$

The second-order partial derivatives w_{yy} in (6) are expressed as follows:

$$\begin{cases} w_{yy(i,j)} = \frac{1}{h^2}\left(-\frac{49}{18}w_{i,j} + \frac{3}{2}\left(w_{i+1,j} + w_{i-1,j}\right) - \frac{3}{20}\left(w_{i+2,j} + w_{i-2,j}\right) + \frac{1}{90}\left(w_{i+3,j} + w_{i-3,j}\right)\right) + O\left(h^6\right), i = \overline{3, n_2 - 3}, j = \overline{1, n_1 - 1}, \\ w_{yy(1,j)} = \frac{1}{h^2}\left(\frac{137}{180}w_{0,j} - \frac{49}{60}w_{1,j} - \frac{17}{12}w_{2,j} + \frac{47}{18}w_{3,j} - \frac{19}{12}w_{4,j} + \frac{31}{60}w_{5,j} - \frac{13}{180}w_{6,j}\right) + O\left(h^4\right), j = \overline{1, n_1 - 1}, \\ w_{yy(2,j)} = \frac{1}{h^2}\left(-\frac{5}{2}w_{2,j} + \frac{4}{3}\left(w_{1,j} + w_{3,j}\right) - \frac{1}{12}\left(w_{0,j} + w_{4,j}\right)\right) + O\left(h^4\right), j = \overline{1, n_1 - 1}, \\ w_{yy(n_2-1,j)} = \frac{1}{h^2}\left(\frac{137}{180}w_{n_2,j} - \frac{49}{60}w_{n_2-1,j} - \frac{17}{12}w_{n_2-2,j} + \frac{47}{18}w_{n_2-3,j} - \frac{19}{12}w_{n_2-4,j} + \frac{31}{60}w_{n_2-5,j} - \frac{13}{180}w_{n_2-6,j}\right) + O\left(h^4\right), j = \overline{1, n_1 - 1}, \\ w_{yy(n_2-2,j)} = \frac{1}{h^2}\left(-\frac{5}{2}w_{n_2-2,j} + \frac{4}{3}\left(w_{n_2-1,j} + w_{n_2-3,j}\right) - \frac{1}{12}\left(w_{n_2,j} + w_{n_2-4,j}\right)\right) + O\left(h^4\right), j = \overline{1, n_1 - 1}. \end{cases} \tag{8}$$

Similarly, the formulas for the derivative w_{xx} are written analogously to formulas (8). From [2], we also include the general boundary condition for vorticity (equation (6), sixth step of the general algorithm) in the open cavity with fourth-order accuracy, obtained by differentiating the last equation for the stream function in system (1) twice with respect to y:

$$w(x,y) = -\psi_{xx} - \psi_{yy} = \frac{1}{h_1^2}\left(\frac{415}{72}\psi_0 - 8\psi_1 + 3\psi_2 - \frac{8}{9}\psi_3 + \frac{1}{8}\psi_4\right) - \frac{25}{6}\frac{v(0,y)}{h_1} - \psi_{yy}, v = -\psi_x,$$
$$m = \overline{0, n_2}, y_m = mh_2, \Delta = h_2\left(n_2 - n_3\right), 1 - \Delta = h_2 n_3, \tag{9}$$

$$\overline{w}_{m,0} = \begin{cases} \frac{1}{h_1^2}\left(\frac{415}{72}\overline{\psi}_{m,0} - 8\overline{\psi}_{m,1} + 3\overline{\psi}_{m,2} - \frac{8}{9}\overline{\psi}_{m,3} + \frac{1}{8}\overline{\psi}_{m,4}\right) - \frac{25}{6}\frac{\overline{v}_{m,0}}{h_1} + 2\frac{\left(\overline{y_m} - H/L\right)}{\left(\Delta/L\right)^2}, m = \overline{n_3, n_2}, \\ \frac{1}{h_1^2}\left(\frac{415}{72}\overline{\psi}_{m,0} - 8\overline{\psi}_{m,1} + 3\overline{\psi}_{m,2} - \frac{8}{9}\overline{\psi}_{m,3} + \frac{1}{8}\overline{\psi}_{m,4}\right) - \frac{25}{6}\frac{\overline{v}_{m,0}}{h_1}, m = \overline{0, n_3}, \textit{left}, \end{cases} \tag{10.1}$$

$$\overline{w}_{m,n_1} = \begin{cases} \frac{1}{h_1^2}\left(\frac{415}{72}\overline{\psi}_{m,n_1} - 8\overline{\psi}_{m,n_1-1} + 3\overline{\psi}_{m,n_1-2} - \frac{8}{9}\overline{\psi}_{m,n_1-3} + \frac{1}{8}\overline{\psi}_{m,n_1-4}\right) + \frac{25}{6}\frac{\overline{v}_{m,n_1}}{h_1} + 2\frac{\left(\overline{y_m} - H/L\right)}{\left(\Delta/L\right)^2}, m = \overline{n_3, n_2}, \\ \frac{1}{h_1^2}\left(\frac{415}{72}\overline{\psi}_{m,n_1} - 8\overline{\psi}_{m,n_1-1} + 3\overline{\psi}_{m,n_1-2} - \frac{8}{9}\overline{\psi}_{m,n_1-3} + \frac{1}{8}\overline{\psi}_{m,n_1-4}\right) + \frac{25}{6}\frac{\overline{v}_{m,n_1}}{h_1}, m = \overline{0, n_3}, \quad \textit{right}, \end{cases} \tag{10.2}$$

$$\overline{w}_{0,n}=\begin{cases}\dfrac{1}{h_2^2}\left(\dfrac{415}{72}\overline{\psi}_{0,n}-8\overline{\psi}_{1,n}+3\overline{\psi}_{2,n}-\dfrac{8}{9}\overline{\psi}_{3,n}+\dfrac{1}{8}\overline{\psi}_{4,n}\right)+\dfrac{25}{6}\dfrac{\overline{u}_{0,n}}{h_2},\ n=\overline{0,n_1},\ u=\psi_y,\ bottom,\\ \dfrac{1}{h_2^2}\left(\dfrac{415}{72}\overline{\psi}_{n_2,n}-8\overline{\psi}_{n_2-1,n}+3\overline{\psi}_{n_2-2,n}-\dfrac{8}{9}\overline{\psi}_{n_2-3,n}+\dfrac{1}{8}\overline{\psi}_{n_2-4,n}\right)-\dfrac{25}{6}\dfrac{\overline{u}_{n_2,n}}{h_2},\ n=\overline{0,n_1},\ top.\end{cases} \tag{10.3}$$

In deriving the boundary equation (9) for the vorticity function, all stream function derivatives of order higher than two were eliminated. This significantly improves the stability of boundary finite-difference conditions of the type (9) and (10) for velocity fields with first-kind discontinuities. Table 1 presents the classification of blood vessels according to their Reynolds number and diameter.

Table 1

Classification of blood vessels

Type	Diameter	Blood velocity	Re	Governing equations
Capillaries	(5–10) μm	(0.5–1.0) mm/s	0.00075–0.003	–
Arterioles	(10–100) μm	(0.5–10.0) cm/s	0.015–3,000	(1), (13)
Arteries	(2–10) mm	(10.0–50.0) cm/m	60–1500	(1), (13)
Aorta	(2–3) cm	0.5 m/s	3000	(1), (13)

Experience [1] shows that, for a physically rapid solution of system (1) in arterioles and arteries, it is necessary to select an inertial time interval $T=\dfrac{L}{u_{\max}}$, while the hydrodynamic problem is solved using system (1).

We consider a simplest mathematical model of fibrin formation, which accounts for the concentration dynamics of two metabolites: an activator of the coagulation process (thrombin) s and an inhibitor z, which slows down blood coagulation:

$$\begin{cases}\dfrac{\partial s}{\partial t}+u\dfrac{\partial s}{\partial x}+v\dfrac{\partial s}{\partial y}=D\left(s_{xx}+s_{yy}\right)+\dfrac{\alpha s^2}{s+s_0}-k_1 s-\gamma s z,\\ \dfrac{\partial z}{\partial t}+u\dfrac{\partial z}{\partial x}+v\dfrac{\partial z}{\partial y}=D\left(z_{xx}+z_{yy}\right)+\beta s\left(1-\dfrac{z}{c}\right)\left(1+\dfrac{z^2}{z_0^2}\right)-k_2 z.\end{cases} \tag{11}$$

Here, u, v are the velocity components; the coefficients α, β, k_1, γ, D, c, v_0, k_2 are dimensional, and their numerical values are taken from [3, p. 16].

Table 2

Dimensional coefficients in system of equations (11)

α, min^{-1}	β, min^{-1}	$\dfrac{\gamma}{\min\cdot\mathrm{nM}}$	$v_0(z_0)$, nM	c, nM	$u_0(s_0)$, nM	k_1, min^{-1}	k_2, min^{-1}
2.0	0.0015	5.0	0.0525	5.0	2.95	0.05	0.35

The diffusion coefficients of thrombin and the inhibitor are assumed equal to $D = 10^{-11}$ m^2/s [2, p. 99]. The diffusion velocities of thrombin and the inhibitor can be calculated using the formula $v=2\sqrt{\alpha D}=2\sqrt{10^{-11}2/60}=1.155\cdot10^{-6}$ m/s. These diffusion velocities are significantly smaller than the blood velocity in an arteriole (3 mm/s) and in an artery (50 cm/s), which justifies the inclusion of advection terms on the left-hand side of system (11).

$$\begin{cases}\dfrac{\partial\overline{s}}{T\partial\overline{t}}+\dfrac{u_{\max}}{L}\overline{u}\dfrac{\partial\overline{s}}{\partial\overline{x}}+\dfrac{u_{\max}}{L}\overline{v}\dfrac{\partial\overline{s}}{\partial\overline{y}}=\dfrac{D}{L^2}\left(\overline{s}_{\overline{x}\overline{x}}+\overline{s}_{\overline{y}\overline{y}}\right)+\dfrac{\alpha\overline{s}^2}{\overline{s}+1}-k_1\overline{s}-\gamma\overline{s}\overline{z}z_0,\\ \dfrac{\partial\overline{z}}{T\partial\overline{t}}+\dfrac{u_{\max}}{L}\overline{u}\dfrac{\partial\overline{z}}{\partial\overline{x}}+\dfrac{u_{\max}}{L}\overline{v}\dfrac{\partial\overline{z}}{\partial\overline{y}}=\dfrac{D}{L^2}\left(\overline{z}_{\overline{x}\overline{x}}+\overline{z}_{\overline{y}\overline{y}}\right)+\dfrac{s_0}{z_0}\beta\overline{s}\left(1-\dfrac{z_0\overline{z}}{c}\right)\left(1+\overline{z}^2\right)-k_2\overline{z},\end{cases}\Leftrightarrow$$

$$\begin{cases}\dfrac{\partial\overline{s}}{\partial\overline{t}}+\overline{u}\dfrac{\partial\overline{s}}{\partial\overline{x}}+\overline{v}\dfrac{\partial\overline{s}}{\partial\overline{y}}=\dfrac{D}{Lu_{\max}}\left(\overline{s}_{\overline{x}\overline{x}}+\overline{s}_{\overline{y}\overline{y}}\right)+\dfrac{L}{u_{\max}}\left(\dfrac{\alpha\overline{s}^2}{\overline{s}+1}-k_1\overline{s}-\gamma\overline{s}\overline{z}z_0\right),\\ \dfrac{\partial\overline{z}}{\partial\overline{t}}+\overline{u}\dfrac{\partial\overline{z}}{\partial\overline{x}}+\overline{v}\dfrac{\partial\overline{z}}{\partial\overline{y}}=\dfrac{D}{Lu_{\max}}\left(\overline{z}_{\overline{x}\overline{x}}+\overline{z}_{\overline{y}\overline{y}}\right)+\dfrac{L}{u_{\max}}\left(\dfrac{s_0}{z_0}\beta\overline{s}\left(1-\dfrac{z_0\overline{z}}{c}\right)\left(1+\overline{z}^2\right)-k_2\overline{z}\right),\end{cases}\Leftrightarrow$$

$$\begin{cases} \dfrac{\partial \bar{s}}{\partial \bar{t}} + \bar{u}\dfrac{\partial \bar{s}}{\partial \bar{x}} + \bar{v}\dfrac{\partial \bar{s}}{\partial \bar{y}} = \dfrac{D}{\nu \mathrm{Re}}\left(\bar{s}_{\bar{x}\bar{x}} + \bar{s}_{\bar{y}\bar{y}}\right) + \dfrac{L}{u_{\max}}\left(\dfrac{\alpha \bar{s}^2}{\bar{s}+1} - k_1 \bar{s} - \gamma \bar{s}\bar{z}z_0\right), \\ \dfrac{\partial \bar{z}}{\partial \bar{t}} + \bar{u}\dfrac{\partial \bar{z}}{\partial \bar{x}} + \bar{v}\dfrac{\partial \bar{z}}{\partial \bar{y}} = \dfrac{D}{\nu \mathrm{Re}}\left(\bar{z}_{\bar{x}\bar{x}} + \bar{z}_{\bar{y}\bar{y}}\right) + \dfrac{L}{u_{\max}}\left(\dfrac{s_0}{z_0}\beta \bar{s}\left(1 - \dfrac{z_0 \bar{z}}{c}\right)\left(1 + \bar{z}^2\right) - k_2 \bar{z}\right), \\ \dfrac{d\bar{\varphi}}{d\bar{t}} = \bar{s}(\bar{t}). \end{cases} \tag{12}$$

The last equation in system (12) is the thrombin growth equation $\bar{\varphi}(\bar{t})$ obtained by integrating the activator $\bar{s}(\bar{t})$ over the dimensionless time $\bar{t}$. According to [2–5], the activator $\bar{s}(\bar{t})$, the inhibitor $\bar{z}(\bar{t})$, and thrombin $\bar{\varphi}(\bar{t})$ take only non-negative values, which was enforced by the authors in the numerical implementation.

For an arteriole [5], the diameter is $2d = 2$ mm, the blood viscosity is $\eta = 3{,}5 \cdot 10^{-3}$ Pa·s, and the kinematic viscosity of blood is $\nu = \dfrac{\mu}{\rho} = \dfrac{3.5 \cdot 10^{-3}\,\mathrm{Pa \cdot s}}{1050\ \mathrm{kg/m^3}} = 3.33(3) \cdot 10^{-6}\,\dfrac{\mathrm{m}^2}{\mathrm{s}}$. The blood velocity [5] in an aneurysm of diameter $L \approx 4d = 4$ mm is $u_{\max} = 3$ mm/s. Then the Reynolds number is calculated as $\mathrm{Re} = \dfrac{u_{\max} L}{\nu} = \dfrac{3 \cdot 10^{-3} \cdot 4 \cdot 10^{-3}}{3.33(3) \cdot 10^{-6}} = 3.6$. We introduce the following dimensionless variables $\bar{s} = s / s_0$, $\bar{z} = z / z_0$, and compute the corresponding dimensionless coefficients:

$$\frac{D}{\nu \mathrm{Re}} = \frac{10^{-11}}{3.33(3) \cdot 10^{-6} \cdot 3.6} = 8.33(3) \cdot 10^{-7},\ z_0 / C = 0.0525/5 = 1.05 \cdot 10^{-2},\ z_0 / C = 0.0525/5 = 1.05 \cdot 10^{-2},$$

$$\alpha \frac{L}{u_{\max}} = \frac{2 \cdot 4 \cdot 10^{-3}}{60 \cdot 3 \cdot 10^{-3}} = 0.044(4),\ k_1 \frac{L}{u_{\max}} = \frac{0.05 \cdot 4 \cdot 10^{-3}}{60 \cdot 3 \cdot 10^{-3}} = 0.0011(1),$$

$$\frac{L\gamma}{u_{\max}} z_0 = \frac{4 \cdot 10^{-3}}{3 \cdot 10^{-3}} \cdot \frac{5}{60} \cdot 0.0525 = 0.005833(3),\ k_2 \frac{L}{u_{\max}} = \frac{0.35 \cdot 4 \cdot 10^{-3}}{60 \cdot 3 \cdot 10^{-3}} = 0.0077(7),$$

$$\frac{L\beta}{u_{\max}} \frac{s_0}{z_0} = \frac{4 \cdot 10^{-3}}{3 \cdot 10^{-3}} \cdot \frac{0.0015}{60} \cdot \frac{2.95}{0.0525} = 0.00187301587301(587301).$$

We denote the right-hand sides in the dynamical equations for the inhibitor and activator in system (12) and obtain the splitting method [11] with splitting multiplicity N:

$$F_{\bar{s}}\left(\bar{t} = \tau_0\left(k + (i/N)\right), \bar{x}, \bar{y}\right) = \frac{D}{\nu \mathrm{Re}}\left(\bar{s}_{\bar{x}\bar{x}} + \bar{s}_{\bar{y}\bar{y}}\right) + \frac{L}{u_{\max}}\left(\frac{\alpha \bar{s}^2}{\bar{s}+1} - k_1 \bar{s} - \gamma \bar{s}\bar{z}z_0\right),$$

$$F_{\bar{z}}\left(\bar{t} = \tau_0\left(k + (i/N)\right), \bar{x}, \bar{y}\right) = \frac{D}{\nu \mathrm{Re}}\left(\bar{z}_{\bar{x}\bar{x}} + \bar{z}_{\bar{y}\bar{y}}\right) + \frac{L}{u_{\max}}\left(\frac{s_0}{z_0}\beta \bar{s}\left(1 - \frac{z_0 \bar{z}}{c}\right)\left(1 + \bar{z}^2\right) - k_2 \bar{z}\right),$$

$$\begin{cases} \dfrac{\bar{s}^{k+((i+1)/N)} - \bar{s}^{k+(i/N)}}{\tau_0 / N} + u^k \cdot \bar{s}_x^{k+(i/N)} + v^k \cdot \bar{s}_y^{k+(i/N)} = F_{\bar{s}}\left(\bar{t} = \tau_0\left(k + (i/N)\right), \bar{x}, \bar{y}\right), \\ \dfrac{\bar{z}^{k+((i+1)/N)} - \bar{z}^{k+(i/N)}}{\tau_0 / N} + u^k \cdot \bar{z}_x^{k+(i/N)} + v^k \cdot \bar{z}_y^{k+(i/N)} = F_{\bar{z}}\left(\bar{t} = \tau_0\left(k + (i/N)\right), \bar{x}, \bar{y}\right), i = \overline{0, N-1},\ k = 0,1,2,\ldots. \end{cases} \tag{13}$$

The splitting multiplicity $N = 70$ in system (13) for the inhibitor and activator differs from the multiplicity $n = 200$ used for the vorticity equation (6). It is only necessary to synchronize the time steps of systems (6) and (13) such that, after completion of both subroutine loops, the increment of their dimensionless time coincides, i. e., equals τ_0.

If the boundary conditions for the inhibitor and activator at the solid wall are specified for the no-penetration case (for example, at the bottom of the cavity), then from formula (5.1) we obtain formula (14.1) with eleventh-order accuracy:

$$\begin{aligned} 0 = \bar{s}_y(0, j) = \frac{1}{(-h_2)}\Bigg(& -\frac{83711}{27720}\bar{s}_{0,j} + 11\bar{s}_{1,j} - \frac{55}{2}\bar{s}_{2,j} + 55\bar{s}_{3,j} - \frac{165}{2}\bar{s}_{4,j} + \frac{462}{5}\bar{s}_{5,j} - \\ & -77\bar{s}_{6,j} + \frac{330}{7}\bar{s}_{7,j} - \frac{165}{8}\bar{s}_{8,j} + \frac{55}{9}\bar{s}_{9,j} - \frac{11}{10}\bar{s}_{10,j} + \frac{1}{11}\bar{s}_{11,j}\Bigg) + O\left(h^{10}\right), j = \overline{1, n_1 - 1} \Leftrightarrow \\ \bar{s}_{0,j} = \frac{27720}{83711}\Bigg(& 11\bar{s}_{1,j} - \frac{55}{2}\bar{s}_{2,j} + 55\bar{s}_{3,j} - \frac{165}{2}\bar{s}_{4,j} + \frac{462}{5}\bar{s}_{5,j} - \end{aligned} \tag{14.1}$$

$$-77\bar{s}_{6,j}+\frac{330}{7}\bar{s}_{7,j}-\frac{165}{8}\bar{s}_{8,j}+\frac{55}{9}\bar{s}_{9,j}-\frac{11}{10}\bar{s}_{10,j}+\frac{1}{11}\bar{s}_{11,j}\Big)+O\left(h^{11}\right),\ j=\overline{1,n_1-1}.$$

Similarly, we obtain formula (14.2) with fifth-order accuracy:

$$\bar{s}_{0,j}=\frac{60}{137}\left(5\bar{s}_{1,j}-5\bar{s}_{2,j}+\frac{10}{3}\bar{s}_{3,j}-\frac{5}{4}\bar{s}_{4,j}+\frac{1}{5}\bar{s}_{5,j}\right)+O\left(h^5\right),\ j=\overline{1,n_1-1}. \tag{14.2}$$

Problem Initialization. The initial values for the inhibitor and activator fields are set, following A.I. Lobanov [3], as a step function for the activator. These initial conditions were used in systems (1) and (13), with the solutions shown below in Fig. 2–7:

$$\begin{cases}\bar{z}_{i,j}(t=0)=0,\forall i=\overline{0,n_2},\ j=\overline{0,n_1},\\ \bar{s}_{i,j}(t=0)=\begin{cases}1,\forall i=\overline{0,n_2},\ j=\overline{0,n_1/2},\\ 0,\forall i=\overline{0,n_2},\ j=\overline{n_1/2,n_1}.\end{cases}\end{cases} \tag{15}$$

We also assume that the boundary conditions for the activator and inhibitor on the rectangular boundary of the cavity (aneurysm) are homogeneous. Dirichlet conditions:

$$\bar{s}\big|_{\Gamma/\Gamma_2}=0,\bar{z}\big|_{\Gamma/\Gamma_2}=0. \tag{16}$$

The initial velocity field is defined as follows: the vertical velocity component $v_{i,j}(t=0)$ is absent, while the horizontal component $u_{i,j}(t=0)$ follows a Poiseuille distribution (4):

$$\begin{cases}v_{i,j}(t=0)=0,\forall i=\overline{0,n_2},\ j=\overline{0,n_1},\\ u_{i,j}(t=0)=\begin{cases}\left(1-\left(\dfrac{\overline{y_i}-\overline{H}}{\overline{\Delta}}\right)^2\right),\ \overline{H}-\overline{\Delta}=h_2n_3\le\overline{y_i}\le\overline{H}=h_2n_2,\overline{y_i}=i\cdot h_2,i=\overline{n_3,n_2},\\ 0,i=\overline{0,n_3}.\end{cases}\end{cases} \tag{17}$$

From [5], we select an arteriole diameter of $2d=2$ mm and a blood velocity $u=3$ mm/s. The aneurysm diameter and length are twice that, $2D=L=4$ мм. The corresponding Reynolds number is $\mathrm{Re}=\dfrac{u_{\max}L}{\nu}=\dfrac{3\cdot10^{-3}\cdot4\cdot10^{-3}}{3.333\cdot10^{-6}}=3.6$. The **transit time** of a fluid particle $T=\dfrac{L}{u_{\max}}=\dfrac{4\cdot10^{-3}}{3\cdot10^{-3}}=1.33(3)$ s along the aneurysm exceeds the period of cardiac pulsations (1 second); therefore, during the time interval $T=1.33(3)$ s two cardiac pulsations occur, resulting in two mechanical mixing events of the blood within the aneurysm walls.

Homogeneous zero boundary conditions were chosen for the inhibitor and activator on the cavity walls, based on the assumption that their concentrations at points far from the aneurysm are zero. On the upper segment of the cavity, formula (14.2) was applied for both the activator and inhibitor, as symmetric solutions are sought for all unknown fields. System (12) has a trivial solution $\bar{s}(\bar{t})=\bar{z}(\bar{t})\equiv0$. As shown in [3], the trivial solutions $\bar{s}(\bar{t})=\bar{z}(\bar{t})\equiv0$ are stable if the inhibitor and activator values remain below their threshold levels $\bar{s}(\bar{t})=\bar{z}(\bar{t})\equiv0$. This justifies the use of homogeneous zero boundary conditions.

The initial fibrin field $\varphi(\bar{t})$ in (12), obtained by integrating the activator field over time, at $T=1.33(3)$ *s* is shown in Fig. 2.

From Fig. 2, it follows that even at the initial stage of fibrin formation, noticeable transport occurs — both advection along the blood flow and diffusion, according to system (13).

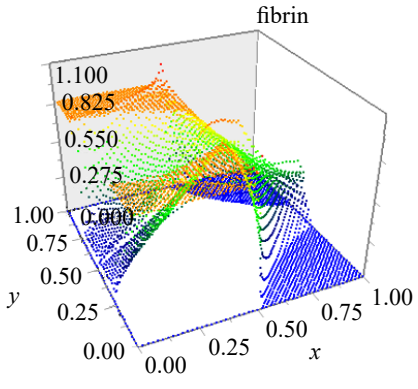

a)

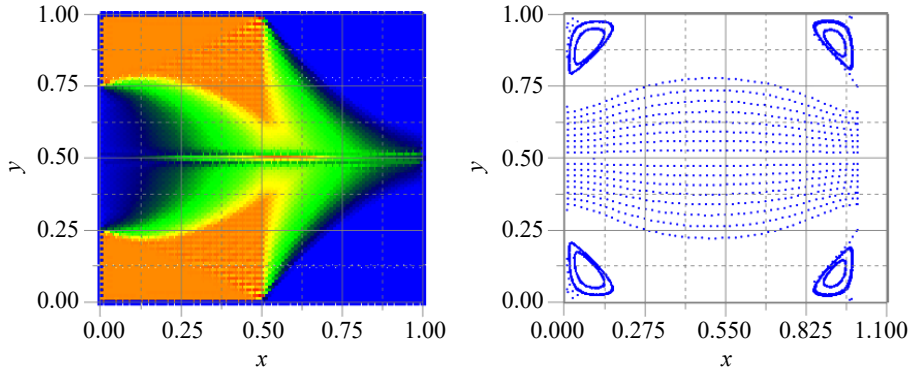

Fig. 2. Fields in an arteriole using formula (14.2) at $T = 1.33(3)$ s,
Re = 3.6, $n_1 \times n_2 = 100 \times 50$, $\Delta / H = 0.5$; $L = 4$ mm, $2H = 4$ mm, $u_{\max} = 3$ mm/s, $\tau = \frac{6}{16} h_1^2$, $m = 53000$ steps,
splitting multiplicities $n = 200$ in (6), $N = 70$ in (13):
a — fibrin surface; *b* — fibrin distribution in the aneurysm; *c* — streamlines in the aneurysm

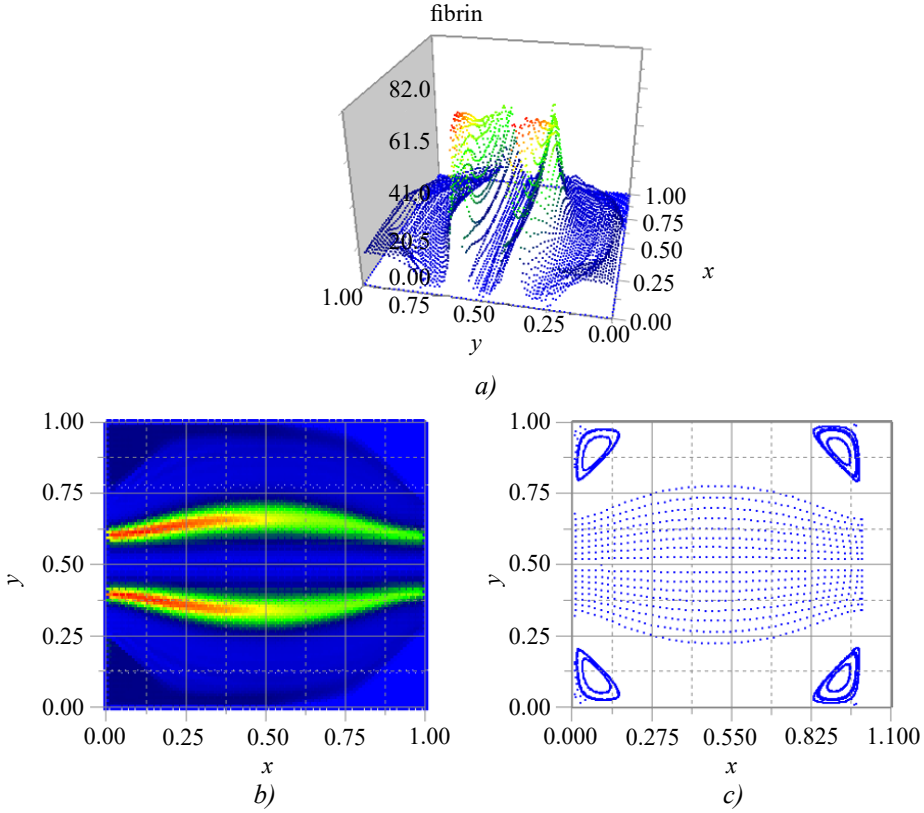

Fig. 3. Fields in an arteriole using formula (14.2) at $T = 20$ s,
Re = 3.6, $n_1 \times n_2 = 100 \times 50$, $\Delta / H = 0.5$; $L = 4$ mm, $2H = 4$ mm, $u_{\max} = 3$ mm/s, $\tau = \frac{6}{16} h_1^2$, $m = 800000$ steps,
splitting multiplicities $n = 200$ in (6), $N = 70$ in (13):
a — fibrin surface; *b* — fibrin distribution in the aneurysm; *c* — streamlines in the aneurysm

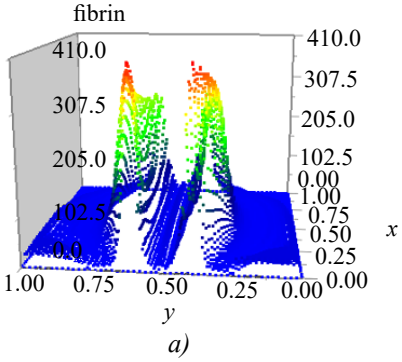

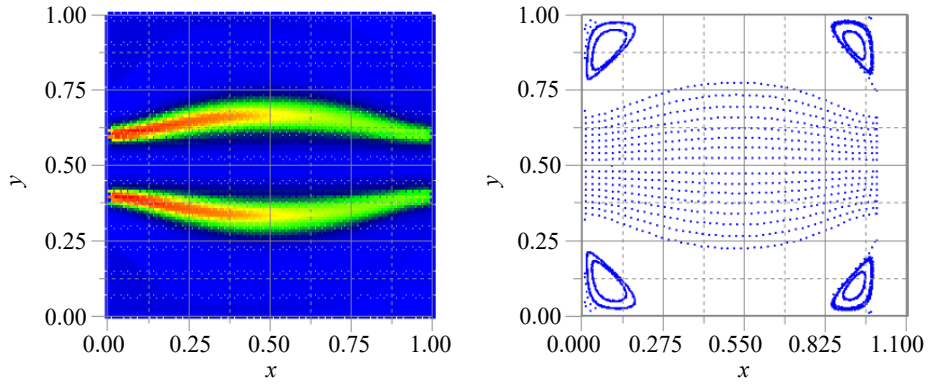

Fig. 4. Fields in an arteriole using formula (14.2) at $T = 26$ s,
$\mathrm{Re} = 3.6$, $n_1 \times n_2 = 100 \times 50$, $\Delta / H = 0.5$; $L = 4$ mm, $2H = 4$ mm, $u_{\max} = 3$ mm/s, $\tau = \frac{6}{16} h_1^2$, $m = 1200000$ steps,
splitting multiplicities $n = 200$ in (6), $N = 70$ in (13):
a — fibrin surface; *b* — fibrin distribution in the aneurysm; *c* — streamlines in the aneurysm

Fig. 4 concludes the graphical representation of thrombus formation in an arteriole aneurysm at the end of the first phase (30 seconds). From Table 1, we select an artery diameter of $2d = 1$ cm and a blood velocity $u = 0.5$ m/s. The aneurysm diameter and length are twice that, $2H = L = 2$ cm. The corresponding Reynolds number is $\mathrm{Re} = \frac{u_{\max} L}{\nu} = \frac{0.5 \cdot 2 \cdot 10^{-2}}{3.33(3) \cdot 10^{-6}} = 3000$. The transit time of a fluid particle $T = \frac{L}{u_{\max}} = \frac{2 \cdot 10^{-2}}{0.5} = 0.04$ s along the aneurysm is less than the period of cardiac pulsations (1 second); therefore, during this interval $T = 0.04$ s only a single cardiac pulsation occurs, resulting in blood mixing within the aneurysm with low probability.

The initial fibrin field $\bar{\varphi}(\bar{t})$ in (12), obtained by integrating the activator field over time, at $T = 0.04$ s is shown in Fig. 5.

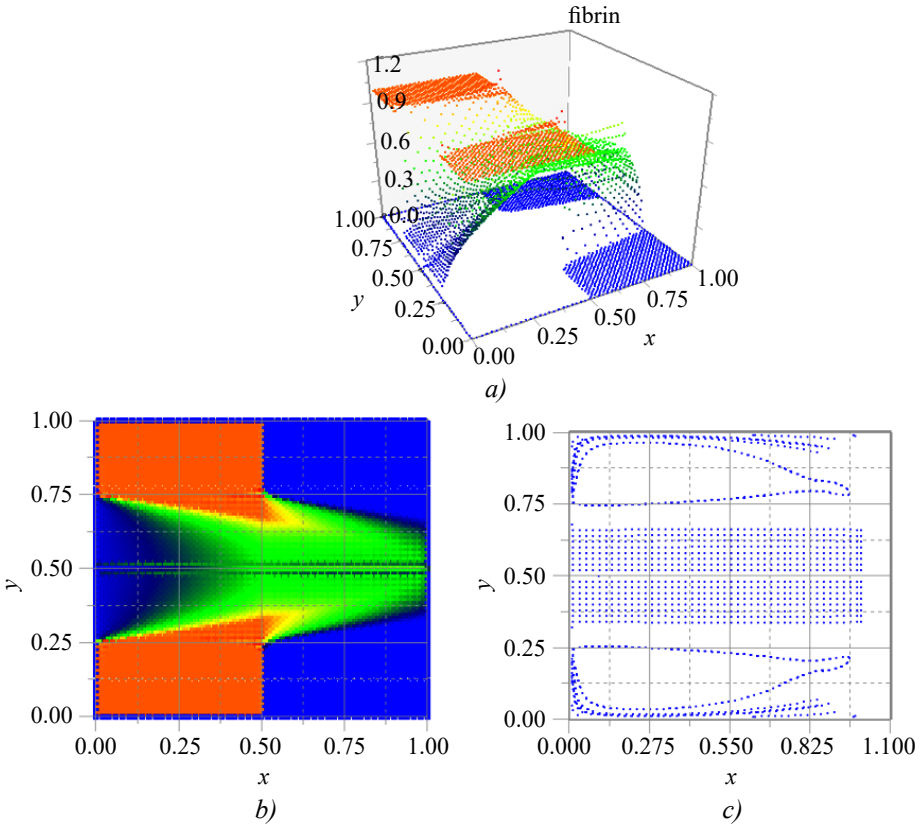

Fig. 5. Fields in an artery using formula (14.2) at $T = 0.04$ s,
$\mathrm{Re} = 3000$, $n_1 \times n_2 = 100 \times 50$, $\Delta / H = 0.5$; $L = 2$ cm, $2H = 2$ cm, $u_{\max} = 0.5$ m/s, $\tau = \frac{6}{16} h_1^2$, $m = 53000$ steps,
splitting multiplicities $n = 200$ in (6), $N = 70$ in (13):
a — fibrin surface; *b* — fibrin distribution in the aneurysm; *c* — streamlines in the aneurysm

Compared to Fig. 2*b*, in Fig. 5*b* the advection of the activator is more pronounced than its diffusion. In Fig. 6*b*, the fibrin transport along the flow and its swirling near the right segment of the cavity, forming a “fibrin stalk”, can be observed. Consequently, a fibrin film forms along the geometric boundary of the cavity, blocking oxygen access to the aneurysm walls and creating blood stasis within the aneurysm.

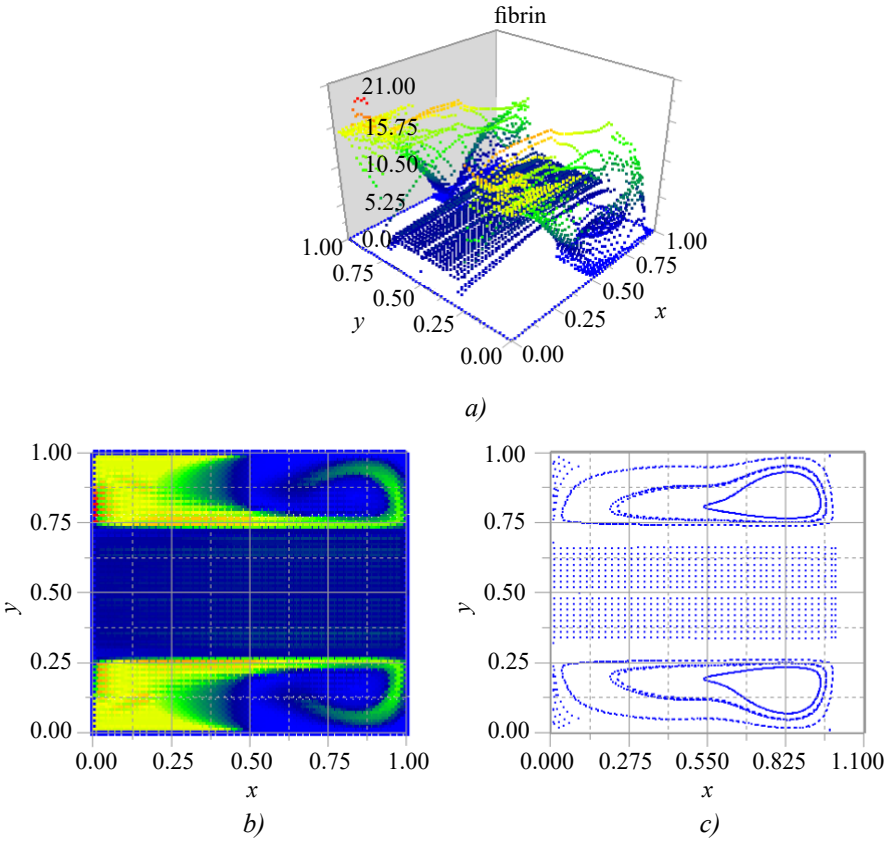

Fig. 6. Fields in an artery using formula (14.2) at $T = 0.6$ s,
$\mathrm{Re} = 3000$, $n_1 \times n_2 = 100 \times 50$, $\Delta / H = 0.5$; $L = 2$ cm, $2H = 2$ cm, $u_{\max} = 0.5$ m/s, $\tau = \frac{6}{16} h_1^2$, $m = 800000$ steps,
splitting multiplicities $n = 200$ in (6), $N = 70$ in (13):
a — fibrin surface; *b* — fibrin distribution in the aneurysm; *c* — streamlines in the aneurysm

Qualitatively, Fig. 6 and 7 are similar; however, the “fibrin stalk” in Fig. 6*b* has already transformed into a “fibrin ring” in Fig. 7*b*. Fig. 6 and 7 demonstrate that in a turbulent environment, each fibrin filament rapidly changes its value even along its length, resembling loose hair strands blown by the wind.

Next, we consider the periodic structure of fibrin in an arteriole near the aneurysm wall at $t = 10$ s after the onset of blood coagulation, as shown in Fig. 8.

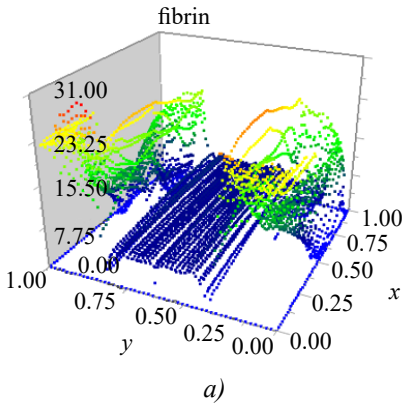

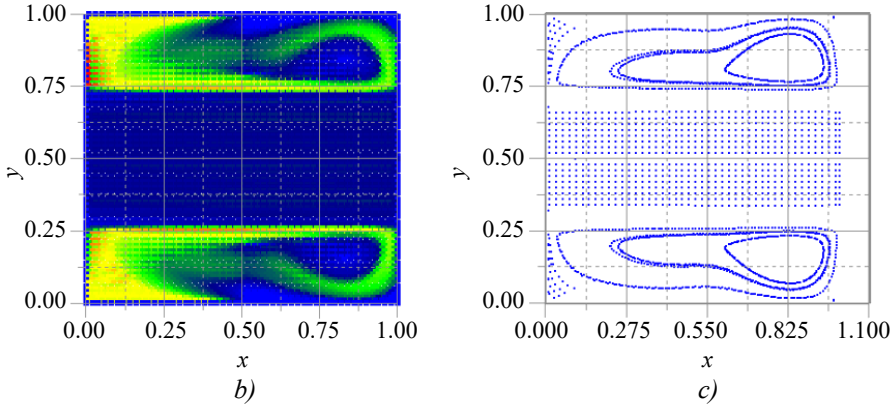

Fig. 7. Fields in an artery using formula (14.2) at $T = 0.9$ s,
$\mathrm{Re} = 3000$, $n_1 \times n_2 = 100 \times 50$, $\Delta / H = 0.5$; $L = 2$ cm, $2H = 2$ cm, $u_{\max} = 0.5$ m/s, $\tau = \frac{6}{16} h_1^2$, $m = 1200000$ steps,
splitting multiplicities $n = 200$ in (1), $N = 70$ in (13):
a — fibrin surface; *b* — fibrin distribution in the aneurysm; *c* — streamlines in the aneurysm

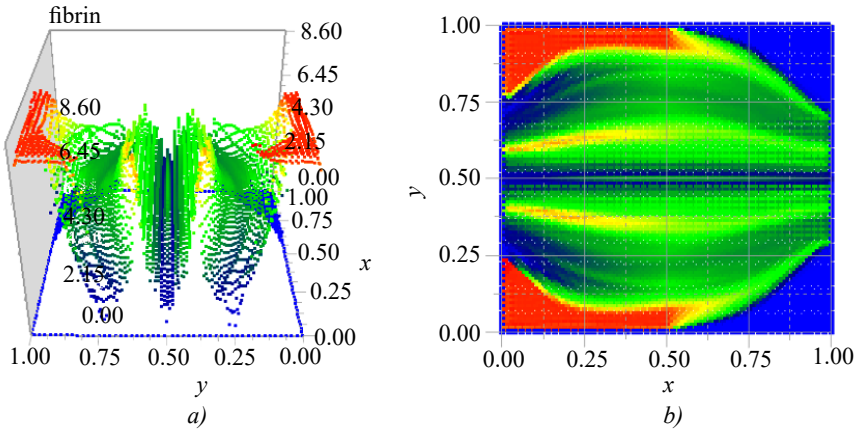

Fig. 8. Fibrin field in an arteriole using formula (14.2) at $T = 10$ s,
$\mathrm{Re} = 3.8$, $n_1 \times n_2 = 100 \times 50$, $\Delta / H = 0.5$; $L = 4$ mm, $2H = 4$ mm, $u_{\max} = 3$ mm/s, $\tau = \frac{6}{16} h_1^2$, $m = 400000$ steps,
splitting multiplicities $n = 200$ in (6), $N = 70$ in (13):
a — fibrin surface; *b* — fibrin distribution in the aneurysm

Fig. 8*a* and 8*b* show that fibrin moves along the aneurysm wall in a thin layer against the direction of blood flow (at a velocity of $u_{\max} = 3$ mm/s). It turns at the far wall (potentially adhering to it) and returns to the near wall, forming a "fibrin horseshoe" with the maximum fibrin density located outside the aneurysm region. That is, the fibrin horseshoe grows both within the bulk of the flow and against the flow direction. In Fig. 8*b*, a periodic spatial variation of fibrin density along the aneurysm wall is also visible. Similarly, in Fig. 3*b* and 4*b*, the fibrin horseshoe in the center of the arteriole aneurysm reaches its maximum density (shown in red) near the left wall, confirming that fibrin growth occurs opposite to the direction of blood flow.

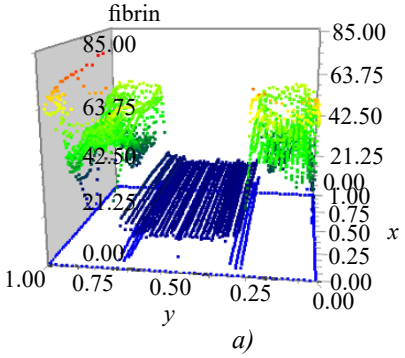

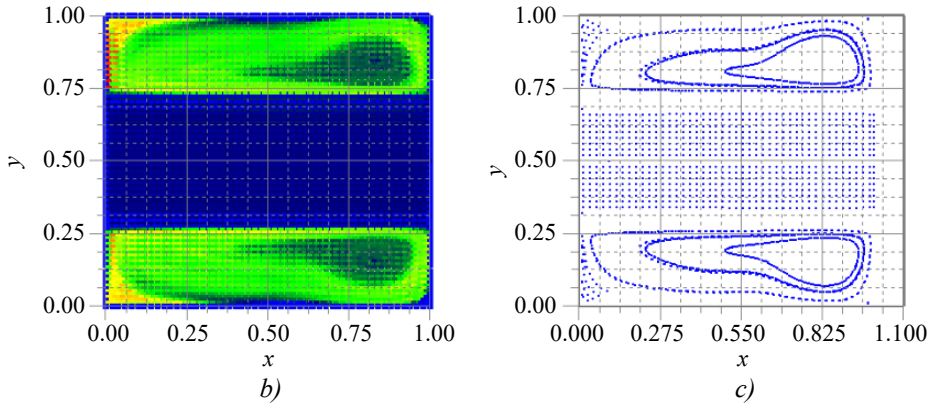

Fig. 9. Field distributions in the artery using (14.2) at $T = 2.54$ s

Re = 3000, $n_1 \times n_2 = 100 \times 50$, $\Delta / H = 0.5$; $L = 2\ cm, 2H = 2\ cm$, $u_{\max} = 0.5\ m/s$, $\tau = \frac{6}{16} h_1^2$, $m = 3387700$ steps,

splitting multiplicity $n = 200$ in (1), $N = 70$ in (13):

a — fibrin surface; *b* — fibrin distribution within the aneurysm; *c* — streamline field in the aneurysm

Fig. 9*b* shows that by $t = 2.54$ s, a homogeneous thrombus with a maximum dimensionless density of 85 units forms throughout the entire volume of the aneurysm (compared to Fig. 7*b*). The question of the threshold fibrin density is also crucial—the density at which it can be considered a solid body and impermeable to blood flow. In this case, blood must flow around the ultra-dense fibrin clots. It is equally important to obtain an experimental dependence of blood viscosity on the dimensionless fibrin density to account for it in the systems of equations (1) and (12).

Discussion

1. In the initial phase (Fig. 2*b* and 5*b*), fibrin forms in regions where the activator concentration exceeds the threshold and is transported to other parts of the aneurysm by advection and diffusion.

2. In arterioles, during the initial phase at $t = 1{,}333$ s (Fig. 2*a* and 2*b*), the maximum fibrin concentration (red tones) is observed near the aneurysm walls. However, at $t = 20$ s (Fig. 3*a* and 3*b*), a fibrin horseshoe appears, with maximum fibrin values in the central flow, approximately twice as high as near the wall.

3. In arteries with high blood velocity (Re = 3000) fibrin accumulates within the aneurysm, separating its boundaries from the blood flow by a “fibrin filament” (Fig. 6*b*).

4. Due to the nonlinear terms in systems (12) and (13), fibrin motion in arterioles (Re = 3.6) occurs against the flow (Fig. 3*b*), whereas in arteries (Re = 3000) it occurs in the direction of blood flow (Fig. 6*b*).

5. In Fig. 8*a* and 8*b*, near the aneurysm wall with low blood velocity, a spatial structure with periodic variations in fibrin density is observed. This result is consistent with [2–4], whose solutions can exhibit layered fibrin formation in stationary blood.

6. Fig. 3*b* and 6*b* show that even in the symmetry plane of the aneurysm, where fibrin density is minimal (blue tones), the value remains greater than zero. This indicates that the presence of an aneurysm causes blood densification and increased viscosity throughout the aneurysm, although solid fibrin does not form at every point.

7. The range of dimensionless fibrin in this study is of the same order as in [2–4], i. e., from 50 to 750 dimensionless units (in our examples, less than 500 dimensionless units).

8. Doubling the aneurysm diameter relative to the vessel diameter increases the Reynolds number (Re = 3000 in the artery) and, as seen in Fig. 6 and 7, generates a flow reversal point near the vortex core. Therefore, the presence of an aneurysm leads to velocity field discontinuities and an increase in vorticity in the vicinity of the flow reversal point.

Conclusion. This study presents the systems of equations (1), (12), and (13) with boundary and initial conditions (14), (15), (16), and (17), constituting a simplified unsteady model of blood flow and fibrin (thrombus) formation in aneurysms of blood vessels. The proposed model allows for a qualitative investigation of the mechanisms of thrombus formation in arterial and arteriolar aneurysms, as well as in components of medical devices.

References

1. Volosova N.K., Volosov K.A., Volosova A.K., Karlov M.I., Pastukhov D.F., Pastukhov Yu.F. Modelling circulation in the aneurysms of blood vessels. *Computation Mathematics and Information Technologies*. 2025;9(3):30–43. (In Russ.) https://doi.org/10.23947/2587-8999-2025-9-3-30-43

2. Ataulakhanov F.I., Guria G.T., Sorochkina A.Yu. Spatial aspects of the dynamics of blood coagulation. Phenomenological model. *Biophysics*. 1994;39(1):97−106. (In Russ.)

3. Lobanov A.I., Storozhilova T.K., Zarnitsyna V.I., Ataullakhanov F.I. Comparison of two mathematical models to describe the spatial dynamics of the blood coagulation process. *Mathematical modeling*. 2003;15(1):14−28. (In Russ.)

4. Volosov K.A., Vdovina E.K., Pugina L.V. Modeling of “pulsatile” modes of blood coagulation dynamics. *Math modeling*. 2014;26(12):14–32. (In Russ.)

5. Kalugina M.D., Limareva M.Yu., Lobanov A.I. Non-stacionary models of growth of platelet thrombus. *Russian Biomechanics Jornal.* 2024;26(4):179–188. (In Russ.) https://doi.org/10.15593/RZhBiomeh/2024.4.15

6. Petrov A.G. High-precision numerical schemes for solving plane boundary value problems for a polyharmonic equation and their application to problems of hydrodynamics. *Applied Mathematics and Mechanics*. 2023;87(3):343–368. (In Russ.) https://doi.org/10.31857/S0032823523030128

7. Sukhinov A.I., Kolgunova O.V., Girmai M.Z., Nakhom O.S. A two -dimensional hydrodynamic model of coastal systems, taking into account evaporation. *Computation Mathematics and Information Technologies*. 2023;7(4):9–21. (In Russ.) https://doi.org/10.23947/2587-8999-2023-7-4-9-21

8. Ershova T.Ya. Boundary value problem for a third-order differential equation with a strong boundary layer. *Bulletin of Moscow University. Episode 15: Computational mathematics and cybernetics*. 2020;1:30–39. (In Russ.) https://doi.org/10.3103/S0278641920010057

9. Sitnikova M.A., Skulsky O.I. Flow of momentary anisotropic fluid in thin layers. *Bulletin of Perm University. Mathematics. Mechanics. Informatics*. 2015;28(1):56–62. (In Russ.)

10. Sidoryakina V.V., Solomaha D.A. Symmetrized versions of the Seidel and upper relaxation methods for solving two-dimensional difference problems of elliptic. *Computational Mathematics and Information Technologies*. 2023;7(3):12–19. (In Russ.) https://doi.org/10.23947/2587-8999-2023-7-3-12-19

11. Volosova N.K., Volosov K.A., Volosova A.K., Karlov M.I., Pastuhov D.F., Pastuhov Yu.F. The *N*-fold distribution of the obvious variable scheme for the equalization of the vortex in the viscous incompatible fluid. *Bulletin of the Perm University. Mathematics. Mechanics. Informatics*. 2023; 63(4):12–21. (In Russ.) https://doi.org/10.17072/1993-0550-2023-4-12-21

12. Bahvalov N.S., Zhidkov N.P., Kobelkov G.M. *Numerical methods: a textbook for students of physics and mathematics specialties of higher educational institutions.* Binom. lab. Knowledge; 2011. 636 p. (In Russ.)

About the Authors:

Natalya K. Volosova, Post-graduate Student of Bauman Moscow State Technical University (2nd Baumanskaya St. 5–1, Moscow, 105005, Russian Federation), ORCID, navalosova@yandex.ru

Konstantin A. Volosov, Doctor of Physical and Mathematical Sciences, Professor of the Department of Applied Mathematics of the Russian University of Transport (Obraztsova St. 9–9, Moscow, GSP-4, 127994, Russian Federation), ORCID, SPIN-code, konstantinvolosov@yandex.ru

Aleksandra K. Volosova, Candidate of Physical and Mathematical Sciences, Chief Analytical Department “Tramplin” LLC, Russian University of Transport (Obraztsova St. 9–9, Moscow, GSP-4, 127994, Russian Federation), ORCID, SPIN-code, alya01@yandex.ru

Mikhail I. Karlov, Candidate of Physical and Mathematical Sciences, Associate Professor of the Department of Mathematics, Moscow Institute of Physics and Technology (9, Institutsky Lane, GSP-4, Dolgoprudny, 141701, Russian Federation), SPIN-code, karlov.mipt@gmail.com

Dmitriy F. Pastukhov, Candidate of Physical and Mathematical Sciences, Associate Professor of Polotsk State University (Blokhin St. 29, Novopolotsk, 211440, Republic of Belarus), ORCID, SPIN-code, dmitrij.pastuhov@mail.ru

Yuriy F. Pastukhov, Candidate of Physical and Mathematical Sciences,Associate Professor of Polotsk State University (Blokhin St. 29, Novopolotsk, 211440, Republic of Belarus), ORCID, SPIN-code, pulsar1900@mail.ru

Contributions of the authors:

N.K. Volosova: ideas; formulation or evolution of overarching research goals and aims; writing — original draft preparation; software.

K.A. Volosov: supervision; methodology.

A.K. Volosova: translation; study of the history of the task; literature.

M.I. Karlov: formal analysis.

D.F. Pastukhov: visualization; validation.

Yu.F. Pastukhov: testing of existing code components.

***Conflict of Interest Statement:* the authors declare no conflict of interest.**

All authors have read and approved the final manuscript.

Об авторах:

Наталья Константиновна Волосова, аспирант Московского государственного технического университета им. Н.Э. Баумана (105005, Российская Федерация, г. Москва, ул. 2-я Бауманская, 5, стр. 1), ORCID, navalosova@yandex.ru

Константин Александрович Волосов, доктор физико-математических наук, профессор кафедры прикладной математики Российского университета транспорта (127994, ГСП-4, Российская Федерация, г. Москва, ул. Образцова, 9, стр. 9), ORCID, SPIN-код, konstantinvolosov@yandex.ru

Александра Константиновна Волосова, кандидат физико-математических наук, начальник аналитического отдела ООО «Трамплин» Российского университета транспорта (127994, ГСП-4, Российская Федерация, г. Москва, ул. Образцова, 9, стр. 9), ORCID, SPIN-код, alya01@yandex.ru

Михаил Иванович Карлов, кандидат физико-математических наук, доцент кафедры математики Московского физико-технического института (141701, ГСП-4, Российская Федерация, г. Долгопрудный, Институтский переулок, 9), SPIN-код, karlov.mipt@gmail.com

Дмитрий Феликсович Пастухов, кандидат физико-математических наук, доцент кафедры технологий программирования Полоцкого государственного университета (211440, Республика Беларусь, г. Новополоцк, ул. Блохина, 29), ORCID, SPIN-код, dmitrij.pastuhov@mail.ru

Юрий Феликсович Пастухов, кандидат физико-математических наук, доцент кафедры технологий программирования Полоцкого государственного университета (211440, Республика Беларусь, г. Новополоцк, ул. Блохина, 29), ORCID, SPIN-код, pulsar1900@mail.ru

Заявленный вклад авторов:

Н.К. Волосова: постановка задачи; написание черновика рукописи; формулировка идей исследования, целей и задач; разработка программного обеспечения.

К.А. Волосов: научное руководство; разработка методологии.

А.К. Волосова: перевод; изучение истории задачи; поиск литературы.

М.И. Карлов: формальный анализ.

Д.Ф. Пастухов: визуализация; валидация.

Ю.Ф. Пастухов: тестирование существующих компонентов кода.

Конфликт интересов: **авторы заявляют об отсутствии конфликта интересов.**

Все авторы прочитали и одобрили окончательный вариант рукописи.

Received / Поступила в редакцию 27.08.2025
Reviewed / Поступила после рецензирования 25.09.2025
Accepted / Принята к публикации 21.10.2025

MATHEMATICAL MODELLING
МАТЕМАТИЧЕСКОЕ МОДЕЛИРОВАНИЕ

UDC 519.6

https://doi.org/10.23947/2587-8999-2025-9-4-38-45

Original Empirical Research

Mathematical Modelling of Suspension Uplift by Wind Gusts

Valentina V. Sidoryakina ✉, **Alexander E. Chistyakov**
Don State Technical University, 1, Gagarin Square, Rostov-on-Don, Russian Federation
✉ cvv9@mail.ru

Abstract

Introduction. The study of suspension uplift processes (e. g., particles of dust, sand, soil, etc.) by wind gusts in the surface layer is aimed at fundamentally understanding the mechanisms of wind erosion, dust storm formation, pollutant transport, and related phenomena. This area of scientific research has significant practical importance for combating desertification, erosion, drought, as well as for increasing crop yields and preserving natural ecosystems. Predicting these processes allows for the assessment and timely response to negative effects associated with them. The objective of this work is to propose and implement a mathematical model that enables numerical experiments with various scenarios of suspension uplift by wind gusts.

Materials and Methods. The paper presents a continuous mathematical model of multicomponent air medium motion in the atmospheric surface layer. The model accounts for factors such as turbulent mixing, variable density, Archimedes' force, tangential stress at media interfaces, etc. A distinctive feature of the mathematical model is the presence of suspension particles (their composition and aggregate state) in the air medium, as well as the influence of anthropogenic factors — suspension sources. The approach based on mathematical modelling aims to ensure the universality of the numerical implementation.

Results. The mathematical model has been implemented as a software package. Numerical experiments simulating the uplift of suspension by wind gusts in computational domains have been conducted.

Discussion. The results of this work can be in demand for a wide range of tasks related to human health protection, environmental safety, and land-use planning in arid and steppe regions of the country.

Conclusion. Further research by the authors may be directed towards modelling the movement of dust-laden air flows for natural landscapes containing forest plantations.

Keywords: wind gust, suspended matter, turbulent mixing, aerodynamics, mathematical model, numerical experiment

Funding. The study was supported by the Russian Science Foundation grant No. 22–11–00295–П. https://rscf.ru/en/project/22-11-00295/

For Citation. Sidoryakina V.V., Chistyakov A.E. Mathematical Modelling of Suspension Uplift by Wind Gusts. *Computational Mathematics and Information Technologies*. 2025;9(4):38–45. https://doi.org/10.23947/2587-8999-2025-9-4-38-45

Оригинальное эмпирическое исследование

Математическое моделирование подъема взвеси ветровыми порывами

В.В. Сидорякина ✉, **А.Е. Чистяков**
Донской государственный технический университет, г. Ростов-на-Дону, Российская Федерация
✉ cvv9@mail.ru

Аннотация

Введение. Изучение процесса подъема взвеси (например, частиц пыли, песка, почвы и др.) ветровыми порывами в приземном слое направлено на фундаментальное понимание механизмов ветровой эрозии, возникновения пыльных бурь, переноса загрязняющих веществ и др. Эта область научных исследований имеет важное практическое значение для борьбы с опустыниванием, эрозией, засухой, а также для повышения урожайности и сохранения природных экоси-

стем. Прогнозирование данных процессов позволяет оценивать и своевременно реагировать на негативные эффекты, связанные с данными процессами. Цель настоящей работы — предложить и реализовать математическую модель, которая позволит проводить численные эксперименты с различными сценариями подъема взвеси ветровыми порывами.
Материалы и методы. В работе представлена непрерывная математическая модель движения многокомпонентной воздушной среды в приземном слое атмосферы, которая учитывает такие факторы, как турбулентное перемешивание, переменную плотность, силу Архимеда, тангенциальное напряжение на границах раздела сред и др. Отличительной особенностью математической модели является присутствие в воздушной среде частиц взвеси (их состава и агрегатного состояния), а также влияние техногенных факторов — источников взвеси. Подход, основанный на математическом моделировании, призван обеспечить универсальность численной реализации.
Результаты исследования. Математическая модель реализована в виде комплекса программ. Проведены численные эксперименты, моделирующие подъем взвеси ветровыми порывами в расчетных областях.
Обсуждение. Результаты данной работы могут быть востребованы для широкого круга задач, связанных с охраной здоровья человека, экологической безопасностью и планированием природопользования в засушливых и степных регионах страны.
Заключение. Дальнейшие исследования авторов могут быть направлены на моделирование движения воздушного потока, содержащего пыль, для природных ландшафтов, содержащих лесонасаждения.

Ключевые слова: ветровой порыв, взвешенное вещество, турбулентное перемешивание, аэродинамика, математическая модель, численный эксперимент

Финансирование. Исследование выполнено за счет гранта Российского научного фонда № 22–11–00295–П. https://rscf.ru/project/22-11-00295/

Для цитирования. Сидорякина В.В., Чистяков А.Е. Математическое моделирование подъема взвеси ветровыми порывами. *Computational Mathematics and Information Technologies*. 2025; 9(4):38–45. https://doi.org/10.23947/2587-8999-2025-9-4-38-45

Introduction. The uplift of dust, sand, and other suspended particles in the lower atmospheric layers by wind gusts is a complex physical process. It depends on wind force (especially gusts), atmospheric turbulence, the physical characteristics of the particles, soil roughness and moisture, the presence of vegetation cover, and other factors. Upon reaching a critical (threshold) velocity, wind can “pick up” dust, sand, and fine soil particles and transport them over long distances, thereby destroying the upper fertile soil layer and causing wind erosion. One of the vivid manifestations of wind erosion is associated with the formation of dust storms.

Dust storms, combined with strong winds in southern Russia (primarily in the Rostov, Volgograd, and Astrakhan regions, Krasnodar and Stavropol territories), are caused by a combination of the following factors: intense heat, which dries out the soil; wind intensification up to 12–15 m/s, which lifts and transports dust and sand particles; vast expanses of plowed land not covered by vegetation. Seasonally, dust storms occur in early spring and early autumn (their greatest intensity is observed in the second half of the year, specifically in September and October), which is associated with low atmospheric precipitation, soil moisture loss, and a high degree of land plowing. The main and long-term cause is the disappearance of protective forest belts that could restrain the wind, as well as the influx of hot air masses from neighboring desert regions, such as Kalmykia. Here, in zones with semi-desert and desert landscapes, conditions are created for the transport of dust-sand and aerosol material to neighboring regions. The scale and cyclicity of these phenomena have increased in recent years.

In this context, predicting the processes of air mass movement containing dust and fine sand particles, and identifying areas at high risk of wind erosion, becomes relevant. Therefore, the experience of Russian and foreign researchers and their teams, who have applied both fundamental physical models (Euler-Lagrange, Discrete Phase Model — DPM) and modern software packages (ANSYS Fluent, COMSOL, etc.), is interesting and useful [1–5]. The vast majority of research focuses on specific regions and territories, which is related to specific meteorological conditions, local data on topography and soil types, unique dust sources, etc. For Southern Russia, studies on this topic are reflected in the works of scientists from the Southern Mathematical Institute of the Vladikavkaz Scientific Center of the Russian Academy of Sciences, Southern Federal University, Don State Technical University, and others [6–10].

The authors propose for consideration a mathematical model that will allow conducting numerical experiments with various scenarios of dust-laden airflow movement. The work emphasizes modeling the turbulence of the airflow caused by the wind structure, which contributes to the uplift of suspended matter particles from the earth›s surface and is the main cause of dust storm formation. The mathematical model has been implemented as a software package. Numerical experiments have been conducted, simulating wind gusts in the lower atmospheric layers with the uplift and transport of suspension by ascending turbulent flows in computational domains.

Materials and Methods

Mathematical Model of Suspension Propagation in the Atmospheric Surface Layer. The authors consider a comprehensive mathematical model describing the processes of air medium motion and suspension propagation within it, which includes [9, 10]:

– a model of multicomponent air medium motion (defining the velocity field of the air medium), accounting for turbulent exchange, variable density, and the dependence of air medium density on pressure,

– a model of suspension propagation in the air medium, accounting for the phase transition of water from liquid to gaseous state and vice versa, and substance transport,

– a pressure calculation model, accounting for medium compressibility, suspension sources associated with the phase transition of water from liquid to gaseous state and vice versa, as well as turbulent mixing of the multicomponent air medium.

Let us formulate the equations of the multicomponent air medium motion model in the coordinate system $Ox_1x_2x_3$:

– motion equation (Navier-Stokes equations):

$$\frac{dv_j}{dt} = -\frac{1}{\rho}\frac{\partial p}{\partial x_j} + div\left(\mu grad\left(v_j\right)\right) - g_i; \tag{1}$$

– substance transport equation:

$$\frac{\partial \rho}{\partial t} + div\left(\rho\vec{v}\right) = div\left(\mu grad\left(\rho\right)\right) + I_\rho; \tag{2}$$

– equation of state:

$$P = \sum_i \frac{\rho_i}{M_i} RT; \tag{3}$$

– impurity transport equation:

$$\frac{d\varphi_i}{dt} = div\left(\mu grad\left(\varphi_i\right)\right) + I_\varphi; \tag{4}$$

– turbulence model equation:

$$v_{SGS} = \left(C_S\Delta\right)^2 S. \tag{5}$$

In equations (1–5), the following notations are used: t is the temporal variable; v_j ($j = 1, 2, 3$) are the components of the air medium velocity vector $\vec{v}$; p is the pressure; μ is the turbulent exchange coefficient; ρ is the density of the air medium; ρ_i is the density of the i-th phase ($i = 0$ — air, 1 — water in gaseous state, 2 — gas at the source, 3 — water in liquid state, 4 — soot); φ_i are the volume fractions of the i-th phase; I is a function describing the distribution and power of suspension sources; R is the universal gas constant, M is the molar mass, T is the temperature of the gas phase.

To simplify computational calculations for the discrete analogues of the model equations, a transition from 3D to 2D equations is performed. Consider the 3D convection-diffusion-reaction equation:

$$\frac{\partial \rho}{\partial t} + \frac{\partial\left(\rho v_1\right)}{\partial x_1} + \frac{\partial\left(\rho v_2\right)}{\partial x_2} + \frac{\partial\left(\rho v_3\right)}{\partial x_3} = \frac{\partial}{\partial x_1}\left(\mu\frac{\partial \rho}{\partial x_1}\right) + \frac{\partial}{\partial x_2}\left(\mu\frac{\partial \rho}{\partial x_2}\right) + \frac{\partial}{\partial x_3}\left(\mu\frac{\partial \rho}{\partial x_3}\right) + I_\rho. \tag{6}$$

Equation (6) is supplemented with corresponding boundary conditions [9].

As a result of transformations, we obtain:

$$\varepsilon\frac{\partial \rho}{\partial t} + \frac{\partial\left(\varepsilon\rho v_1\right)}{\partial x_1} + \frac{\partial\left(\varepsilon\rho v_3\right)}{\partial x_3} = \frac{\partial}{\partial x_1}\left(\mu\varepsilon\frac{\partial \rho}{\partial x_1}\right) + \frac{\partial}{\partial x_3}\left(\mu\varepsilon\frac{\partial \rho}{\partial x_3}\right) - \frac{\tau}{\rho}\Big|_{x_{2(a)}}^{x_{2(b)}} + \varepsilon I_\rho, \tag{7}$$

where ε is a parameter describing the relative volume of the computational domain free from plants.

Two-Dimensional Mathematical Model of Atmospheric Surface Layer Aerodynamics. Let us further assume $x_1 = x$, $x_2 = y$, $x_3 = z$, and for the components of the air medium velocity vector $\vec{v}$ — $v_1 = u$, $v_2 = v$, $v_3 = w$.

Consider the basic equations of air medium dynamics:

– system of Navier-Stokes equations:

$$\begin{aligned} \varepsilon u'_t + u\varepsilon u'_x + v\varepsilon u'_z &= -\frac{1}{\rho}\left(\varepsilon P\right)'_x + \left(\mu\varepsilon u'_x\right)'_x + \left(\mu\varepsilon u'_z\right)'_z + \varepsilon f_x, \\ \varepsilon w'_t + u\varepsilon w'_x + w\varepsilon w'_z &= -\frac{1}{\rho}\left(\varepsilon P\right)'_z + \left(\mu\varepsilon v'_x\right)'_x + \left(\mu\varepsilon w'_z\right)'_z + \varepsilon f_z; \end{aligned} \tag{8}$$

– continuity equation:

$$\varepsilon\rho'_t + \left(\varepsilon\rho u\right)'_x + \left(\varepsilon\rho w\right)'_z = \left(\varepsilon\mu\rho'_x\right)'_x + \left(\varepsilon\mu\rho'_z\right)'_z + \varepsilon I_\rho; \tag{9}$$

– equation of state:

$$P = \sum_i \frac{\rho_i}{M_i} RT, \tag{10}$$

where ε is a parameter describing the relative volume of the modeled area free from plants.

Assuming the air medium is initially at rest, the initial conditions are:

$$u = 0,\ w = 0,\ P = P_a,$$

where $\vec{v} = \{u, w\}$, P_a is atmospheric pressure.

The system of equations (8)–(10) is considered under the following boundary conditions:

– on an impermeable boundary:

$$\rho_w \eta u'_n = \tau_{x,b}(t),\ \rho_w \eta v'_n = \tau_{z,b}(t),\ \overline{V}_n = 0, P'_n = 0,\ P'_n = 0;$$

– on lateral permeable boundaries:

$$u'_n = 0,\ w'_n = 0,\ P'_n = 0;$$

– on the source:

$$u = U,\ w = W,\ P'_n = 0,$$

where P is the pressure; U, W are the components of the velocity vector at the source; τ_x, τ_z are the components of tangential shear stress.

Splitting Schemes for Physical Processes in Solving Aerodynamic Problems. According to the pressure correction method, the original hydrodynamic model is split into three subproblems [11–14].

The first subproblem is represented by the convection-diffusion-reaction equation, based on which the components of the velocity field at an intermediate time layer are calculated:

$$\begin{aligned} \varepsilon\frac{\tilde{u} - u}{h_t} + u\varepsilon\overline{u}'_x + w\varepsilon\overline{u}'_z &= \left(\mu\varepsilon\overline{u}'_x\right)' + \left(\mu\varepsilon\overline{u}'_z\right)', \\ \varepsilon\frac{\tilde{w} - w}{h_t} + u\varepsilon\overline{w}'_x + w\varepsilon\overline{w}'_z &= \left(\mu\varepsilon\overline{w}'_x\right)' + \left(\mu\varepsilon\overline{w}'_z\right)'. \end{aligned} \tag{11}$$

For the temporal approximation of the convection-diffusion-reaction equation, weighted schemes are used. Here $\overline{u} = \sigma\tilde{u} + (1-\sigma)u$; $\sigma \in [0,1]$ is the scheme weight.

Let us describe the boundary conditions for system (11):

– on an impermeable boundary:

$$\rho_w \eta u'_n = \tau_{x,b}(t),\ \rho_w \eta v'_n = \tau_{z,b}(t);$$

– on lateral permeable boundaries:

$$u'_n = 0,\ w'_n = 0;$$

– on the source:

$$u = U,\ w = W,\ P'_n = 0.$$

The second subproblem allows for the calculation of the pressure distribution

$$\left(\varepsilon P'_x\right)'_x + \left(\varepsilon P'_z\right)'_z = \varepsilon\frac{\hat{\rho} - \rho}{h_t^2} + \frac{\left(\overline{\rho}\varepsilon\tilde{u}\right)'_x}{h_t} + \frac{\left(\overline{\rho}\varepsilon\tilde{w}\right)'_z}{h_t}$$

or

$$\varepsilon\frac{\hat{P} - P}{h_t} + \left(\varepsilon\overline{P}\tilde{u}\right)'_x + \left(\varepsilon\overline{P}\tilde{w}\right)'_z = kh_t\left(\left(\varepsilon\overline{P}'_x\right)'_x + \left(\varepsilon\overline{P}'_z\right)'_z\right),\ k = \frac{RT}{\mathrm{M}}. \tag{12}$$

The third subproblem allows for the determination of the velocity distribution at the new time level using explicit formulas:

$$\varepsilon\frac{\hat{u} - \tilde{u}}{h_t} = -\frac{1}{\rho}\left(\varepsilon\overline{P}\right)'_x,\ \varepsilon\frac{\hat{w} - \tilde{w}}{h_t} = -\frac{1}{\rho}\left(\varepsilon\overline{P}\right)'_z, \tag{13}$$

where h_t is the step in the temporal coordinate; u is the velocity field value at the previous time level; $\tilde{u}$ is the velocity field value at the intermediate time level; $\hat{u}$ is the value at the current time level.

Multiplying the system of equations (13) by $h_t\rho$ and differentiating with respect to the variables *x, y, z* respectively, we obtain:

$$\left(\varepsilon\rho\hat{u}\right)'_x = \left(\varepsilon\rho\tilde{u}\right)'_x - \varepsilon h_t P''_{xx}, \quad \left(\varepsilon\rho\hat{w}\right)'_z = \left(\varepsilon\rho\tilde{w}\right)'_z - \varepsilon h_t P''_{zz}. \tag{14}$$

Using expressions (14) to transform equation (9), we get:

$$\varepsilon\rho'_t + \left(\varepsilon\rho\tilde{u}\right)'_x - \varepsilon h_t P''_{xx} + \left(\varepsilon\rho\tilde{w}\right)'_z - \varepsilon h_t P''_{zz} = \left(\varepsilon\mu\rho'_x\right)'_x + \left(\varepsilon\mu\rho'_z\right)'_z + \varepsilon I_\rho. \tag{15}$$

Taking into account the equation of state, expression (15) takes the form:

$$\varepsilon\frac{\rho}{P}\frac{\partial P}{\partial t} = \varepsilon h_t P''_{xx} + \varepsilon h_t P''_{zz} - \left(\varepsilon\rho\tilde{u}\right)'_x - \left(\varepsilon\rho\tilde{w}\right)'_z + \left(\varepsilon\mu\rho'_x\right)'_x + \left(\varepsilon\mu\rho'_z\right)'_z + \varepsilon I_\rho. \tag{16}$$

The pressure field is computed based on equation (16). It should be noted that the pressure calculation accounts for medium compressibility, thermal expansion, substance sources associated with the phase transition of water from liquid to gaseous state and vice versa, as well as turbulent mixing of the multicomponent air medium.

The construction of finite-difference schemes approximating the considered equations (16) has been performed on hydrodynamic grids using methods described in works [15, 16] and is not presented in this article.

Results. Based on the developed algorithms, a software package was created for the numerical simulation of suspension uplift by wind gusts in a multicomponent air medium. A series of numerical experiments was conducted.

Figures 1 and 2 present the results of a numerical experiment simulating air medium motion under wind gusts. The model domain has dimensions of 30 m × 50 m. The input data are: air medium density 1.29 kg/m³; atmospheric pressure 100 kPa; wind gust speed 10 m/s, wind direction — from left to right. Computational grids with a step of 10 meters in each coordinate direction were used to solve the problem. The temporal step was 0.1 s, and the total simulation time interval was 100 s.

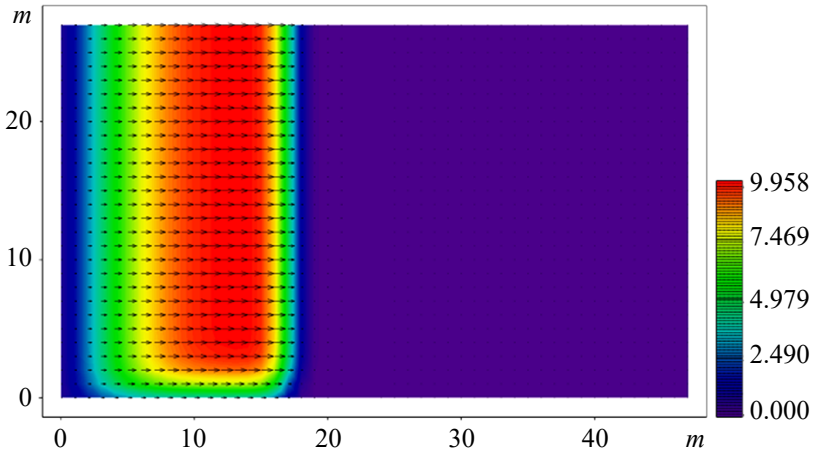

Fig. 1. Image of the initial simulation moment for calculating air medium velocity. Horizontal cross-section

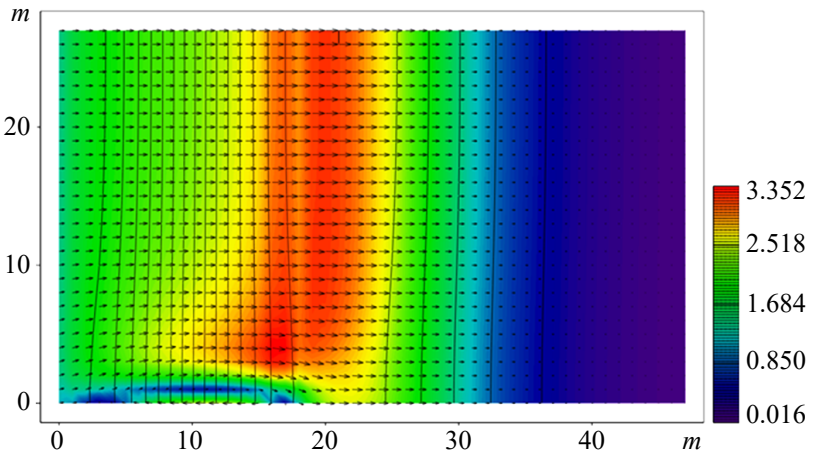

Fig. 2. Simulation result of air medium velocity. Horizontal cross-section

In Fig. 1 and 2, the intensity of air medium motion in m/s is represented according to the color palette. Fig. 2 demonstrates the presence of a vortex in its lower left part, which may be associated with the motion of a flow at different speeds at the

interface between air layers, as well as with the terrain relief (vortex flows often arise due to the “repulsion” of air masses from the surface). The vortex nature of atmospheric flows is observed near the surface and gradually diminishes with height. This leads to the formation of a stable density gradient. The airflow in the surface layer becomes stably stratified, and the vortices weaken. As a result, the flow velocity increases.

Next, we present the results of modeling suspension uplift under wind gusts. The input data are: air medium density 1.29 kg/m³; emission density 1.4 kg/m³; ambient temperature 20 °C; air medium flow velocity 10 m/s; specific emission power 5 L/s. Computational grids with dimensions of 30 m × 50 m were used to solve the model problem. The steps in the spatial variables are 1 m, and the air medium velocity on the left boundary was set to 1 m/s. Weighted schemes were applied to solve the model problem, with the scheme weight set to 0.5. The temporal step was 0.1 s, and the total simulation time interval was 10 s.

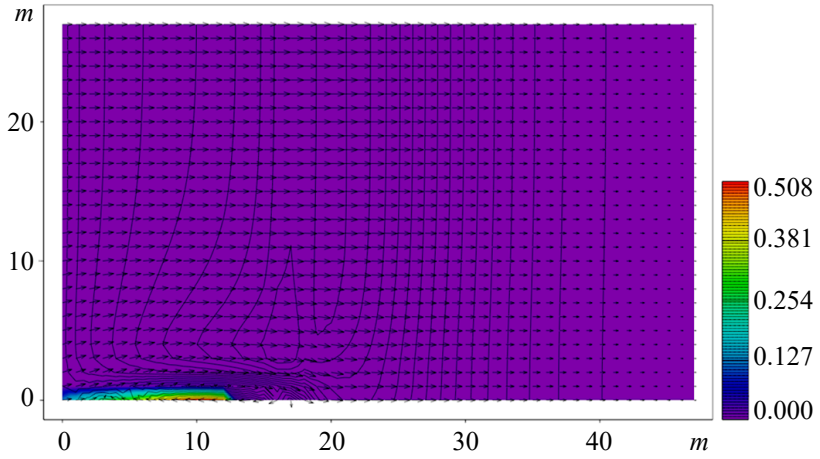

Fig. 3. Image of the initial simulation moment for calculating suspended matter concentration

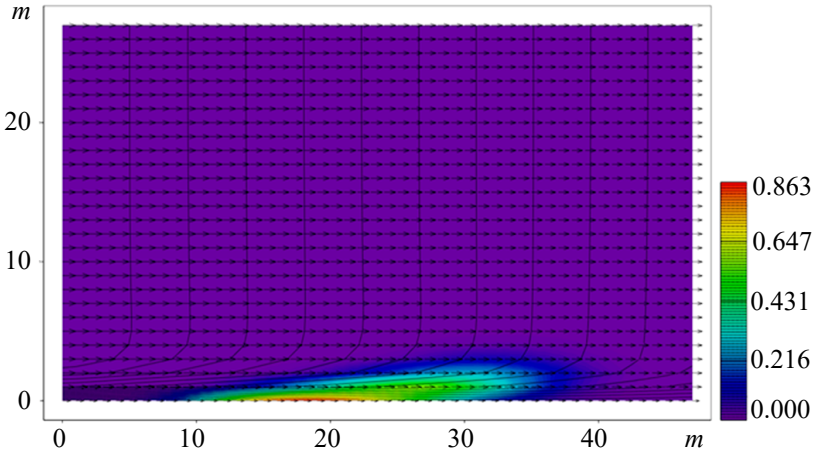

Fig. 4. Simulation results for calculating suspended matter concentration 10 seconds after the start of the simulation

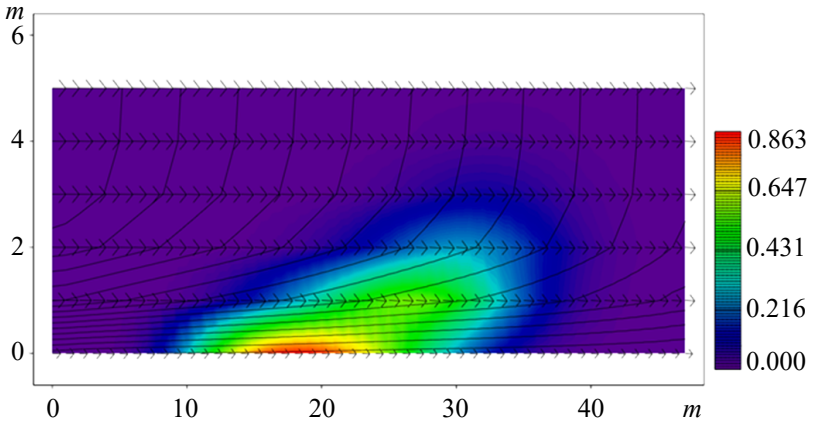

Fig. 5. Simulation results for calculating suspended matter concentration 10 seconds after the start of the simulation — zoom into the substance propagation zone

The color palette in Fig. 3–5 indicates the concentration of suspended matter in the atmospheric surface layer. The simulation results demonstrate the propagation of the impurity in the direction of air medium motion over tens of meters; the impurity uplift exceeded 5 m.

Discussion. The results of this work can be applied to a wide range of tasks related to human health protection, environmental safety, and land-use planning in arid and steppe regions of the country.

Conclusion. Further research by the authors may focus on modeling the movement of dust-laden airflows in natural landscapes containing forest plantations.

References

1. Zhou X.H., Brandle J.R., Takle E.S., Mize C.W. Estimation of the three-dimensional aerodynamic structure of a green ash shelterbelt. *Agricultural and Forest Meteorology.* 2002;111(2):93–108. https://doi.org/10.1016/S0168-1923(02)00017-5

2. Bannister E.J., MacKenzie A.R., Cai X.-M. Realistic Forests and the Modeling of Forest-Atmosphere Exchange. *Reviews of Geophysics*. 2022;60(1):e2021RG000746. https://doi.org/10.1029/2021RG000746

3. Xu X., Yi C., Kutter E. Stably stratified canopy flow in complex terrain. *Atmospheric Chemistry and Physics*. 2015;15(13):7457–7470. https://doi.org/10.5194/acp-15-7457-2015

4. Yan C., Miao S., Liu Y., Cui G. Multiscale modeling of the atmospheric environment over a forest canopy. *Science China Earth Sciences.* 2020;63:875–890. https://doi.org/10.1007/s11430-019-9525-6

5. Zeng P., Takahashi H. A first-order closure model for the wind flow within and above vegetation canopies. *Agricultural and Forest Meteorology*. 2000;103(3):301–313. https://doi.org/10.1016/S0168-1923(00)00133-7

6. Sukhinov A.I., Protsenko E.A., Chistyakov A.E., Shreter S.A. Comparison of computational efficiencies of explicit and implicit schemes for the problem of sediment transport in coastal water systems. In: *Parallel computing technologies (PaVT'2015). Proceedings of the international scientific conference* (Ekaterinburg, March 31 – April 2, 2015). Editors: L.B. Sokolinsky, K.S. Pan. Chelyabinsk: Publishing center of SUSU, 2015. Pp. 297–307. (In Russ.)

7. Sukhinov A.I., Chistyakov A.E., Protsenko E.A. Two-dimensional hydrodynamic model taking into account the dynamic restructuring of the bottom geometry of a shallow reservoir. *Bulletin of SFedU. Engineering sciences*. 2011;8(121):159–167. (In Russ.)

8. Kamenetsky E.S., Radionoff A.A., Timchenko V.Yu., Panaetova O.S. Mathematical Modelling of Dust Transfer from the Tailings in the Alagir Gorge of the RNO-Alania. *Computational Mathematics and Information Technologies*. 2023;7(4):22–29. (In Russ.) https://doi.org/10.23947/2587-8999-2023-7-4-22-29

9. Sukhinov A.I., Khachunts D.S., Chistyakov A.E. A mathematical model of pollutant propagation in near-ground atmospheric layer of a coastal region and its software implementation. *Computational Mathematics and Mathematical Physics.* 2015;55(7):1216–1231. https://doi.org/10.1134/S096554251507012X

10. Belova Yu.V., Protsenko E.A., Atayan A.M., Kurskaya I.A. Simulation of coastal aerodynamics taking into account forest plantations. *Computational Mathematics and Information Technologies*. 2018;2(2):91–105. (In Russ.) https://doi.org/10.23947/2587-8999-2018-2-2-91-105

11. Sukhinov A.I., Chistyakov A.E., Sidoryakina V.V. Parallel solution of sediment and suspension transportation problems on the basis of explicit schemes. *Communications in Computer and Information Science*. 2018;910:306–321. https://doi.org/10.1007/978-3-319-99673-8_22

12. Sidoryakina V.V., Sukhinov A.I., Chistyakov A.E., Protsenko E.A., Protsenko S.V. Parallel algorithms for solving the problem of bottom relief change dynamics in coastal systems. *Computational Methods and Programming*. 2020;21(3):196–206. (In Russ.) https://doi.org/10.26089/NumMet.v21r318

13. Sukhinov A.I., Sidoryakina V.V. Development and correctness analysis of the mathematical model of transport and suspension sedimentation depending on bottom relief variation. *Vestnik of Don State Technical University*. 2018;18(4):350–361. https://doi.org/10.23947/1992-5980-2018-18-4-350-361

14. Sukhinov A.I., Chistyakov A.E., Sidoryakina V.V., Protsenko S.V., Atayan A.M. Locally two-dimensional splitting schemes for parallel solving of the three-dimensional problem of suspended substance transport. *Mathematical Physics and Computer Simulation*. 2021;24(2):38–53. (In Russ.) https://doi.org/10.15688/mpcm.jvolsu.2021.2.4

15. Sidoryakina V.V., Sukhinov A.I. Construction and analysis of the proximity of solutions in L2 for two boundary problems in the model of multicomponent suspension transport in coastal systems. *Journal of Computational Mathematics and Mathematical Physics*. 2023;63(10):1721–1732. (In Russ.) https://doi.org/10.1134/S0965542523100111

16. Litvinov V.N., Chistyakov A.E., Nikitina A.V., Atayan A.M., Kuznetsova I.Yu. Mathematical modeling of hydrodynamics problems of the Azov Sea on a multiprocessor computer system. *Computer Research and Modeling*. 2024;16(3):647–672. (In Russ.) https://doi.org/10.20537/2076-7633-2024-16-3-647-672

About the Authors:

Valentina V. Sidoryakina, Candidate of Physical and Mathematical Sciences, Associate Professor, Department of Mathematics and Informatics, Don State Technical University (1, Gagarin Sq., Rostov-on-Don, 344003, Russian Federation), ORCID, SPIN-code, ResearcherID, MathSciNet, ScopusID, cvv9@mail.ru

Alexander E. Chistyakov, Doctor of Physical and Mathematical Sciences, Professor, Professor of the Department of Software for Computer Engineering and Automated Systems, Don State Technical University (1, Gagarin Sq., Rostov-on-Don, 344003, Russian Federation), ORCID, SPIN-code, ResearcherID, MathSciNet, ScopusID, cheese_05@mail.ru

Contributions of the authors:

V.V. Sidoryakina: formulation of the results and description of their significance, article design.

A.E. Chistyakov: general scientific supervision; problem statement; formulation of research ideas, goals, and objectives; methodology development; derivation of calculation formulas; and numerical experiment execution.

Conflict of Interest Statement: **the authors declare no conflict of interest.**

All authors have read and approved the final manuscript.

Об авторах:

Валентина Владимировна Сидорякина, кандидат физико-математических наук, доцент, кафедры математики и информатики Донского государственного технического университета (344003, Российская Федерация, г. Ростов-на-Дону, пл. Гагарина, 1), ORCID, SPIN-код, ResearcherID, MathSciNet, ScopusID, cvv9@mail.ru

Чистяков Александр Евгеньевич, доктор физико-математических наук, профессор кафедры программного обеспечения вычислительной техники и автоматизированных систем Донского государственного технического университета (344003, Российская Федерация, г. Ростов-на-Дону, пл. Гагарина, 1), ORCID, SPIN-код, ResearcherID, MathSciNet, ScopusID, cheese_05@mail.ru

Заявленный вклад авторов:

В.В. Сидорякина: формулировка достигнутых результатов и описание их значимости, оформление материала статьи.

А.Е. Чистяков: общее научное руководство; постановка задачи; формулировка идей исследования, целей и задач, разработка методологии, получение расчетных формул и проведение численного эксперимента.

Конфликт интересов: **авторы заявляют об отсутствии конфликта интересов.**

Все авторы прочитали и одобрили окончательный вариант рукописи.

Received / Поступила в редакцию 29.10.2025
Reviewed / Поступила после рецензирования 14.11.2025
Accepted / Принята к публикации 15.12.2025

MATHEMATICAL MODELLING
МАТЕМАТИЧЕСКОЕ МОДЕЛИРОВАНИЕ

UDC 004.942:532.1

Original Empirical Research

https://doi.org/10.23947/2587-8999-2025-9-4-46-55

Mathematical Modelling of the Bioproductivity of a Shallow Water Body under Sudden Depression Caused by Scyphozoan Jellyfish

Denis V. Bondarenko, Alla V. Nikitina
Don State Technical University, Rostov-on-Don, Russian Federation
✉ denis.bondarenko.dev@gmail.com

Abstract

Introduction. The relevance of this study is determined by the need for a quantitative assessment of the negative impact of mass outbreaks of scyphozoan jellyfish (*Aurelia aurita* and *Rhizostomeae*) on the bioresources of the Azov Sea, which is subjected to a complex combination of anthropogenic pressures. The theoretical framework of the research is based on the concept of trophic interactions and biological invasions in marine ecosystems. The aim of this study is to develop a mathematical model of the dynamics of the fish community in the Azov Sea that accounts for both competitive and predatory pressure exerted by jellyfish, in order to identify critical biomass thresholds leading to the depression of commercial fish stocks.

Materials and Methods. To investigate the influence of scyphozoan jellyfish on the bioresources of the Azov Sea, a mathematical model of biological kinetics was employed as the primary research tool. The model describes the dynamics of three key ecosystem components (zooplankton, fish, and jellyfish), incorporating mechanisms of competition and predation. The research material consists of a system of theoretical equations with appropriate interaction parameters and initial and boundary conditions.

Results. Numerical simulations demonstrated that under environmental conditions typical of the summer period in the Azov Sea (elevated water temperature and eutrophication), an increase in scyphozoan jellyfish biomass by more than threefold during July–August leads to an abrupt shift of the ecosystem to an alternative stable state dominated by jellyfish. This transition is driven by the combined effects of intense competition for zooplankton and direct predation by jellyfish on the early life stages of fish, and is accompanied by a critical reduction in food availability, which suppresses the recovery of commercial fish populations.

Discussion. The results confirm the high ecological significance of mass aggregations of scyphozoan jellyfish and provide a quantitative justification for the risk of a regime shift in the Azov Sea ecosystem toward an alternative, less productive state dominated by jellyfish. From a theoretical perspective, the study contributes to the development of trophic interaction models that incorporate multiple impact mechanisms of invasive species.

Conclusion. The practical significance of this work lies in the fact that the proposed model serves as a tool for predictive assessment of bioresource status and for substantiating management decisions aimed at mitigating the consequences of eutrophication and biological invasions. Future research will focus on further refinement of the model, including the incorporation of seasonal and climatic factors to improve the accuracy of long-term forecasts.

Keywords: mathematical modelling, bioproductivity, Azov Sea, scyphozoan jellyfish, trophic interactions, alternative stable states, ecological forecasting

Funding. The study was supported by grant No. 22–11–00295–П from the Russian Science Foundation, https://rscf.ru/project/22-11-00295/

For Citation. Bondarenko D.V., Nikitina A.V. Mathematical modelling of the bioproductivity of a shallow water body under sudden depression caused by scyphozoan jellyfish. *Computational Mathematics and Information Technologies*. 2025;9(4):46–55. https://doi.org/10.23947/2587-8999-2025-9-4-46-55

Оригинальное эмпирическое исследование

Математическое моделирование биопродуктивности мелководного водоема при внезапной депрессии сцифоидными медузами

Д.В. Бондаренко ✉, **А.В. Никитина**
Донской государственный технический университет, г. Ростов-на-Дону, Российская Федерация
✉ denis.bondarenko.dev@gmail.com

Аннотация

Введение. Актуальность исследования обусловлена необходимостью количественной оценки негативного влияния массового развития сцифоидных медуз (*Aurelia aurita* и *Rhizostomeae*) на биоресурсы Азовского моря, испытывающего комплекс антропогенных нагрузок. Теоретической основой для решения данной проблемы выступает концепция трофических взаимодействий и инвазий в морских экосистемах. Целью настоящей работы является разработка математической модели динамики рыбного сообщества Азовского моря, учитывающей конкурентное и хищническое давление со стороны медуз, для оценки критических порогов его биомассы, приводящих к депрессии промысловых запасов.

Материалы и методы. Для исследования влияния сцифомедуз на биоресурсы Азовского моря в качестве основного инструмента использована математическая модель биологической кинетики, описывающая динамику трёх ключевых компонентов (зоопланктон, рыбы, медузы) с учётом конкуренции и хищничества. Материалом исследования выступали теоретические уравнения системы с соответствующими параметрами взаимодействий и начально-краевыми условиями.

Результаты исследования. Результаты численного моделирования показали, что при характерных для летнего сезона условиях в Азовском море (высокая температура, эвтрофикация) прирост биомассы сцифомедуз более чем в три раза за период июль-август приводит к резкому переходу экосистемы в альтернативное устойчивое состояние с их доминированием. Этот переход обусловлен комбинированным эффектом интенсивной конкуренции за зоопланктон и прямого хищничества медуз на ранних стадиях развития рыб и сопровождается критическим снижением доступности кормовой базы, что подавляет восстановление промысловых рыбных популяций.

Обсуждение. Проведённое исследование подтверждает высокую экологическую значимость массовых скоплений сцифомедуз и количественно обосновывает риск перехода экосистемы Азовского моря в альтернативное, менее продуктивное состояние, доминируемое медузами. С теоретической точки зрения работа вносит вклад в развитие моделей трофических взаимодействий с учётом множественных механизмов воздействия инвазионных видов.

Заключение. Практическая значимость работы заключается в том, что разработанная модель представляет собой инструмент для прогнозной оценки состояния биоресурсов и обоснования управленческих решений, направленных на смягчение последствий эвтрофикации и биологических инвазий. Перспективы исследования связаны с дальнейшей детализацией модели и включением в неё сезонных и климатических факторов для повышения точности долгосрочных прогнозов.

Ключевые слова: математическое моделирование, биопродуктивность, Азовское море, сцифоидные медузы, трофические взаимодействия, альтернативные устойчивые состояния, экологический прогноз

Финансирование. Исследование выполнено за счет гранта Российского научного фонда № 22–11–00295–П, https://rscf.ru/project/22-11-00295/

Для цитирования. Бондаренко Д.В., Никитина А.В. Математическое моделирование биопродуктивности мелководного водоема при внезапной депрессии сцифоидными медузами. *Computational Mathematics and Information Technologies*. 2025;9(4):46–55. https://doi.org/10.23947/2587-8999-2025-9-4-46-55

Introduction. The Azov Sea is one of the shallowest seas in the world and plays a key role in the fisheries and ecological system of southern Russia. Over recent decades, its ecosystem has been subjected to substantial pressures, including eutrophication, changes in river runoff, pollution, and invasions of alien species [1]. One of the most pronounced recent trends is the mass development of scyphozoan jellyfish, primarily Aurelia aurita and representatives of the order Rhizostomeae. Owing to their high reproductive potential and ecological plasticity, these jellyfish form extensive aggregations in coastal waters during the spring–summer period. In certain years, their total biomass reaches thousands of tons, exerting significant pressure on trophic networks [2].

Under such conditions, it is reasonable to speak of a sudden depression of the water body caused by scyphozoan jellyfish and their impact on the bioproductivity of the aquatic ecosystem. Fig. 1 illustrates aggregations of scyphozoan jellyfish observed in the Azov Sea.

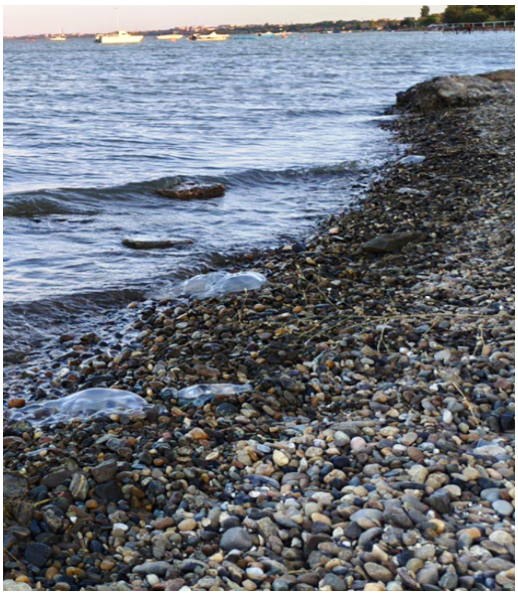

Fig. 1. Coast of the Yeysk Estuary with jellyfish, July 2025

Scyphozoan jellyfish may pose a danger to humans, as contact with their tentacles can cause skin burns, itching, or irritation. Scyphozoan jellyfish (class *Scyphozoa*, phylum *Cnidaria*) are marine organisms characterized by the presence of stinging cells (cnidocytes), which they use for predation and defense. The class comprises a relatively small number of species, approximately 200 in total. Their life cycle is characterized by metagenesis, including an asexual (polypoid) stage and a sexual (medusoid) stage. The medusae of some species reach large sizes and are capable of forming massive aggregations, whereas scyphozoan polyps (scyphistomae) are extremely small, typically only a few millimeters in size.

Common scyphozoan jellyfish species found in the seas of Russia include the moon jellyfish (*Aurelia aurita*), the lion's mane jellyfish (*Cyanea capillata*), and the barrel jellyfish (*Rhizostoma pulmo*). Some scyphozoan species, such as the so-called "sea wasp", are particularly dangerous: contact causes intense pain and burning sensations comparable to a whip strike. Severe pain shock may lead to loss of consciousness, followed by symptoms of intoxication such as dry mouth and breathing difficulties; in rare cases, stings may be fatal.

In the Azov Sea, *Aurelia* aurita and *Rhizostomeae* actively consume zooplankton, including copepods and larvae of crustaceans and mollusks, which constitute the primary food source for juvenile and planktivorous fish species such as Baltic herring, roach, and juvenile pikeperch. This results in intense competition for food resources. In addition, jellyfish exhibit direct predation on fish eggs and larvae. Field observations indicate that at high abundances, jellyfish may consume up to 10–30% of the daily ration of fish larvae [3]. Despite the availability of biological observations, a quantitative assessment of the impact of jellyfish on fish stocks remains insufficient [4–7].

This study presents a mathematical model describing the dynamics of a fish community while explicitly accounting for competitive and predatory pressure exerted by jellyfish. The model enables the estimation of critical jellyfish biomass thresholds at which the productivity of valuable and commercially important fish species in the Azov Sea becomes suppressed [8]. Therefore, the emergence of scyphozoan jellyfish as invasive species may lead to a sudden depression of the state of the main bioresources of the Azov Sea.

Materials and Methods. To quantitatively assess the impact of scyphozoan jellyfish (*Aurelia aurita* and *Rhizostomeae*) on fish communities of the Azov Sea, a dynamic model was developed describing the interaction of three key ecosystem components: $Z(t)$ — zooplankton concentration (resource), $F(t)$ — biomass of the fish community, $J(t)$ — biomass of scyphozoan jellyfish. The model incorporates two primary mechanisms by which jellyfish affect fish populations: competition for a shared food resource—zooplankton, and direct predation by jellyfish on fish eggs and larvae. The structure of these interactions is illustrated in Fig. 2.

In Fig. 2, the following notations are used: (1) consumption of zooplankton by scyphozoan jellyfish; (2) consumption of zooplankton by fish communities; (3) predation by scyphozoan jellyfish on fish eggs and larvae; (4) influence of changes in external environmental factors (temperature, salinity, etc.); (5) influence of terrestrial-driven environmental changes (anthropogenic pressure, river runoff, eutrophication).

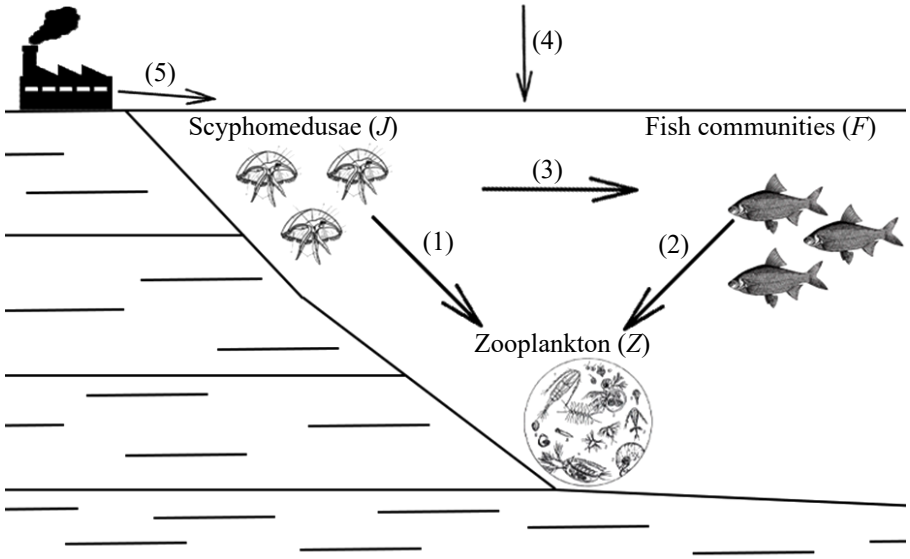

Fig. 2. Structural scheme of trophic interactions between jellyfish, fish, and zooplankton

The biological kinetics model is based on well-established approaches [9, 10] and has the following form:

$$\begin{cases} \dfrac{\partial Z}{\partial t}+u\dfrac{\partial Z}{\partial x}+v\dfrac{\partial Z}{\partial y}+(w+w_{gZ})\dfrac{\partial Z}{\partial z}=\dfrac{\partial}{\partial x}\left(\mu_Z\dfrac{\partial Z}{\partial x}\right)+\dfrac{\partial}{\partial y}\left(\mu_Z\dfrac{\partial Z}{\partial y}\right)+\dfrac{\partial}{\partial z}\left(\nu_Z\dfrac{\partial Z}{\partial z}\right)+\psi_Z, \\ \dfrac{\partial F}{\partial t}+u\dfrac{\partial F}{\partial x}+v\dfrac{\partial F}{\partial y}+(w+w_{gF})\dfrac{\partial F}{\partial z}=\dfrac{\partial}{\partial x}\left(\mu_F\dfrac{\partial F}{\partial x}\right)+\dfrac{\partial}{\partial y}\left(\mu_F\dfrac{\partial F}{\partial y}\right)+\psi_F, \\ \dfrac{\partial J}{\partial t}+u\dfrac{\partial J}{\partial x}+v\dfrac{\partial J}{\partial y}+(w+w_{gJ})\dfrac{\partial J}{\partial z}=\dfrac{\partial}{\partial x}\left(\mu_J\dfrac{\partial J}{\partial x}\right)+\dfrac{\partial}{\partial y}\left(\mu_J\dfrac{\partial J}{\partial y}\right)+\psi_J, \end{cases} \tag{1}$$

$$\psi_Z=rZ\left(1-\frac{Z}{K}\right)-\frac{a_ZFZ}{1+h_aa_ZZ}-\frac{b_ZJZ}{1+h_bb_ZZ},$$

$$\psi_F=\alpha\left(\frac{a_ZFZ}{1+h_aa_ZZ}\right)-d_FF-\varepsilon JF,\quad \psi_J=\beta\left(\frac{b_ZFZ}{1+h_bb_ZZ}\right)+\delta JF-d_JJ.$$

In system (1), the following notations are introduced: $\mathbf{u}=(u, v, w)$ — velocity field of the water flow; $w_{g\varphi}$ — settling (sedimentation) velocity of substance φ, $\varphi\in\{Z, F, G\}$; μ_φ, ν_φ — diffusion coefficients of substance φ, $\varphi\in\{Z, F, G\}$ in the horizontal and vertical directions, respectively; r — intrinsic growth rate of zooplankton; K — environmental carrying capacity; a_z — grazing (consumption) rate coefficient of zooplankton by fish; b_z — grazing (consumption) rate coefficient of zooplankton by jellyfish; h_a — food handling time for fish; h_b — food handling time for jellyfish; α — fish biomass growth coefficient (zooplankton-to-fish conversion efficiency); d_F — natural mortality coefficient; ε — fish biomass loss coefficient accounting for jellyfish predation on fish eggs and larvae; β — jellyfish growth coefficient; δ — nonlinear predation coefficient; d_J — jellyfish mortality coefficient.

Let Γ denote the boundary of the spatial domain G, $\overline{G}=G\cup\Gamma$; where σ is the lateral boundary surface, $\Sigma_{пов}$ is a part of the free water surface, and $\Sigma_{дно}$ — is the bottom surface. $\Gamma=\sigma\cup\Sigma_{пов}\cup\Sigma_{дно}$.

We specify:

– initial conditions at $t = 0$

$$\varphi(x,y,z,0)\equiv\varphi_0(x,y,z); \tag{2}$$

– boundary conditions on the lateral surface σ at any time $\sigma\times(0,T]$

$$\frac{\partial\varphi}{\partial\mathbf{n}}=0,\ \text{if}\ (\mathbf{u}_\Gamma,\mathbf{n})<0, \tag{3}$$

$$\frac{\partial\varphi}{\partial\mathbf{n}}=-\frac{u_\Gamma}{\mu_\varphi}\varphi,\ \text{if}\ (\mathbf{u}_\Gamma,\mathbf{n})\geq 0, \tag{4}$$

where $\mathbf{n}$ is the outward unit normal vector to the boundary of the domain σ; $\mathbf{u}_\Gamma$ is the fluid velocity vector on the boundary S; u_Γ — is the normal component of the flow velocity $\mathbf{n}$ at the domain boundary G;

– boundary conditions at the water surface

$$\frac{\partial \varphi}{\partial \mathbf{n}} = 0; \tag{5}$$

– boundary conditions at the bottom surface $\Sigma_{дно} \times \left(0 < t \le T\right]$

$$\frac{\partial \varphi}{\partial \mathbf{n}} = -\frac{w_{g\varphi}}{\nu_i}\varphi,\ \varphi \in \{Z,F,J\}. \tag{6}$$

To investigate the dynamics of the considered hydrobionts of the Azov Sea ecosystem and to identify the key patterns governing the interactions between scyphozoan jellyfish and fish communities, a qualitative analysis of the proposed nonlinear system of ordinary differential equations is performed. The main focus is placed on the identification of equilibrium states (steady states) and on the analysis of their stability based on the Jacobian matrix. This approach makes it possible to determine the conditions under which coexistence of the selected ecosystem components is feasible, as well as to identify threshold parameter values beyond which a transition to an alternative stable state occurs, such as jellyfish dominance.

Let us consider system (1). The equilibrium states of the system are determined by setting all right-hand sides equal to zero:

$$\frac{dZ}{dt} = 0, \frac{dF}{dt} = 0, \frac{dJ}{dt} = 0.$$

We examine four biologically relevant cases.

1. Trivial equilibrium $E_0 = (K,0,0)$.

This equilibrium corresponds to the absence of both fish and jellyfish populations, while zooplankton reaches the carrying capacity of the environment. Substituting $F = 0$, $J = 0$ into system (1) yields:

$$rZ\left(1 - \frac{Z}{K}\right) = 0 \Rightarrow Z = K.$$

Hence, $E_0 = (K,0,0)$ is an equilibrium point. To analyze its stability, we compute the coefficients of the Jacobian matrix in a neighborhood of E_0:

$$J\left(E_0\right) = \left.\begin{pmatrix} \frac{\partial Z}{\partial Z} & \frac{\partial Z}{\partial F} & \frac{\partial Z}{\partial J} \\ \frac{\partial F}{\partial Z} & \frac{\partial F}{\partial F} & \frac{\partial F}{\partial J} \\ \frac{\partial J}{\partial Z} & \frac{\partial J}{\partial F} & \frac{\partial J}{\partial J} \end{pmatrix}\right|_{(K,0,0)}.$$

After computing the partial derivatives and substituting the equilibrium values, we obtain:

$$J\left(E_0\right) = \begin{pmatrix} -r & -\frac{a_Z K}{1 + h_a a_Z K} & -\frac{b_Z K}{1 + h_b b_Z K} \\ 0 & \alpha\frac{a_Z K}{1 + h_a a_Z K} - d_F & 0 \\ 0 & 0 & \beta\frac{b_Z K}{1 + h_b b_Z K} - d_J \end{pmatrix}.$$

Since the Jacobian matrix is upper triangular, its eigenvalues are given by the diagonal elements:

$$\lambda_1 = -r < 0, \lambda_2 = \alpha\frac{a_Z K}{1 + h_a a_Z K} - d_F, \lambda_3 = \beta\frac{b_Z K}{1 + h_b b_Z K} - d_J.$$

The equilibrium E_0 is asymptotically stable if $\lambda_2 < 0$ and $\lambda_3 < 0$, i. e.

$$\alpha\frac{a_Z K}{1 + h_a a_Z K} < d_F,\ \beta\frac{b_Z K}{1 + h_b b_Z K} < d_J,\ \text{at}\ \alpha > 0,\ \beta > 0.$$

These inequalities define threshold values of the carrying capacity K, below which neither fish nor jellyfish are able to colonize the ecosystem. When these thresholds are exceeded, the equilibrium E_0 becomes unstable, and growth of one or both populations is initiated.

2. Fish-only equilibrium $E_F = \left(Z_F^*, F^*, 0\right)$.

Next, we consider the case where jellyfish are absent, i. e., $J = 0$, $F > 0$. This corresponds to a state in which the fish community is established and maintained through interaction with zooplankton. From system (1), we obtain:

$$\frac{dZ}{dt} = 0 \Rightarrow rZ\left(1 - \frac{Z}{K}\right) = \frac{a_Z F Z}{1 + h_a a_Z Z},$$

$$\frac{dF}{dt}=0\Rightarrow \alpha\frac{a_Z FK}{1+h_a a_Z K}=d_F F\Rightarrow \alpha\frac{a_Z K}{1+h_a a_Z K}=d_F\Rightarrow \frac{a_Z Z}{1+h_a a_Z Z}=\frac{d_F}{\alpha}.$$

Solving the corresponding equations yields:

$$Z_F^*=\frac{d_F}{a_Z\left(\alpha-h_a d_F\right)}\ (upon\ condition\ \alpha>h_a d_F).$$

Substituting Z_J^* into the first equation allows us to determine the equilibrium fish biomass F^*. Thus, a nontrivial equilibrium $E_F=\left(Z_F^*,F,0\right)$, exists provided that $d_F<\alpha\frac{a_Z}{1+h_a a_Z K}$. The stability of E_F depends critically on the ability of jellyfish to invade this equilibrium. If $\beta\frac{b_Z Z_F^*}{1+h_b b_Z Z_F^*}>d_J$, then jellyfish can successfully invade the system, implying that the equilibrium is unstable.

3. Jellyfish-only equilibrium $E_J=\left(Z_F^*,0,J^*\right)$.

We now consider the case opposite to the fish-only equilibrium, namely $F = 0$, $J > 0$. This state corresponds to domination of jellyfish communities. Substituting $F = 0$ into system (1) yields:

$$\frac{dZ}{dt}=0\Rightarrow rZ\left(1-\frac{Z}{K}\right)=\frac{JZ}{1+h_b Z},$$

$$\frac{dJ}{dt}=0\Rightarrow \beta\frac{JZ}{1+h_b Z}=d_J J\Rightarrow \beta\frac{Z}{1+h_b Z}=d_J\Rightarrow \frac{Z}{1+h_b Z}=\frac{d_J}{\beta}.$$

From the remaining equations, we obtain:

$$Z_J^*=\frac{d_J}{\left(\beta-h_b d_J\right)}\ (upon\ condition\ \beta>h_b d_J).$$

Substituting Z_J^* into the first equation, we obtain the equilibrium jellyfish biomass J^*. Thus, a jellyfish-only equilibrium $E_J=\left(Z_F^*,0,J^*\right)$, exists, corresponding to the exclusion of fish by jellyfish. The stability of E_J in this case depends on the impact of fish; specifically, if $\alpha\frac{a_Z Z_J^*}{1+h_a a_Z Z_J^*}>d_F$, then fish are able to invade the system and begin displacing jellyfish, which implies that the equilibrium is unstable.

4. Coexistence conditions and bifurcation.

Coexistence of fish and jellyfish is possible provided that the following conditions are simultaneously satisfied:

$$\alpha\frac{a_Z Z}{1+h_a a_Z Z}>d_F+\varepsilon J,\ \beta\frac{b_Z Z}{1+h_b b_Z Z}+\delta F>d_J.$$

However, numerical analysis indicates that the coexistence region is narrow. As the parameters J and b_z increase, the system loses stability and competitive exclusion occurs, resulting in $F \to 0$. The critical jellyfish biomass threshold at which this transition takes place can be estimated from the condition:

$$\alpha\frac{a_Z Z}{1+h_a a_Z Z}=d_F+\varepsilon J.$$

For a fixed value of $Z\approx Z_J^*$, this equation yields a threshold value, exceeding this value renders the persistence of the fish community impossible.

After analyzing the stability of the equilibrium states, we proceed to a qualitative analysis of the system dynamics, which allows visualization of typical ecosystem trajectories and identification of key behavioral scenarios. To this end, phase portraits are constructed in the projection of fish biomass F and scyphozoan jellyfish biomass J at a fixed zooplankton level Z, This corresponds to a quasi-stationary approximation (dimension reduction), which is commonly employed in models of biological kinetics [11]. We consider a simplified system describing the dynamics of F and J at a constant zooplankton concentration $Z = Z^*$:

$$\begin{cases}\dfrac{dF}{dt}=\alpha\left(\dfrac{a_Z FZ^*}{1+h_a a_Z Z^*}\right)-d_F F-\varepsilon JF,\\ \dfrac{dJ}{dt}=\beta\left(\dfrac{b_Z FZ^*}{1+h_b b_Z Z^*}\right)+\delta JF-d_J J.\end{cases}\qquad(7)$$

This approach eliminates the fast zooplankton dynamics and focuses attention on the long-term interaction between jellyfish and fish under a given level of ecosystem productivity. Fig. 3 presents the phase portrait of system (7) for $Z^* = 1.5$ (dimensionless units).

Analysis of the phase portrait reveals the presence of two attractors:

1. A stable equilibrium characterized by fish dominance, which is observed at low initial jellyfish biomass.
2. A jellyfish-dominated state, which is reached when the jellyfish biomass exceeds a critical threshold.

Between these attractors lies the boundary of the basins of attraction, which determines which of the two scenarios is realized depending on the initial conditions. This behavior indicates the existence of alternative stable states in the ecosystem: under identical external parameters, two qualitatively different equilibrium regimes may occur.

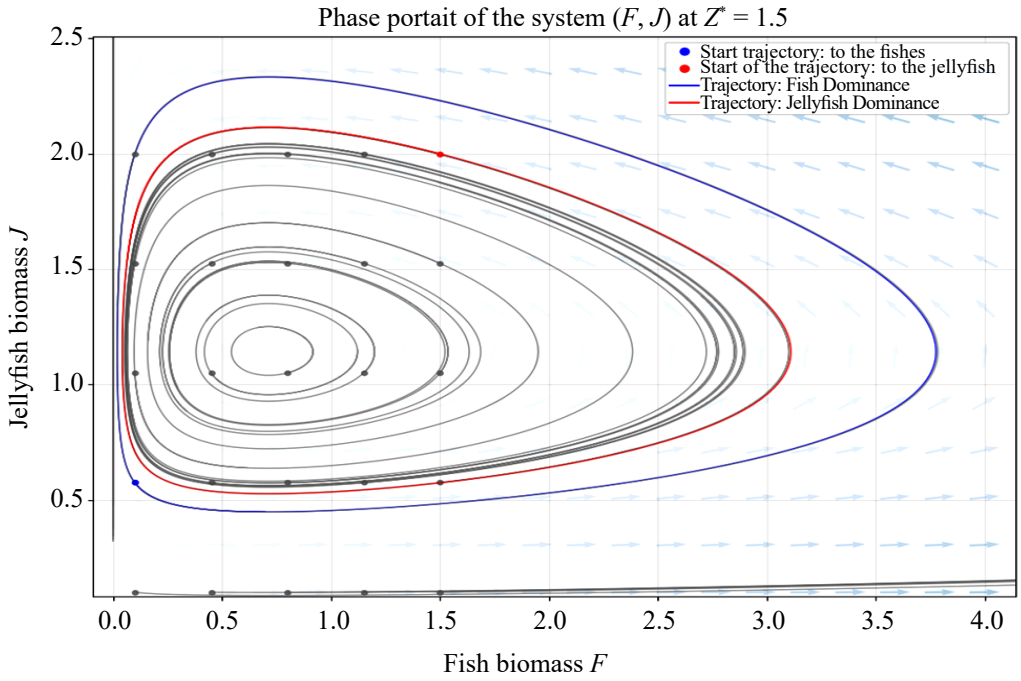

Fig. 3. Phase portrait of the system in the (F, J) plane at $Z^* = 1.5$ (dimensionless units)

To quantitatively assess the transition between these regimes, a bifurcation diagram was constructed, representing the dependence of the equilibrium fish biomass on jellyfish biomass (Fig. 4). Such behavior is typical of systems with positive feedback mechanisms: an increase in jellyfish abundance leads to a decline in zooplankton growth and elevated mortality of fish larvae, which in turn reduces competition for food resources and promotes further growth of the jellyfish population. As a result, the transition to the alternative state becomes weakly reversible in the absence of external intervention, such as mitigation of eutrophication in the aquatic ecosystem [12–14].

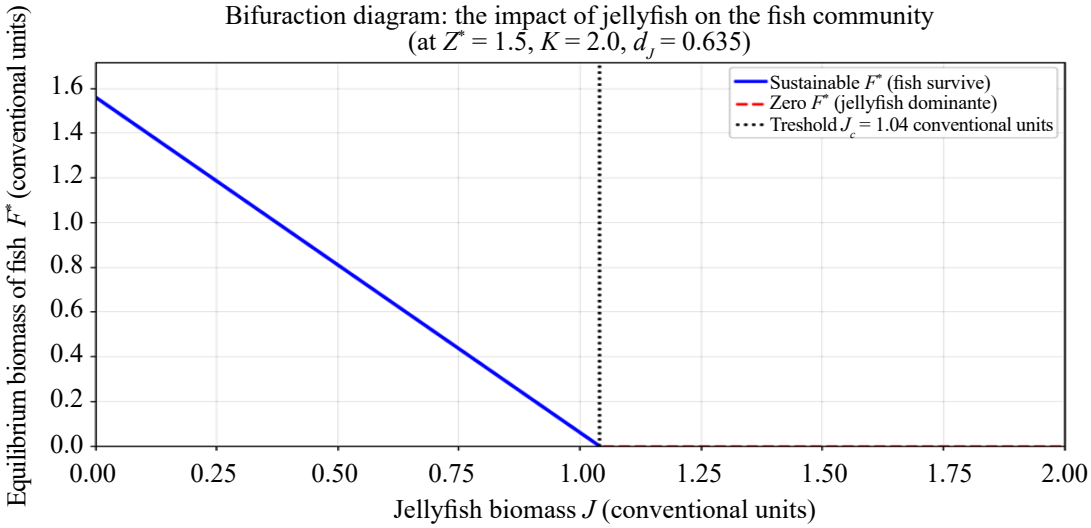

Fig. 4. Bifurcation diagram showing the equilibrium fish biomass as a function of jellyfish biomass

The obtained results confirm that the Azov Sea ecosystem can exist in two alternative stable states:

– a fish-centered state (at moderate jellyfish abundance);

– a jellyfish-centered state (when jellyfish abundance exceeds a critical threshold).

Thus, phase-plane analysis clearly demonstrates the risk of ecological collapse and highlights the necessity of continuous environmental monitoring and ecosystem management in the Azov Sea [9, 10].

Results. Numerical modelling of the Azov Sea ecosystem dynamics for the period from July 1 to August 31, 2025 revealed a substantial impact of scyphozoan jellyfish (*Rhizostomeae* and *Aurelia aurita*) on the state of the fish community through a combined effect of competition for zooplankton and direct predation on early life stages of fish. The initial conditions were chosen to represent a typical ecosystem state at the beginning of July, when jellyfish begin active reproduction, while fish populations exploit high plankton productivity to support juvenile growth [15].

The key model parameters were specified as follows:

• $r = 0.8$ day^{-1} — zooplankton growth rate, corresponding to elevated water temperatures (22–26 °C) and high nutrient availability due to eutrophication;;

• $K = 2.0$ dimensionless units — environmental carrying capacity, reflecting the maximum sustainable zooplankton biomass in the coastal zone;

• $a_z = 1.2$; $b_z = 2$ — zooplankton consumption rates by fish and jellyfish, respectively. The value accounts for the high filtration capacity of *Aurelia aurita*, which is capable of processing large volumes of water;

• $h_a = 0.9$; $h_b = 0.3$ — food handling times. The lower value indicates the higher efficiency of jellyfish as filter feeders compared to fish;

• $\alpha = 0.3$; $\beta = 0.4$ — food-to-biomass conversion efficiency coefficients. The coefficient is higher for jellyfish, reflecting their lower energetic costs for maintenance metabolism;

• $\delta = 0.03$ — additional jellyfish biomass gain due to consumption of fish eggs and larvae, characterizing their predatory activity;

• $d_F = 0.05$; $d_J = 0.635$ — natural mortality rates. Jellyfish mortality increases toward the end of August as a result of strobilation and post-reproductive senescence;

• $\varepsilon = 0.15$ — predation coefficient of jellyfish on fish larvae.

The temporal dynamics of all three system components — zooplankton, fish, and jellyfish — are illustrated in Fig. 5.

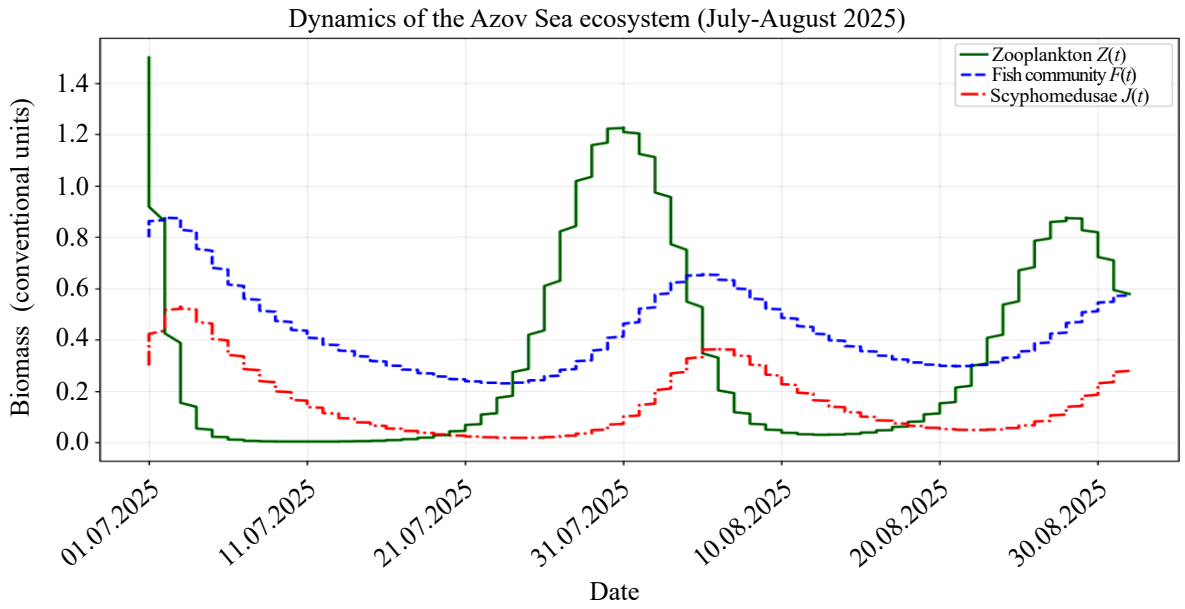

Fig. 5. Results of the numerical experiment illustrating the dynamics of the main hydrobionts and scyphozoan jellyfish in the Azov Sea ecosystem

The numerical simulations show that, for an initial jellyfish biomass of 0.3 (dimensionless units) and under favorable environmental conditions (high water temperature and eutrophication), jellyfish abundance increases by more than threefold by the end of August. This growth leads to a sharp reduction in zooplankton availability and a pronounced suppression of fish biomass growth. The obtained results demonstrate a transition of the ecosystem to a state in which jellyfish temporarily dominate the trophic structure, thereby limiting the recovery of fish populations.

Discussion. In this study, a mathematical model describing the complex trophic interactions between scyphozoan jellyfish and fish communities in the Azov Sea ecosystem was developed, analyzed, and numerically implemented. The proposed model explicitly accounts for both competition for a shared resource—zooplankton—and direct predation by jellyfish on the early life stages of fish, which makes it more realistic than classical “resource–consumer” systems.

The results of numerical experiments for the period July-August 2025 indicate that mass proliferation of jellyfish can lead to a substantial suppression of the productivity of valuable and commercially important fish species, especially under conditions of ongoing eutrophication and increasing water temperature. This points to a risk of a persistent shift of the ecosystem toward a jellyfish-dominated regime, which reduces both ecosystem resilience and fisheries value.

Conclusion. Mathematical modelling confirms the necessity of comprehensive monitoring of gelatinous invasive species and their integration into environmental management frameworks for marine resources in southern Russia. The proposed model can be used as a tool for forecasting ecosystem states, assessing the effectiveness of environmental protection measures, and substantiating the management of fishing pressure in the region. In future work, the model may be extended by incorporating seasonal variability of external factors and the influence of climate change [16].

References

1. Matishov G.G., Stepanyan O.V. R/V “Deneb”: 10 years of marine scientific research. *Physical Oceanography*. 2018;34(6):548–555. (In Russ.)

2. Smirnova E.A., Matishov G.G., Glukhov V.V. Study of the strandings of scyphozoan jellyfish Rhizostoma pulmo (Macri, 1778) on the Yasenskaya Spit of the Azov Sea in September 2024. *Science of the South of Russia*. 2025;21(1):58–62. (In Russ.) https://doi.org/10.7868/S25000640250108

3. Mirzoyan Z.A., Martynyuk M.L., Khrenkin D.V., Afanasiev D.F. Development of scyphozoan jellyfish Rhizostoma pulmo and Aurelia aurita populations in the Sea of Azov. *Aquatic Bioresources and Environment*. 2019;2(2):27–35. (In Russ.) https://doi.org/10.47921/2619-1024_2019_2_2_27

4. Sukhinov A.I., Chistyakov A.E., Belova Yu.V., Kuznetsova I.Yu. Analytical and numerical study of the plankton population dynamics problem in the presence of microplastic. *Mathematical Models and Computer Simulations*. 2024;36(3):95–114. (In Russ.) https://doi.org/10.20948/mm-2024-03-07

5. Ryabenkii V.S. Theory of control of solutions of linear difference schemes in composite domains. *Keldysh Institute Preprints*. 2012;(011):1–32. (In Russ.)

6. Lovisari M., Kelly O.R., McDonald A.R. Hydrocarbon Oxidation by a Porphyrin-π-Cation Radical Complex. *Angewandte Chemie International Edition*. 2023;62(20):202303083. https://doi.org/10.1002/anie.202303083

7. Sukhinov A.I., Chistyakov A.E., Yakobovskiy M.V. Accuracy of the numerical solution of the convection-diffusion equation using finite difference schemes with the second and fourth order of approximation error. *Bulletin of the South Ural State University. Series: Computational Mathematics and Computer Science*. 2016;5(1):47–62. (In Russ.)

8. Sukhinov A.I., Atayan A.M., Belova Yu.V., Litvinov V.N., Nikitina A.V., Chistyakov A.E. Processing of field measurement data from expeditionary studies for mathematical modeling of hydrodynamic processes of the Azov Sea. *Computational Continuum Mechanics*. 2020;13(2):161–174. (In Russ.)

9. Samarskiy A.A., Nikolaev E.S. *Methods for solving grid equations*. Moscow: Nauka; 1978. 591 p. (In Russ.)

10. Kudinov N.V., Filina A.A., Nikitina A.V. Modeling of vertical movements of seawater in stratified reservoirs. *Advanced Engineering Research.* 2023;23(2):212–224. (In Russ.) https://doi.org/10.23947/2687-1653-2023-23-2-212-224

11. Litvinov V.N., Rudenko N.B., Gracheva N.N. Development of a model of a parallel-pipeline computing process for solving a system of grid equations. *Advanced Engineering Research*. 2023;23(3):329–339. (In Russ.) https://doi.org/10.23947/2687-1653-2023-23-3-329-339

12. Belova Yu.V., Nikitina A.V. Application of observational data assimilation methods for modeling the spread of pollutants in a reservoir and managing sustainable development. *Safety of technogenic and natural systems*. 2024;8(3):39–48. (In Russ.) https://doi.org/10.23947/2541-9129-2024-8-3-39-48

13. Belova Yu.V. Filina A.A., Chistyakov A.E. Forecasting the dynamics of summer phytoplankton species based on satellite data assimilation methods. *Computational Mathematics and Information Technologies*. 2024;8(4):27–34. (In Russ.) https://doi.org/10.23947/2587-8999-2024-8-4-27-34

14. Babar Z.B., Rizwan K., Munir S. Multifunctional Smart Nano-membranes for the Removal of Oil-Based Pollutants from Marine Sources: A Tool for Sustainable Environment. *Water, Air, & Soil Pollution*. 2024;235(2):80. https://doi.org/10.1007/s11270-023-06864-x

15. Sukhinov A.I., Sidoryakina V.V. Approximation of boundary conditions of the second and third kind in boundary value problems for convection-diffusion equations with application to environmental hydrophysics. *Computational Mathematics and Information Technologies*. 2025;9(3):16–29. (In Russ.) https://doi.org/10.23947/2587-8999-2025-9-3-16-29

16. The state of jellyfish stocks in the Black and Azov Seas (according to periods until 2000) under the conditions of economic activity in the water area of the region and adjacent territories. Assessment of jellyfish stocks, distribution map and catch forecast: research report. Rostov-on-Don: AzNIIRKH Publishing House; 1981. 18 p. (In Russ.)

About the Authors:

Denis V. Bondarenko, assistant department of software for computing equipment and automated systems Don State Technical University (1, Gagarin Sq., Rostov-on-Don, 344003, Russian Federation), ORCID, SPIN-code, ScopusID, denis.bondarenko.dev@gmail.com

Alla V. Nikitina, doctor of engineering science, Professor department of software for computing equipment and automated systems Don State Technical University (1, Gagarin Sq., Rostov-on-Don, 344003, Russian Federation), ORCID, SPIN-code, ScopusID, nikitina.vm@gmail.com

Contributions of the authors:

D.V. Bondarenko: calculations; text preparation; graphic design; source analysis.

A.V. Nikitina: development of the main concept; research goals and objectives; analysis of research results; formulation of conclusions; proofreading.

Conflict of Interest Statement: **the authors declare no conflict of interest.**

All authors have read and approved the final manuscript.

Об авторах:

Денис Вадимович Бондаренко, ассистент кафедры программного обеспечения вычислительной техники и автоматизированных систем Донского государственного технического университета (344003, Российская Федерация, г. Ростов-на-Дону, пл. Гагарина, 1), ORCID, SPIN-код, ScopusID, denis.bondarenko.dev@gmail.com

Алла Валерьевна Никитина, доктор технических наук, профессор кафедры программного обеспечения вычислительной техники и автоматизированных систем Донского государственного технического университета (344003, Российская Федерация, г. Ростов-на-Дону, пл. Гагарина, 1), ORCID, SPIN-код, ScopusID, nikitina.vm@gmail.com

Заявленный вклад авторов:

Д.В. Бондаренко: проведение расчетов; подготовка текста; оформление графических материалов; работа с источниками.

А.В. Никитина: формирование основной концепции; цели и задачи исследования; анализ результатов исследований; формулирование выводов; корректировка текста.

Конфликт интересов: ***авторы заявляют об отсутствии конфликта интересов.***

Все авторы прочитали и одобрили окончательный вариант рукописи.

Received / Поступила в редакцию 27.10.2025
Reviewed / Поступила после рецензирования 12.11.2025
Accepted / Принята к публикации 10.12.2025

INFORMATION TECHNOLOGIES
ИНФОРМАЦИОННЫЕ ТЕХНОЛОГИИ

UDC 519.6:574.5:504.45

Original Empirical Research

https://doi.org/10.23947/2587-8999-2025-9-4-56-67

Mathematical Modelling of Green Microalgae Invasion and Rehabilitation of the Taganrog Bay: Ecological-Hygienic and Medical Consequences

Yuliya V. Belova[1] ✉, **Olesya V. Kolgunova**[2], **Mariya I. Gabueva**[3]

[1] Don State Technical University, Rostov-on-Don, Russian Federation

[2] North Ossetian State University, Vladikavkaz, Russian Federation

[3] North Ossetian State Medical Academy, Vladikavkaz, Russian Federation

✉ yvbelova@yandex.ru

Abstract

Introduction. The Taganrog Bay of the Azov Sea is one of the most eutrophic and ecologically vulnerable water areas in Russia, where massive blooms of toxic cyanobacteria (*Microcystis, Aphanizomenon, Anabaena, Nodularia*) regularly occur during summer. Their proliferation is accompanied by the accumulation of cyanotoxins (microcystin, anatoxin, cylindrospermopsin, saxitoxin), posing a serious threat to public health. This paper considers an approach to the biological rehabilitation of the bay based on the controlled introduction of the freshwater green microalgae *Chlorella vulgaris*, which competes with cyanobacteria for nutrients. The aim of the study is to develop and apply a comprehensive mathematical model describing phytoplankton kinetics and substance transport processes under conditions of increasing bay salinity, as well as to assess the ecological-hygienic and medical consequences of the proposed method.

Materials and Methods. The research object is the Taganrog Bay of the Azov Sea. The modelling is based on the three-dimensional hydrodynamic model "Azov3D", previously used to calculate currents and vertical mixing under conditions of changing salinity. Water environment parameters (salinity, temperature, current velocities) were used as input data for solving the linearized hydrobiological problem. The source of bathymetric data was digitized nautical charts processed using automated depth recognition algorithms. The model grid was generated considering the actual coastline configuration and bottom topography. Calculations were performed on the computing cluster of the Southern Federal University. The numerical method is based on finite-difference schemes previously applied for hydrobiological calculations in the Azov Sea.

Results. It is shown that a 30% increase in salinity leads to a shift in the cyanobacteria habitat from the Azov Sea water area to the eastern part of the Taganrog Bay, which is consistent with hydrological observations. Model calculations demonstrate an increase in the proportion of green algae with the controlled introduction of *Chlorella vulgaris* cultures, reflecting the potential for biomelioration. The forecast of the spatial distribution of populations shows stable dominance of green and blue-green algae, constituting 60–70% of the bay's phytoplankton biomass, under various impact scenarios.

Discussion. The results indicate that mathematical modelling is an effective tool for predicting the dynamics of phytoplankton populations under changing hydrological conditions. The model allows for assessing the influence of biological regulation and salinization scenarios, providing a basis for management decisions in the field of ecological rehabilitation of water bodies.

Conclusion. The application of *Chlorella vulgaris* may be a promising biomelioration method but requires further verification based on field observations and controlled field experiments. The modelling results indicate the possibility of adaptive ecological management of the Taganrog Bay and minimizing the risk of toxic blooms.

Keywords: phytoplankton dynamics, *Chlorella vulgaris*, eutrophication modelling, hydrodynamic model, convection-diffusion equations, substance transport, cyanobacterial bloom, numerical modelling, biological regulation, Taganrog Bay

Acknowledgements. The authors express sincere gratitude to Alexander Ivanovich Sukhinov, Doctor of Physical and Mathematical Sciences, Professor, Corresponding Member of the Russian Academy of Sciences, for his attentive attitude and assistance in the work, constructive comments, and valuable recommendations, which contributed to improving the quality of the research.

Funding. The study was supported by the Russian Science Foundation grant No. 22–11–00295–П, https://rscf.ru/en/project/22-11-00295/

For Citation. Belova Yu.V., Kolgunova O.V., Gabueva M.I. Mathematical Modelling of Green Microalgae Invasion and Rehabilitation of the Taganrog Bay: Ecological-Hygienic and Medical Consequences. *Computational Mathematics and Information Technologies*. 2025;9(4):56–67. https://doi.org/10.23947/2587-8999-2025-9-4-56-67

Оригинальное эмпирическое исследование

Математическое моделирование инвазии зеленых микроводорослей и оздоровления Таганрогского залива: эколого-гигиенические и медицинские последствия

Ю.В. Белова[1] ✉, **О.В. Колгунова**[2], **М.И. Габуева**[3]

[1] Донской государственный технический университет, г. Ростов-на-Дону, Российская Федерация

[2] Северо-Осетинский государственный университет, г. Владикавказ, Российская Федерация

[3] Северо-Осетинская государственная медицинская академия, г. Владикавказ, Российская Федерация

✉ yvbelova@yandex.ru

Аннотация

Введение. Таганрогский залив Азовского моря является одной из наиболее эвтрофных и экологически уязвимых акваторий России, где в летний период регулярно формируются массовые цветения токсичных цианобактерий (*Microcystis, Aphanizomenon, Anabaena, Nodularia*). Их развитие сопровождается накоплением цианотоксинов (микроцистин, анатоксин, цилиндроспермопсин, сакситоксин), представляющих серьёзную угрозу для здоровья населения. В работе рассматривается подход к биологической реабилитации залива на основе контролируемого внесения пресноводных зелёных микроводорослей *Chlorella vulgaris*, конкурирующих с цианобактериями за биогенные элементы. Цель исследования заключается в разработке и применении комплексной математической модели, описывающей кинетику фитопланктона и процессы переноса веществ в условиях осолонения залива, а также в оценке эколого-гигиенических и медицинских последствий предложенного метода.

Материалы и методы. Объектом исследования является Таганрогский залив Азовского моря. Моделирование выполнено на основе трёхмерной гидродинамической модели «Azov3D», ранее применённой для расчётов течений и вертикального перемешивания в условиях изменяющейся солёности. Параметры водной среды (солёность, температура, скорости течений) использовались как входные данные для решения линеаризованной гидробиологической задачи. Источник батиметрических данных — оцифрованные лоцманские карты, обработанные с применением автоматизированных алгоритмов распознавания глубин. Сеточная основа модели формировалась с учётом реальной конфигурации береговой линии и рельефа дна. Расчёты выполнялись на вычислительном кластере Южного федерального университета. Численный метод основан на разностных схемах, применяемых ранее для гидробиологических расчётов в Азовском море.

Результаты исследования. Показано, что увеличение солёности на 30 % приводит к смещению ареала цианобактерий из акватории Азовского моря в восточную часть Таганрогского залива, что согласуется с гидрологическими наблюдениями. Модельные расчёты демонстрируют усиление доли зелёных водорослей при контролируемом внесении культур *Chlorella vulgaris*, что отражает потенциал биомелиорации. Прогноз пространственного распределения популяций показывает устойчивое доминирование зеленых и синезеленых водорослей, составляющих 60–70 % биомассы фитопланктона залива, при различных сценариях воздействия.

Обсуждение. Результаты показывают, что математическое моделирование является эффективным инструментом для прогнозирования динамики фитопланктонных популяций в условиях изменяющейся гидрологии. Модель позволяет оценить влияние биологической регуляции и сценариев осолонения, предоставляя основу для принятия управленческих решений в сфере экологического оздоровления водоёмов.

Заключение. Применение *Chlorella vulgaris* может быть перспективным методом биомелиорации, однако требует дальнейшей проверки с опорой на натурные наблюдения и контролируемые полевые эксперименты. Модельные результаты указывают на возможность адаптивного экологического управления Таганрогским заливом и минимизации риска токсичных цветений.

Ключевые слова: динамика фитопланктона, *Chlorella vulgaris*, моделирование эвтрофикации, гидродинамическая модель, уравнения конвекции-диффузии, перенос веществ, цветение цианобактерий, численное моделирование, биологическая регуляция, Таганрогский залив

Благодарности. Авторы выражают искреннюю благодарность Сухинову Александру Ивановичу, доктору физико-математических наук, профессору, член-корреспонденту РАН за внимательное отношение и помощь в работе, конструктивные замечания и ценные рекомендации, которые способствовали улучшению качества исследования.

Финансирование. Исследование выполнено за счет гранта Российского научного фонда № 22–11–00295–П, https://rscf.ru/project/22-11-00295/

Для цитирования. Белова Ю.В., Колгунова О.В., Габуева М.И. Математическое моделирование инвазии зелёных микроводорослей и оздоровления Таганрогского залива: эколого-гигиенические и медицинские последствия. *Computational Mathematics and Information Technologies.* 2025;9(4):56–67. https://doi.org/10.23947/2587-8999-2025-9-4-56-67

Introduction. The Azov Sea, and particularly the Taganrog Bay, is among the most eutrophic and ecologically vulnerable water areas in Russia. The influx of nutrients from the Don River basin, high water temperatures in summer, and limited water exchange lead to the massive proliferation of cyanobacteria (*Microcystis, Aphanizomenon, Anabaena, Nodularia*) [1–3]. A number of cyanobacteria produce toxic metabolites—microcystins, nodularin, cylindrospermopsin, saxitoxin—which pose a threat to human health [4–8]. The blue-green (cyanobacterial) algae *Microcystis aeruginosa, Aphanizomenon flos-aquae*, and representatives of the genus Anabaena are the primary species forming massive "blooms" in the freshened zone of Taganrog Bay [9–12]. Upon the decay of these organisms, anatoxins a and a(s), which affect the nervous system, appear in the water. It was previously hypothesized that poisoning by decomposing cells of blue-green algae causes the so-called Haff disease [2].

Monitoring by the Southern Scientific Centre of the Russian Academy of Sciences indicates that peak phytoplankton concentrations, primarily cyanobacteria, in the Taganrog Bay reach levels classified by the WHO as posing a high risk to the population during swimming and water contact [2–4]. The concentration of toxic algae, primarily cyanotoxin producers, can be reduced through the spatially distributed introduction of biologically significant quantities of the green microalgae *Chlorella vulgaris*, which provides effective competition for nutrients. This paper presents a hydrobiological model and the results of numerical modelling of various scenarios for the spatial distribution of green algae to achieve acceptable ecological and hygienic outcomes through biological regulation of cyanobacterial abundance.

We present initial data illustrating the biological and ecological-hygienic characteristics of toxic microalgae species (hydrobiota) in the Taganrog Bay. According to long-term observations by the SSC RAS [2, 3], the background summer phytoplankton abundance ranges from 7.5–53 thousand cells/ml, reaching up to 152 thousand cells/ml during peak blooms (2015). The corresponding biomass is 23.8 g/m³ [2]; the maximum biomass over the long-term period is 70–80 g/m³ [3]; and the proportion of cyanobacteria in the biomass structure reaches 90% [2, 3]. Such concentrations correspond to harmful algal blooms (HABs) and, according to the WHO classification presented in Table 1, belong to levels at which adverse health effects for the population are possible [4].

Table 1

Cyanobacterial Concentrations and WHO Risk Classification

Indicator	Concentration	Conditions	Risk (WHO)	Sources
Background Abundance	7.500–53.000 cells/ml	Summer	Low	[2, 3]
Peak Bloom Abundance	≈152.000 cells/ml	Taganrog Bay	High (> 100.000)	[2]
Biomass (background)	0.9–5.5 g/m³	Summer	Low	[2]
Biomass (bloom)	23.8 g/m³	Bloom	Moderate–High	[2]
Long-term Maximum Biomass	70–80 g/m³	Azov Sea	HAB (Harmful Algal Bloom)	[3]
Microcystin-LR (Drinking Water MPC)	1 µg/L	Water	Acceptable	[4, 5]
Microcystin-LR (Recreational Water)	> 20 µg/L	Bathing	Hazardous	[4]

(MPC – Maximum Permissible Concentration)

Currently, the following pathways of cyanotoxin impact on humans are known: dermal contact (cutaneous pathway), inhalation, hemodialysis, and ingestion (oral pathway). When distinguishing these pathways, it should be noted that several routes of exposure can act simultaneously on a person. Cases of skin irritation and allergic reactions following contact with cyanobacteria in marine coastal waters have been recorded for at least 30 years. Symptoms have included rashes, blisters, allergic reactions resembling hay fever, asthma, conjunctivitis, and irritation of the ears and eyes. In eighty-five percent of patients, following initial neurotoxicosis, toxic symptoms developed, including painful hepatomegaly, as well as biochemical and histological signs of liver damage. Sixty fatalities were reported, caused either directly by hepatotoxicity or indirectly by complications including gastrointestinal bleeding, sepsis, and cardiovascular problems [8].

A study by A.Yu. Zhidkova et al. showed that an increase in the level of eutrophication in the Taganrog Bay is accompanied by a rise in gastrointestinal diseases, skin conditions, and allergic reactions among the population of coastal areas [1]. The authors note a direct link between the deterioration of water quality and the dynamics of visits to healthcare institutions.

An increase in acute allergic and toxic reactions during swimming should also be noted. At cyanobacterial concentrations exceeding 20–100 thousand cells/ml (levels typical for the Taganrog Bay in summer), the following are possible: skin itching, dermatitis, rashes, conjunctivitis, rhinitis, cough, throat irritation, asthma exacerbation, nausea, vomiting, and diarrhea from accidental water ingestion.

These effects are described in reports by the WHO and EPA [4, 7, 8] and are supported by statistically robust data for the region adjacent to the Azov Sea coast [1, 2]. Particular attention is drawn to cases of severe and acute intoxications, including those leading to hepatotoxic effects (microcystin, nodularin). Confirmed cases of consequences, including acute toxic hepatitis, a sharp increase in transaminase, damage to liver vessels, hemorrhagic necrosis, and others, are detailed in works [4, 6, 8]. To ensure the integrity of the analysis, both acute neurotoxic effects (saxitoxin, anatoxin) and hepato- and nephrotoxic effects, as well as long-term chronic consequences of cyanotoxin exposure, including potential carcinogenic risks, have been considered. Summary data on cyanobacterial and cyanotoxin concentrations, the nature of toxic action, and possible clinical manifestations are presented in Table 2.

Thus, harmful cyanobacterial blooms pose a significant threat to the health of the Azov region›s population and require systematic monitoring and prevention. Mathematical modelling is a relatively inexpensive, rapid, and accessible method for forecasting adverse situations associated with abundant cyanobacterial blooms in summer.

A number of domestic and international publications are devoted to modelling blooms of potentially harmful cyanobacteria. In [13], the influence of phosphorus on stimulating the development of blue-green algae is investigated. The article [14] presented a non-stationary three-component mathematical model of competition between two types of phytoplankton, including toxic ones, and their grazing by zooplankton.

Table 2

Cyanobacteria and Cyanotoxin Concentrations, Types of Exposure, and Possible Clinical Manifestations in Humans

Cyanobacteria Concentration / Toxin Level	Exposure Type	Clinical Manifestations	Sources
7.5–53 thousand cells/ml	Contact	Mild skin reactions	[2, 3]
~152 thousand cells/ml	Bathing	Rash, itching, gastrointestinal disorders	[1, 2, 4]
20–80 g/m³ biomass	Repeated contact	Diarrhea, vomiting, dermatitis	[3, 4]
Microcystin-LR ≥ 1 µg/L	Drinking water	Hepatotoxicity	[4, 5, 6]
Microcystin-LR ≥ 20 µg/L	Bathing	Acute intoxication	[4]
Saxitoxin > 3 µg/L	Ingestion via water/fish	Neurotoxic symptoms, paralysis	[7]
Cylindrospermopsin ~1 µg/L	Contact, water	Hepato- and nephrotoxicity	[9]
Chronic low doses	Long-term residence	Increased risk of oncological and chronic diseases	[1, 8]

One of the methods for limiting mass cyanobacterial blooms is the biological regulation (biomelioration) of water bodies through the controlled introduction of cultures of the green microalgae *Chlorella vulgaris* [15]. The essence of the method is that green algae are introduced into the water body before the beginning of the blue-green algae growing season, where they absorb most of the nutrients, thereby limiting or even stopping the reproduction and growth of harmful cyanobacteria. In turn, green microalgae serve as a food base for zooplankton and juvenile fish, contributing to the stabilization of the water body›s trophic structure [16]. At typical concentrations, no negative impact of green algae on the aquatic ecosystem or harmful effects on human health have been detected. Furthermore, green algae have found application in agriculture as fertilizers, feed additives for livestock, and for wastewater treatment [17].

However, it is important to distinguish between the controlled introduction of *Chlorella vulgaris* cultures for biomelioration and the uncontrolled mass development of green algae. The latter can deteriorate the organoleptic properties of water, increase the concentration of dissolved organic matter, and promote bacterial contamination, which in turn leads to an increase in the formation of disinfection by-products during chlorination [5–7, 9]. These effects are not attributable to biomelioration biotechnology but to spontaneous green algal blooms under conditions of nutrient excess.

Given the pronounced eutrophication of the Azov Sea coastal waters, the use of green microalgae *Chlorella vulgaris* as a biological regulator of cyanobacterial abundance is of particular interest. Results from laboratory and semi-field experiments show that during co-cultivation of *Chlorella vulgaris* and toxic species (*Microcystis aeruginosa, Aphanizomenon flos-aquae, Anabaena spp.*), pronounced competition for available forms of nitrogen and phosphorus is

observed, leading to a reduction in cyanobacterial growth rates and partial cell death within several weeks of the growing season. These data allow the consideration of controlled green microalgae introduction as a potential tool for biological regulation, the effectiveness of which is largely determined by the spatial distribution of biomass, initial phytoplankton concentrations, and the level of nutrient loading [18, 19].

In view of the above, the mathematical modelling of biological water body rehabilitation is a relevant task and is of interest from the perspective of regulating blue-green algae abundance under conditions of their geographically distributed introduction into the aquatic environment of the Taganrog Bay. The aim of this work is to conduct mathematical modelling of the remediation of the Taganrog Bay through the introduction of green microalgae and to assess the ecological-hygienic and medical consequences.

To achieve this aim, the authors of this study propose using a complex of mathematical models of phytoplankton population dynamics and hydrodynamics, accounting for advective and diffusive transport, weather conditions, geometry of the computational domain, growth limitation of microalgae by nutrient availability, and salinity and temperature regimes [20]. Modern finite-difference schemes and numerical methods were used to solve the stated problem.

Materials and Methods. The mathematical model of biological kinetics is based on the works of A.I. Sukhinov and E.V. Yakushev [21, 22]. The mathematical model, the nonlinear right-hand sides of the equations, and the formulation of the initial boundary value problem are described in detail in [22]. A brief description of the mathematical model and its linearization are provided below.

This model is based on a system of unsteady convection-diffusion-reaction equations of parabolic type with nonlinear source functions and first-order derivatives. Advective terms are presented in symmetric form, which guarantees the skew-symmetry of the transport operator and enables a correct problem formulation. For each substance F_i, included in the model, the equation has the form:

$$\frac{\partial q_i}{\partial t}+\frac{1}{2}\left(\nabla\cdot\left(\mathbf{V}q_i\right)+\left(\mathbf{V}\cdot\nabla\right)q_i\right)=\operatorname{div}\left(k\cdot\nabla q_i\right)+R_{q_i}, \tag{1}$$

where q_i is the concentration of the i-th ($i=\overline{1,8}$) component, mg/L; $\mathbf{V}=\{u, v, w\}$ is the water flow velocity vector, m/s; $k=(k_h, k_h, k_v)$ is the turbulent exchange coefficient, m²/s; ∇ denotes the gradient operator; $(x, y, z)\in G$; $0<t\le T$; R_{qi} is the source function of biogenic substances, mg/(L·s); $i\in M$, $M=\{F_1, F_2, DOP, POP, PO_4, NO_3, NO_2, NH_4\}$; F_1 denotes the concentration of green algae, F_2 — blue-green algae. The following biogenic components are specified: *DOP* refers to dissolved organic phosphorus, *POP* — suspended organic phosphorus, PO_4 — phosphates, NO_3 — nitrates, NO_2 — nitrites, NH_4 — ammonium (ammonium nitrogen).

The biochemical interactions between the components of system (1), i. e., the right-hand side functions $R_{qi}=R_{qi}(x, y, z, t)$, are, in general, nonlinear dependencies that may depend on the temperature and salinity of the aquatic environment. They have the following form:

$$R_{F_i}=C_{F_i}(1-K_{F_iR})q_{F_i}-K_{F_iD}q_{F_i}-K_{F_iE}q_{F_i},\ i=1,2,$$

$$R_{DOP}=\sum_{i=1}^{3}s_PK_{F_iE}q_{F_i}+K_{PD}q_{POP}-K_{DN}q_{DOP},$$

$$R_{POP}=\sum_{i=1}^{3}s_PK_{F_iD}q_{F_i}-K_{PD}q_{POP}-K_{PN}q_{POP},$$

$$R_{PO_4}=\sum_{i=1}^{3}s_PC_{F_i}\left(K_{F_iR}-1\right)q_{F_i}+K_{PN}q_{POP}+K_{DN}q_{DOP},$$

$$R_{NO_3}=\sum_{i=1}^{3}s_NC_{F_i}\left(K_{F_iR}-1\right)\frac{f_N^{(1)}\left(q_{NO_3},q_{NO_2},q_{NH_4}\right)}{f_N\left(q_{NO_3},q_{NO_2},q_{NH_4}\right)}\cdot\frac{q_{NO_3}}{q_{NO_2}+q_{NO_3}}q_{F_i}+K_{23}q_{NO_2}, \tag{2}$$

$$R_{NO_2}=\sum_{i=1}^{3}s_NC_{F_i}(K_{F_iR}-1)\frac{f_N^{(1)}\left(q_{NO_3},q_{NO_2},q_{NH_4}\right)}{f_N\left(q_{NO_3},q_{NO_2},q_{NH_4}\right)}\cdot\frac{q_{NO_2}}{q_{NO_2}+q_{NO_3}}q_{F_i}+K_{42}q_{NH_4}-K_{23}q_{NO_2},$$

$$R_{NH_4}=\sum_{i=1}^{3}s_NC_{F_i}\left(K_{F_iR}-1\right)\frac{f_N^{(2)}\left(q_{NH_4}\right)}{f_N\left(q_{NO_3},q_{NO_2},q_{NH_4}\right)}q_{F_i}+\sum_{i=1}^{3}s_N\left(K_{F_iD}+K_{F_iE}\right)q_{F_i}-K_{42}q_{NH_4},$$

where K_{F_iR} is the specific respiration rate of phytoplankton; K_{F_iD} is the specific mortality rate of phytoplankton; K_{F_iE} is the specific excretion rate of phytoplankton; K_{PD} is the specific rate of POP autolysis; K_{PN} is the specific rate of POP phosphatefication; K_{DN} is the specific rate of DOP phosphatefication; K_{42} is the specific rate of ammonium oxidation to

nitrites during nitrification; K_{23} is the specific rate of nitrite oxidation to nitrates during nitrification; S_P, S_N are normalization coefficients for the content of N and P in organic matter. The growth rate of phytoplankton populations is expressed as a function dependent on salinity S and temperature T:

$$C_{F_{1,2}} = K_{NF_{1,2}} f_T(T) f_S(S) min\left\{ f_P\left(q_{PO_4}\right), f_N\left(q_{NO_3}, q_{NO_2}, q_{NH_4}\right)\right\},$$

where K_{NF} is the maximum specific growth rate of phytoplankton.

The growth of microalgae also depends on the concentration of main nutrients — nitrogen compounds (nitrates, nitrites, ammonia) and phosphorus (phosphates, dissolved organic phosphorus, suspended organic phosphorus). The functional dependencies for these are written in the Michaelis-Menten form. All these factors are limiting, and their influence reflects Liebig's law.

The functional dependencies on abiotic factors are expressed by the following formulas:

$$f_T(T) = \exp\left(-a_i\left\{\left(T - T_{opt}\right)/T_{opt}\right\}^2\right),$$

$$f_S(S) = \exp\left(-b_2\left\{\left(S - S_{opt}\right)/S_{opt}\right\}^2\right),$$

$$f_S(S) = \begin{cases} k_s, \text{ for } S \le S_{opt}, \\ \exp\left(-b_1\left\{\left(S - S_{opt}\right)/S_{opt}\right\}^2\right), \text{ for } S > S_{opt}, \end{cases}$$

where $k_s = 1$; T_{opt}, S_{opt} are the optimal salinity and temperature for the given aquatic species; $a_i > 0$, $b_i > 0$; $i = 1,2$ are coefficients characterizing the width of the tolerance range of the aquatic organisms to salinity and temperature, respectively.

For system (1), an initial boundary value problem is formulated with the addition of appropriate initial and boundary conditions. The initial conditions for system (1) have the form:

$$\begin{gathered} q_i(x,y,z,0) = q_{0i}(x,y,z),\ i \in M,\ t = 0,\ (x,y,z) \in \overline{G}, \\ \mathbf{V}(x,y,z,0) = \mathbf{V}_0(x,y,z),\ T(x,y,z,0) = T_0(x,y,z),\ S(x,y,z,0) = S_0(x,y,z), \end{gathered} \tag{3}$$

where G is the computational domain of the enclosed water body, bounded by the lateral surface (cylindrical surface) σ, the bottom $\partial\Sigma_H = \partial\Sigma_H(x,y)$ and Σ_0 — the undisturbed free water surface; Σ is the piecewise smooth boundary of G, defined for $0 < t \le T$ at $\Sigma = \Sigma_0 \cup \Sigma_H \cup \sigma$.

Taking into account the introduced notations, the boundary conditions for equation (1) are formulated as follows on σ:

$$\begin{gathered} q_i = 0, \text{ if } u_n < 0, \\ \frac{\partial q_i}{\partial n} = 0, \text{ if } u_n \ge 0, \\ \frac{\partial q_i}{\partial z} = 0 \text{ on } \Sigma_o, \\ \frac{\partial q_i}{\partial z} = -\varepsilon_i q_i \text{ on the bottom } \Sigma_H, \end{gathered} \tag{4}$$

where ε_i are non-negative constants, $i \in M$; ε_i account for the sedimentation of algae to the bottom, their sinking, and the uptake of nutrients by bottom sediments for $i \in \{F_1, F_2\}$.

On a uniform temporal grid $\omega_\tau = \{t_n = n\tau,\ n = 0,1..., N;\ N\tau = T\}$ within the interval $0 < t \le T$ the nonlinearity of the right-hand side functions of the initial boundary value problem system (1)–(4) was linearized for the continuous model. Solutions of the linearized problem will be denoted as functions of the form $\tilde{q}_i^n$, $n = 1,2..., N$ taking into account the initial and boundary conditions. The linearization involves specifying the concentration functions of the substances appearing in the right-hand sides of the equations from the previous time layer t_{n-1}. If $n = 1$, the known initial conditions (3) are used.

Let us formulate the non-linearized (original) system (1) as a chain of coupled initial-boundary value problems of the form:

$$\frac{\partial q_i^n}{\partial t} + \frac{1}{2}\left(\operatorname{div}\left(\mathbf{V} \cdot q_i^n\right) + q_i^n \cdot \operatorname{div}\mathbf{V}\right) = \operatorname{div}\left(\mathbf{k} \cdot \operatorname{grad}\ q_i^n\right) + R_{q_i}^n, \tag{5}$$

where $i \in M$, $(x, y, z) \in G$, $n = 1,2..., N$, $t_{n-1} < t \le t_n$, $t \in \omega_\tau = \{t_n = n\tau,\ n = ,2..., N\}$ with initial and boundary conditions considered on the interval $t_{n-1} < t \le t_n$ for each of the equations.

Linearization involves specifying the concentration functions of the substances appearing in the right-hand sides of the equations from the previous, relative to the current, time layer:

$$\frac{\partial \tilde{q}_i^n}{\partial t} + \frac{1}{2}\left(\operatorname{div}\left(\mathbf{V}\cdot\tilde{q}_i^n\right) + \tilde{q}_i^n \cdot \operatorname{div}\mathbf{V}\right) = \operatorname{div}\left(\mathbf{k}\cdot\operatorname{grad}\,\tilde{q}_i^n\right) + \tilde{R}_{q_i}^n,$$
$$\tilde{R}_{q_i}^{n-1} = R_{q_i}\left(x, y, z, t_{n-1}, \tilde{q}_i^{n-1}\right),\ i \in M. \tag{6}$$

It has been proven that the norm of the error $\left\|z_i^n\right\|_{L_2(G)}$ tends to zero for any n and i under conditions motivated by hydrophysical and biogeochemical constraints. Inequalities have been obtained that guarantee the closeness of the solutions of the linearized and nonlinear problems for each substance F_i in $L_2(G)$ on a sequence of grids ω_τ at $\tau \to 0$:

$$\left\|z_1^n\left(x, y, z, t_n\right)\right\|_{L_2(G)} \underset{C_1 \equiv const > 0}{\leq} C_1\tau \underset{n=1,2,\ldots,N}{}.$$

The presented mathematical model requires input data with initial values for the concentrations of the studied substances, salinity, temperature, water flow velocities, etc. In 2022–2024, researchers from the Azov-Black Sea Branch of FSBSI "VNIRO" — "AzNIIRKH" investigated the hydrobiological characteristics of the Azov Sea, particularly water salinity and temperature. Values of salinity at the points of the hydrobiological survey grid are presented in [11]. Field measurement data are consistent with the assumption of the authors of this article regarding a 30% increase in the salinity of the Azov Sea, specifically in the Taganrog Bay, relative to normal values for the water body, as reflected in [10]. A forecast of the development of the main phytoplankton population species during summer under various salinization scenarios for the Azov Sea was also made.

As a result of the salinization of the Azov Sea, the habitat of blue-green algae has shifted to the eastern part of the Taganrog Bay, while they are almost absent in the main part of the sea, which is confirmed by data from "AzNIIRKH" [10].

Taking into account the above, it can be assumed that the obtained phytoplankton population habitats under salinity values increased by 30% from normal can be used as initial distributions of phytoplankton population concentrations for conducting a computational experiment on the biological rehabilitation of the water body. The forecast of the geographical position of phytoplankton populations shown in Fig. 1 reflects the ratio of green and blue-green algae, whose biomass in the Taganrog Bay constitutes 60–70% of the total phytoplankton biomass [3].

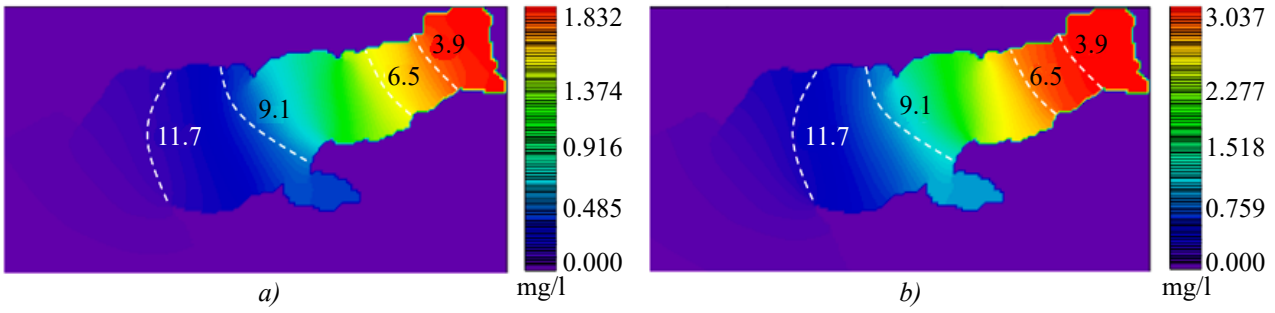

Fig. 1. Phytoplankton population habitats in summer:
a — green algae; *b* — blue-green algae

At the beginning of the growing season, nutrients are abundant, entering the Taganrog Bay with the runoff of the Don River during winter. At the start of the experiment, the distributions of major nutrients are set as uniform. The phosphate concentration is 0.04 mg/L, and the nitrate concentration is 0.204 mg/L. According to data from "AzNIIRKH" [10], the average phytoplankton biomass concentration in the Taganrog Bay is 1 mg/L, with cyanobacteria accounting for 70% of the biomass. The habitats of the initial phytoplankton population distributions are shown in Fig. 1, with the maximum concentration of green algae being 0.1 mg/L and that of cyanobacteria 0.7 mg/L. For the experiment, the optimal temperature for green algae is set at 25 °C, and for blue-green algae at 28 °C. The distributions of salinity and temperature values input into the software module for modelling the biological rehabilitation of the water body are shown in Fig. 2 [23].

When solving the linearized problem (1)–(10), the input data include the com-ponents of the water flow velocity vector at the nodes of the hydrodynamic com-putational grid, calculated based on the 3D hydrodynamic model implemented in the "Azov3D" software suite [24], as well as the values of salinity S_0, temperature T_0 and calculated concentrations q_{0i} at the time t_0. The boundaries of the computational domain were determined using depth values obtained from pro-cessing navigational charts [25].

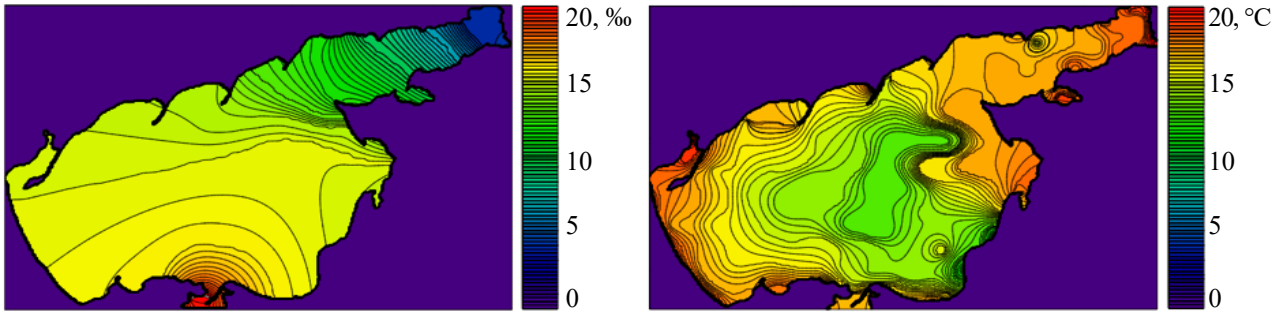

a) *b)*

Fig. 2. Initial data. Distributions of values:
a — salinity; *b* — temperature

The numerical solution of the problem involves constructing a discrete model (finite-difference scheme) using the input data and applying a numerical method for solving the grid equations. The modelling domain is assumed to be inscribed in a three-dimensional stepped region and is covered by a computational grid $\omega_\tau \times \omega_h$, uniform in time and the three spatial directions:

$$\omega_\tau = \{t_n = n\tau,\ n = 0,1..., N,\ N\tau = T\},$$

$$\omega_h = \{x_j = j \cdot h_x,\ y_k = k \cdot h_y,\ z_l = l \cdot h_z;\ \mathrm{j} = 0,1..., N_x,\ k = 0,1..., N_y,\ \mathrm{l} = 0,1..., N_z\},$$

where τ is the time step; $0 \le t \le T$ is the time interval; h_x, h_y, h_z are the steps in the spatial directions *Ox*, *Oy*, and *Oz*, respectively; N_x, N_y, N_z are the maximum number of grid nodes in each spatial direction; L_x, L_y, L_z are the maximum dimensions of the computational domain in space.

The linearization discussed above allows obtaining a system of linear grid equations. The discretization of problem (1), based on the system of convection-diffusion-reaction equations, is carried out using implicit monotonic schemes constructed on hydrodynamic grids.

The biological rehabilitation experiment proceeds as follows: a suspension of green algae is introduced at the beginning of their growing season, i. e., in March–April. By the start of the blue-green algae growing season (in May–June), the green algae have consumed most of the nutrients, leaving insufficient amounts for a massive bloom of blue-green algae.

The chlorella suspension is best introduced into areas of the water body with the highest convection, such as river channels, tips of spits, etc. The water flow velocity values were obtained from the "Azov3D" software suite, which implements a three-dimensional unsteady mathematical model of hydrodynamics. In the Azov Sea, easterly and northeasterly winds prevail from October to April. Such directions are formed under the influence of a spur of the Siberian anticyclone [26]. Therefore, the flow pattern obtained under an easterly wind direction was chosen as input data for conducting a computational experiment on the biological rehabilitation of the Taganrog Bay under conditions of increased salinity. The flow pattern in the Azov Sea under an easterly wind speed of 5 m/s is shown in Fig. 3. Red dots mark the locations of suspension introduction. The selection of points considered the flow velocities, the fact that *Chlorella vulgaris* is a freshwater alga, and the accessibility for introducing the suspension from the shore. The concentration of Chlorella vulgaris in the suspension is 1167 mg/L, the release rate is 5 L/s, with a total of 25 tons released, 2.5 tons at each of the 10 release points.

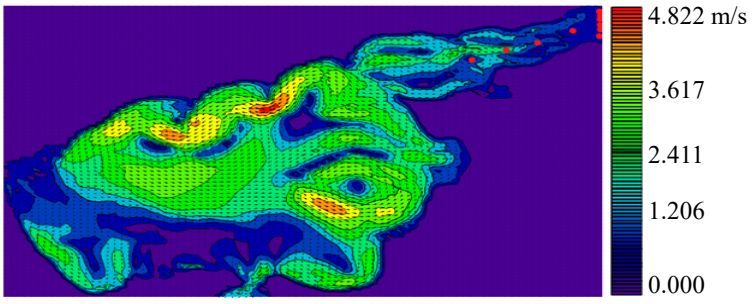

Fig. 3. Flow pattern in the Azov Sea under an easterly wind of 5 m/s

Results. As part of this study, modelling of the biological rehabilitation of the Taganrog Bay under conditions of salinization, based on the introduction of green microalgae, was conducted. As a result of the computational experiment,

the authors obtained distributions of green algae and blue-green algae concentrations at time intervals of 15 days (Fig. 4) and 30 days (Fig. 5) for a *Chlorella vulgaris* suspension concentration of 1167 mg/L and a total volume of 25 tons.

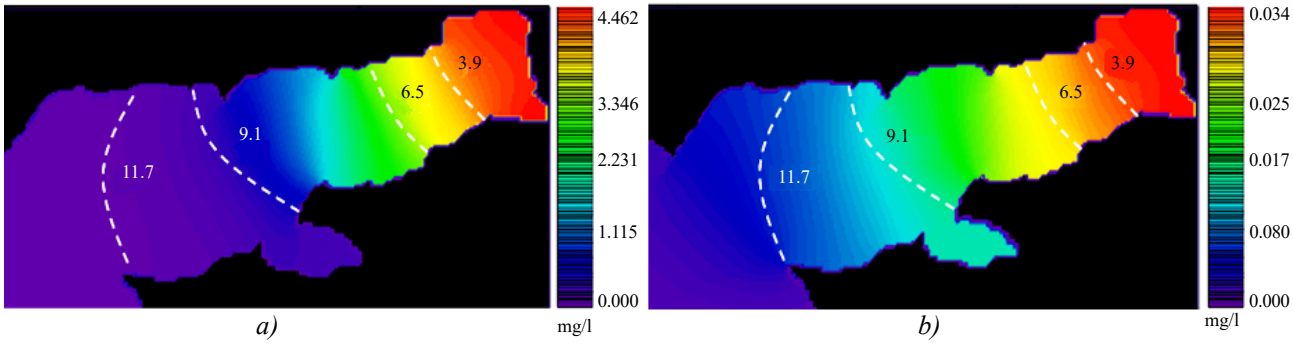

Fig. 4. Concentration distributions 15 days
after introducing the *Chlorella vulgaris* suspension (concentration 1167 mg/L):
a — green algae; *b* — blue-green algae

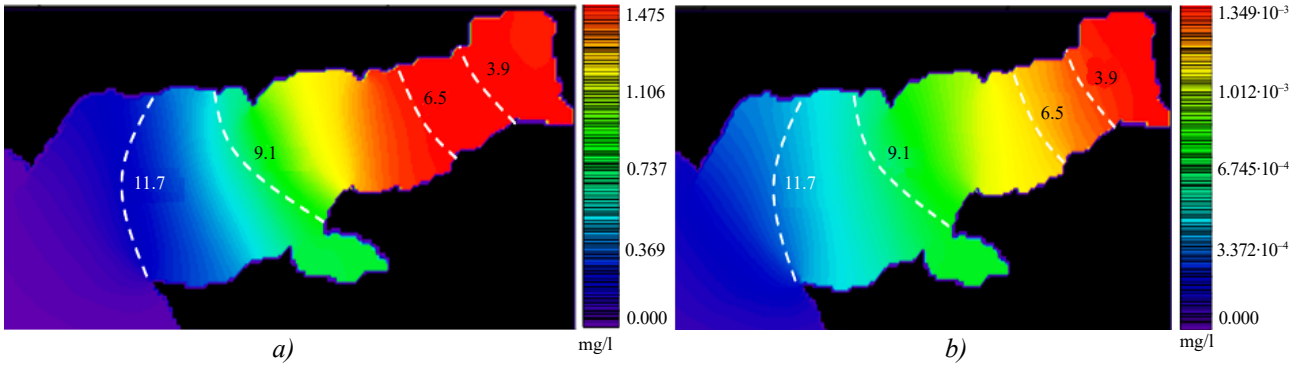

Fig. 5. Concentration distributions 30 days
after introducing the *Chlorella vulgaris* suspension (concentration 1167 mg/L):
a — green algae; *b* — blue-green algae

Fig. 6 shows the distributions of green algae and blue-green algae (surface layer) over a 30-day time interval for a *Chlorella vulgaris* suspension concentration of 2333 mg/L and a total volume of 25 tons.

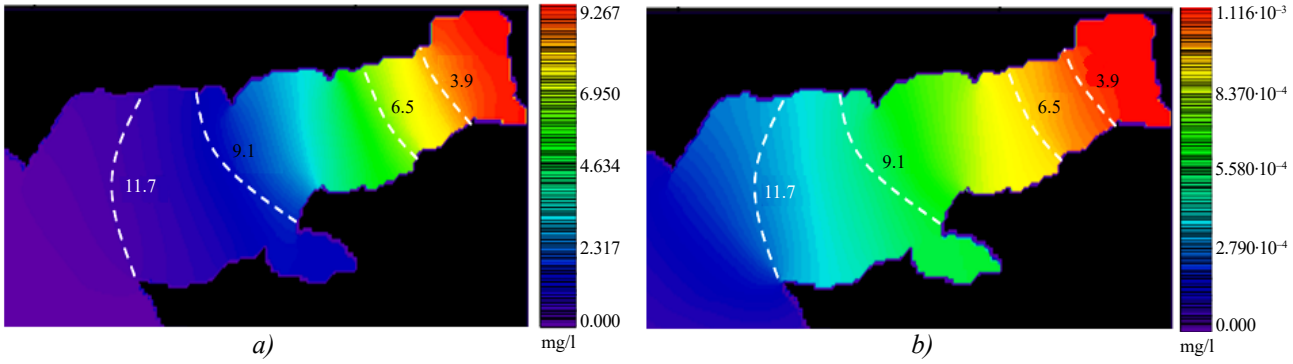

Fig. 6. Concentration distributions 30 days
after introducing the *Chlorella vulgaris* suspension (concentration 2333 mg/L):
a — green algae; *b* — blue-green algae

Fig. 4–6 depict the concentration values of the two microalgae species on the water surface.

Discussion. The concentration distributions of green and blue-green algae obtained from the modelling indicate the success of the computational experiment on the biological rehabilitation of the Taganrog Bay for the given concentration and volume of the introduced suspension. The experiment simulated the introduction of a *Chlorella vulgaris* phytoplankton suspension into the water body during the spring period, prior to the growing season of the potentially toxic blue-green algae *Aphanizomenon flos-aquae*. The introduction points were selected in the freshened zone (salinity values up to 7–8‰),

which allowed the freshwater green algae to survive and grow successfully. The green microalgae consumed phosphates (PO_4) and nitrates (NH_4), leading to a nutrient deficiency by the beginning of the blue-green algae growing season.

At the start of the experiment, the concentration of blue-green algae exceeded that of green algae (0.7 mg/L and 0.1 mg/L, respectively). After 15 days, the concentration of blue-green algae was 131 times lower than that of green algae (0.034 mg/L and 4.462 mg/L, respectively). After 30 days, the difference in concentrations increased further (1.349×10^{-3} mg/L and 1.475 mg/L, respectively). Additionally, as shown in Fig. 6, doubling the concentration of the introduced green algae (to 2333 mg/L while keeping the volume constant) resulted in a potentially hazardous *Chlorella vulgaris* concentration of 9.267 mg/L after 30 days. Such a concentration of green algae, combined with other phytoplankton species, could lead to eutrophication of the water body and fish kills.

Furthermore, increasing the quantity of introduced green algae is costly and, therefore, economically unviable. The computational experiment empirically determined the optimal concentration and volume of the *Chlorella vulgaris* suspension to be introduced. It is important to note that the results of the computational experiment were obtained using reliable data on salinity, temperature, and the distributions of modeled substances, confirmed by field studies and long-term observations.

From the perspective of assessing ecological-hygienic and medical consequences, the scenario where green algae concentration exceeds that of blue-green algae (Fig. 5) is favorable, and no significant negative impacts from blue-green algae on recreational conditions in the Taganrog Bay are expected. Moreover, the concentration of green algae does not exceed permissible limits and is considered acceptable.

Conclusion. The modelling results were obtained using modern and high-precision mathematical modelling methods. The study's findings demonstrate the advantage of employing an integrated approach in mathematically modelling processes occurring in complex natural systems. These methods can be successfully used to simulate various scenarios for the development and rehabilitation of water bodies.

Despite the obtained results, the invasion of *Chlorella* into the ecosystem of the Taganrog Bay cannot be considered as the sole method for improving the ecological state of the water body. However, it can be an effective tool for water body rehabilitation when combined with other methods.

References

1. Zhidkova A.Y., Podberesnij V.V., Zarubina R.V., Kononova O.A. The effect of eutrophication on human health on the example of the Gulf of Taganrog of the Sea of Azov. *IOP Conference Series: Earth and Environmental Science.* 2020;548:052053. https://doi.org/10.1088/1755-1315/548/5/052053

2. Matishov G.G., Fushtei T.V. On the problem of harmful algal blooms in the Azov Sea. *Electronic Journal "Research in Russia"*. 2003;6:213–225. (In Russ.)

3. Kovaleva G.V. Issue VIII: Modelling and Analysis of Natural Hazards in the Sea of Azov Region. In book: *Studies of the Southern Scientific Centre of the Russian Academy of Sciences (Series)*. Rostov-on-Don: SSC RAS Publishers; 2020. 328 p. (In Russ.)

4. World Health Organization. Guidelines on recreational water quality: Volume 1 — Coastal and Fresh Waters. *Geneva: WHO*; 2021. ISBN: 978-92-4-003130-2. URL: https://www.who.int/publications/i/item/9789240031302 (дата обращения: 11.09.2025).

5. Hygienic standards and safety requirements for environmental factors. SanPiN 1.2.3685–21. No. 62296. Moscow: Ministry of Health of Russia; 2021. URL: https://docs.cntd.ru/document/573500115 (accessed: 09.09.2025).

6. Chernova E.N., Shevchenko A.N. Determination of cyanotoxins in drinking water by HPLC. *Hygiene and Sanitation.* 2018;97(8):692–697. https://doi.org/10.18821/0016-9900-2018-97-8-692-697

7. Hallegraeff G.M. Harmful algal blooms: A global overview. *Elsevier Oceanography Series*. 2003;65:25–50. https://doi.org/10.1016/S0422-9894(03)80050-9

8. Backer L.C., Carmichael W.W. Human health effects from exposure to cyanobacteria and their toxins. *Environmental Health Perspectives*. 2016;124(11):1333–1343. https://doi.org/10.1289/EHP.1510459

9. Griffiths D.J., Saker M.L. Cylindrospermopsis raciborskii and cylindrospermopsin. *Environmental Toxicology*. 2003;18(2):78–93. https://doi.org/10.1002/tox.10113

10. AzNIIRKH. Summer cyanobacterial blooms in the Taganrog Bay. 7 September 2018. (In Russ.) URL: https://azniirkh.vniro.ru/ (accessed: 11.09.2025).

11. Berdnikov S.V., Kulygin V.V., Dashkevich L.V. Causes of the rapid increase in salinity of the Sea of Azov in the 21st century. *Marine Hydrophysical Journal*. 2023;39(6):760–778. (In Russ.)

12. Chorus I., Welker M., editors. *Toxic cyanobacteria in water: A guide to their public health consequences, monitoring and management*. 2nd ed. Boca Raton: CRC Press; 2021.

13. Xiao M., Burford M.A., Wood S.A., et al. Schindler's legacy: From eutrophic lakes to phosphorus utilization strategies. *FEMS Microbiology Reviews*. 2022;46(6):fuac029. https://doi.org/10.1093/femsre/fuac029

14. Neverova G., Zhdanova O. Mathematical modeling of plankton evolutionary dynamics. *Mathematics*. 2023;11(22):4673. https://doi.org/10.3390/math11224673

15. Bogdanov N.I. *Biological rehabilitation of water bodies*. Penza: PGSKhA Publishing; 2008;18–26. (In Russ.)
16. Aly S.M., ElBanna N.I., Fathi M. Chlorella in aquaculture. *Aquaculture International*. 2024;32:1559–1586. https://doi.org/10.1007/s10499-023-01229-x
17. Bogdanov N.I. *Chlorella suspension in the diet of farm animals. Russian Academy of Agricultural Sciences, Research Institute of Agriculture*. 2nd ed. Penza; 2007;17. (In Russ.)
18. Pavlyuk T.E., Nikolaev A.D., Ivanova I.V., et al. Correction of algal communities with Chlorella introduction. *Water Resources*. 2023;50(3):324–333. https://doi.org/10.31857/S0321059623030106
19. Gao J., Shao N., Sun Y., et al. Impact of Chlorella vulgaris on pond microbiota. *Sustainability*. 2023;15(9):7362. https://doi.org/10.3390/su15097362
20. Kudinov N.V., Filina A.A., Nikitina A.V., Bondarenko D.V., Razveeva I.F. Simulation of vertical movements of seawater in stratified reservoirs. *Advanced Engineering Research (Rostov-on-Don)*. 2023;23(2):212–224. https://doi.org/10.23947/2687-1653-2023-23-2-212-224
21. Yakushev E.V., Pollehne F., Jost G., et al. Analysis of oxic/anoxic interfaces. *Marine Chemistry*. 2007;107:388–410. https://doi.org/10.1016/j.marchem.2007.06.003
22. Sukhinov A., Belova Y., Chistyakov A., Beskopylny A., Meskhi B. Modeling phytoplankton population geographic dynamics. *Mathematics*. 2021;9:3025. https://doi.org/10.3390/math9233025
23. Belova Yu.V., Chistyakov A.E. Modeling the Dynamics of Harmful Phytoplankton Species Concentration in Taganrog Bay of the Azov Sea. *Safety of Technogenic and Natural Systems*. 2025;9(4):284–293. https://doi.org/10.23947/2541-9129-2025-9-4-284-293
24. Sukhinov A.I., Nikitina A.V., Atayan A.M., Litvinov V.N., Belova Yu.V., Chistyakov A.E. Supercomputer simulation of hydrobiological processes. *Mathematical Models and Computer Simulations*. 2022;14:677–690. (In Russ.) https://doi.org/10.20948/mm-2022-01-06
25. Rakhimbaeva E.O., Alyshov T.A., Belova Yu.V. Automatic depth value recognition. *Computational Mathematics and Information Technologies*. 2025;9(1):52–60. https://doi.org/10.23947/2587-8999-2025-9-1-52-60
26. Unified State System of Information on the World Ocean (ESIMO). *Oceanographic data portal*; 2025. URL: http://esimo.oceanography.ru/ (accessed: 11.09.2025).

About the Authors:

Yulia V. Belova, Candidate of Physico-Mathematical Sciences, Associate Professor of the Department of Mathematics and Computer Science at the Don State Technical University (1, Gagarin Sq., Rostov-on-Don, 344003, Russian Federation), ORCID, SPIN-code, yvbelova@yandex.ru

Olesya V. Kolgunova, Candidate of Physico-Mathematical Sciences, Senior Lecturer at the Department of Applied Mathematics and Computer Science, North Ossetian State University (44–46, Vatutina St., Vladikavkaz, 362025, Russian Federation), ORCID, SPIN-code, kolev2003@mail.ru

Maria I. Gabuyeva, fourth-year student of the Medical Faculty of the North Ossetian State Medical Academy (40, Pushkinskaya St., Vladikavkaz, 362019, Russian Federation), ORCID, gabueva72@xmail.ru

Contributions of the authors:

Yu.V. Belova: ideas; conducting a research and investigation process, specifically performing the computational experiments; preparation, creation of the published work, specifically visualization; making graphic materials.

O.V. Kolgunova: formulation of overarching research goals and aims; preparation, creation of the published work, specifically critical review; conclusions correction; text revision.

M.I. Gabueva: Preparation, creation of the published work, specifically writing the initial draft; formatting the research article; working with sources.

Conflict of Interest Statement: **the authors declare no conflict of interest.**

All authors have read and approved the final manuscript.

Об авторах:

Юлия Валериевна Белова, кандидат физико-математических наук, доцент кафедры математики и информатики Донского государственного технического университета (344003, Российская Федерация, г. Ростов-на-Дону, пл. Гагарина, 1), ORCID, SPIN-код, yvbelova@yandex.ru

Олеся Владимировна Колгунова, кандидат физико-математических наук, старший преподаватель кафедры прикладной математики и информатики Северо-Осетинского государственного университета (362025, Российская Федерация, г. Владикавказ, ул. Ватутина, 44–46), ORCID, SPIN-код, kolev2003@mail.ru

Мария Игоревна Габуева, студент четвертого курса лечебного факультета Северо-Осетинской государственной медицинской академии (362019, Российская Федерация, г. Владикавказ, ул. Пушкинская, 40), ORCID, gabueva72@xmail.ru

Заявленный вклад авторов:

Ю.В. Белова: формулирование основной концепции исследования; осуществление научно-исследовательского процесса, включая проведение вычислительных экспериментов; создание и подготовка рукописи: визуализация результатов исследования и полученных данных; оформление графических материалов.

О.В. Колгунова: формулирование целей и задач исследования; создание и подготовка рукописи: критический анализ черновика рукописи; корректировка выводов; доработка текста.

М.И. Габуева: создание и подготовка рукописи: написание черновика рукописи; оформление научной статьи; работа с источниками.

Конфликт интересов: **авторы заявляют об отсутствии конфликта интересов.**

Все авторы прочитали и одобрили окончательный вариант рукописи.

Received / Поступила в редакцию 27.10.2025
Reviewed / Поступила после рецензирования 28.11.2025
Accepted / Принята к публикации 15.12.2025